JYVÄSKYLÄ STUDIES IN COMPUTING
273

Nataliya Stankevich

Hidden and Self-Excited Attractors in Radiophysical and Biophysical Models

JYVÄSKYLÄN YLIOPISTO

JYVÄSKYLÄ STUDIES IN COMPUTING 273

Nataliya Stankevich

Hidden and Self-Excited Attractors in Radiophysical and Biophysical Models

Esitetään Jyväskylän yliopiston informaatioteknologian tiedekunnan suostumuksella
julkisesti tarkastettavaksi yliopiston Agora-rakennuksen Alfa-salissa
joulukuun 16. päivänä 2017 kello 12.

Academic dissertation to be publicly discussed, by permission of
the Faculty of Information Technology of the University of Jyväskylä,
in building Agora, Alfa hall, on December 16, 2017 at 12 o'clock noon.

UNIVERSITY OF JYVÄSKYLÄ

JYVÄSKYLÄ 2017

Hidden and Self-Excited Attractors in Radiophysical and Biophysical Models

JYVÄSKYLÄ STUDIES IN COMPUTING 273

Nataliya Stankevich

Hidden and Self-Excited Attractors in Radiophysical and Biophysical Models

UNIVERSITY OF JYVÄSKYLÄ

JYVÄSKYLÄ 2017

Editors
Timo Männikkö
Faculty of Information Technology, University of Jyväskylä
Pekka Olsbo, Ville Korkiakangas
Publishing Unit, University Library of Jyväskylä

Permanent link to this publication: http://urn.fi/URN:ISBN:978-951-39-7294-3

URN:ISBN:978-951-39-7294-3
ISBN 978-951-39-7294-3 (PDF)

ISBN 978-951-39-7293-6 (nid.)
ISSN 1456-5390

Jyväskylä University Printing House, Jyväskylä 2017

ABSTRACT

Stankevich, Nataliya
Hidden and self-excited attractors in radiophysical and biophysical models
Jyväskylä: University of Jyväskylä, 2017, 44 p.(+included articles)
(Jyväskylä Studies in Computing
ISSN 1456-5390; 273)
ISBN 978-951-39-7293-6 (nid.)
ISBN 978-951-39-7294-3 (PDF)
Finnish summary
Diss.

One of the central tasks of investigation of dynamical systems is the problem of analysis of the steady (limiting) behavior of the system after the completion of transient processes, i.e., the problem of localization and analysis of attractors (bounded sets of states of the system to which the system tends after transient processes from close initial states). Transition of the system with initial conditions from the vicinity of stationary state to an attractor corresponds to the case of a self-excited attractor. However, there exist attractors of another type: hidden attractors are attractors with the basin of attraction which does not have intersection with a small neighborhoods of any equilibrium points. Classification "hidden vs self-excited" attractors was introduced by Leonov and Kuznetsov.

Discovery of the hidden chaotic attractor has shown the need for further study of the scenarios concerned with the appearance and properties of hidden attractors, since the appearance of such attractors in the system can lead to a qualitative change in the dynamics of the system. In the present work two directions have been chosen, for which the possibility of the appearance of hidden attractors can be critical: radiophysics and biophysics. The features of radiophysical generators which can be used for systems of secure communication based on the dynamical chaos are considered in detail. Using the Chua circuit as an example, we investigate the problem of synchronization between two coupled generators in case when the observed regimes are represented by hidden and self-excited attractors. This example shows that in case of hidden attractors under certain initial conditions desynchronization of the coupled subsystems is possible, and the system of secure communication becomes inoperative. Alternative new radiophysical generators with self-excited attractors are also proposed. In such generators, the dynamical chaos is stable to the variation of parameters, initial conditions. In the context of the biophysics problems, a simplified model describing the dynamics of beta-cells based on the Hodgkin-Huxley formalism is presented. It has a typical for such systems bursting attractor which became hidden. This model can be used for the description of various pathological states of cells formation.

Keywords: hidden attractors, self-excited attractors, multistability, radiophysical generator, Chua circuits, pancreatic beta-cell

Author

Nataliya Stankevich
Faculty of Information Technology,
University of Jyväskylä, Finland;
Faculty of Mathematics and Mechanics,
St. Petersburg State University, Russia;
Department of Radio-electronics and Communications,
Saratov State Technical University, Russia

Supervisors

Professor Pekka Neittaanmäki
Faculty of Information Technology,
University of Jyväskylä, Finland

Professor Nikolay V. Kuznetsov
Faculty of Information Technology,
University of Jyväskylä, Finland;
Faculty of Mathematics and Mechanics,
St. Petersburg State University, Russia

Professor Gennady A. Leonov
Faculty of Mathematics and Mechanics,
St. Petersburg State University, Russia

Reviewers

Professor Sergei Abramovich
School of Education and Professional Studies,
State University of New York at Potsdam, USA

Professor Marius-F. Danca
Romanian Institute of Science and Technology;
Department of Mathematics and Computer Science,
Avram Iancu University, Romania

Opponent

Professor Anton Shiriaev
Department of Engineering Cybernetics,
Norwegian University of Science and Technology,
Trondheim, Norway

ACKNOWLEDGEMENTS

This thesis has been completed in the Doctoral School of the Faculty of Information Technology, University of Jyväskylä.

I greatly appreciate the support from the Faculty of Information Technology (University of Jyväskylä). Also this work was funded by the Russian Science Foundation (14-21-00041).

I would like to express my sincere gratitude to my supervisors Prof. Nikolay V. Kuznetsov, Prof. Gennady A. Leonov, and Prof. Pekka Neittaanmäki for their guidance and continuous support.

I am very grateful to Prof. Sergei Abromovich (School of Education and Professional Studie) and Professor Marius-F. Danca (Avram Iancu University) for their valuable comments.

I would like to thank Prof. Timo Tiihonen for very important comments and remarks.

I would like to thank my collaborators from Saratov group of theoretical nonlinear dynamics: Prof. Alexander Kuznetsov, Prof. Sergey Kuznetsov, Prof. Evgeniy Seleznev. I would like to thank my colleges working in biophysics and biology: Prof. Erik Mosekilde (Denmark Technical University) and Dr. rer. nat. habil. Aneta Koseska (Max Planck Institute for Molecular Physiology).

I would like to thank Dr. Yuliya Emelyanova and Dr. Natallia Makarava for English corrections and Prof. Anatoly Karavaev for important remarks.

Finally, I am eternally grateful to my parents Tatyana N. Stankevich and Vladimir Ya. Stankevich, who brought me up and gave me my life principles and views, and to whom I will be forever indebted and to my son Fadey V. Stankevich.

LIST OF FIGURES

LIST OF TABLES

CONTENTS

LIST OF INCLUDED ARTICLES

PI N. V. Stankevich, N. V. Kuznetsov, G. A. Leonov, L. Chua. Scenario of the Birth of Hidden Attractors in the Chua Circuit. *International Journal of Bifurcation and Chaos, Vol.27, Issue 12, 1730038(18 pages)*, 2017.

PII N. V. Kuznetsov, O. A. Kuznetsova, G. A. Leonov, T. N. Mokaev, N. V. Stankevich. Hidden attractors localization in Chua circuit via the describing function method. *IFAC PapersOnLine, Vol.50, pp.2651-2656*, 2017.

PIII N. V. Kuznetsov, G. A. Leonov, and N. V. Stankevich. Synchronization of Hidden Chaotic Attractors on the Example of Radiophysical Oscillators. *Proceeding of PIERS IEEEXplore*, 2017.

PIV P. V. Kuptsov, S. P. Kuznetsov, N.V. Stankevich. A family of models with blue sky catastrophes of different classes. *Regular and Chaotic dynamics, Vol.5, pp. 551-565*, 2017.

PV O. B. Isaeva, D. V. Savin, E. P. Seleznev, and N. V. Stankevich. Hyperbolic Chaos and Quasiperiodic Dynamics in Experimental Nonautonomous Systems of Coupled Oscillators. *Proceeding of PIERS IEEEXplore*, 2017.

PVI N. V. Stankevich, O. V. Astakhov, E. P. Seleznev. Generation of Chaotic and Quasi-periodic Oscillations in Multi-contour Self-generator. *Proceeding of PIERS IEEEXplore*, 2017.

PVII N. V. Stankevich, E. Mosekilde. Coexistence between bursting and silent states in a biophysical model of Hodgkin-Huxley-type. *CHAOS, Vol.27, Issue 11, accepted*, 2017.

1 INTRODUCTION AND THE STRUCTURE OF THE WORK

1.1 Introduction

One of the central tasks of investigation of dynamical systems is the problem of analysis of the steady (limiting) behavior of the system after the completion of transient processes, i.e., the problem of localization and analysis of attractors (bounded sets of states of the system to which the system tends after transient processes from close initial states). To solve this problem in mathematics the theory of dynamical systems and methods of analysis of its attractors were developed. So, in the 19^{th} century effective criteria for analyzing stability and the appearance of periodic attractors in dynamical systems were developed by Poincaré and Lyapunov. During the 20^{th} century various scenarios of transition to chaos were investigated (Feigenbaum, Shilnikov, Sharkovskiy), and chaotic attractors were discovered in dynamical systems (Ueda, Lorenz). Special difficulties for investigation is due to the multistable dynamical systems, in which several attractors can coexist. Thus, the Hilbert's 16^{th} Problem about the number and mutual arrangement of limit cycles (periodic attractors) in two-dimensional polynomial systems has not been solved in the general case as up to now.

From the point of view of numerical simulations for the searching and visualizing of an attractor in the phase space, it is necessary to determine initial conditions inside the area of the attraction of attractor and numerically observe transient process of trajectory attraction from the initial point to the attractor with the increase of time. Transition of the system with initial conditions from the vicinity of stationary state to an attractor corresponds to the case of a self-excited attractor, this case allows one to carry out an effective numerical search and visualization of this attractor. However, there exist attractors of another type: hidden attractors are attractors with the basin of attraction which does not have intersection with a small neighborhoods of any equilibrium points. Classification "hidden vs self-excited" attractors was introduced by Leonov and Kuznetsov in 2010 when they uncovered a hidden attractor in the radiophysical Chua circuit, and thus allowed

one to combine the notion of transition process in engineering systems, visualization in numerical mathematics, the basin of attraction and the stability of the theory of dynamical system.

A wide range of complex dynamical systems from the biology, neurons, cells (Laurent and Kellershohn, 1999; Pmerening et al., 2003; Ozbudak et al., 2004; Kelso, 2012; Pisarchik and Feudel, 2014) to engineering applications (De Rossi et al., 1998; Joshi and Xiao, 2003; Marquardt et al., 2006; Paraïso et al., 2010) may have many coexisting attractors, so called multistable attractors. The final state, i.e., the attractor toward which the multistable system evolves strongly depends on the initial conditions. Additionally, such systems can be sensitive towards noise and system parameters so a sudden shift to a contrasting regime may occur. To understand the dynamics of these systems one has to identify all possible attractors and their basins of attraction. Recently, it has been shown that multistability can be connected with the occurrence of hidden attractors (Leonov et al., 2011; Leonov and Kuznetsov, 2013; Dudkowski et al., 2016). Numerical localization of the hidden attractors is not straightforward since there are no transient processes leading to them from the neighborhoods of unstable fixed points and one has to use the special analytical numerical procedures. From the viewpoint of applications, the identification of hidden attractors is the major issue. The knowledge about the emergence and properties of hidden attractors can help to predict that the system will remain on the most desirable attractor and reduce the risk of the sudden jump to undesired behavior. The main goal of this work is to obtain a new models demonstrating hidden attractors, which can be applied in biophysics and radio physics and to study scenarios of formation of hidden attractors.

1.2 Structure of the work

The present work consists of an introduction, summaries of the results and includes seven articles (see Figure 1). In the introduction, an overview of the hidden attractors theory development history and the main definitions are given; also applications which were studied are mentioned. The main chapter includes two parts:

- radiophysical applications;
- biophysical applications.

For different kinds of models a general studying algorithm was applied (see Figure 2). For each situation, each own model was proposed, representing a system of ordinary differential equations which were solved by numerical integration in the MatLab with using package Ode45 (it is the Runge-Kutta adaptive step-sized method of numerical integration). Also, the numerical bifurcation analysis was carried out by using software package XPP AUTO (Ermentrout, 2002).

Softwares GnuPlot and CorelDraw were used for visualization of the obtained results and the graphical illustrations.

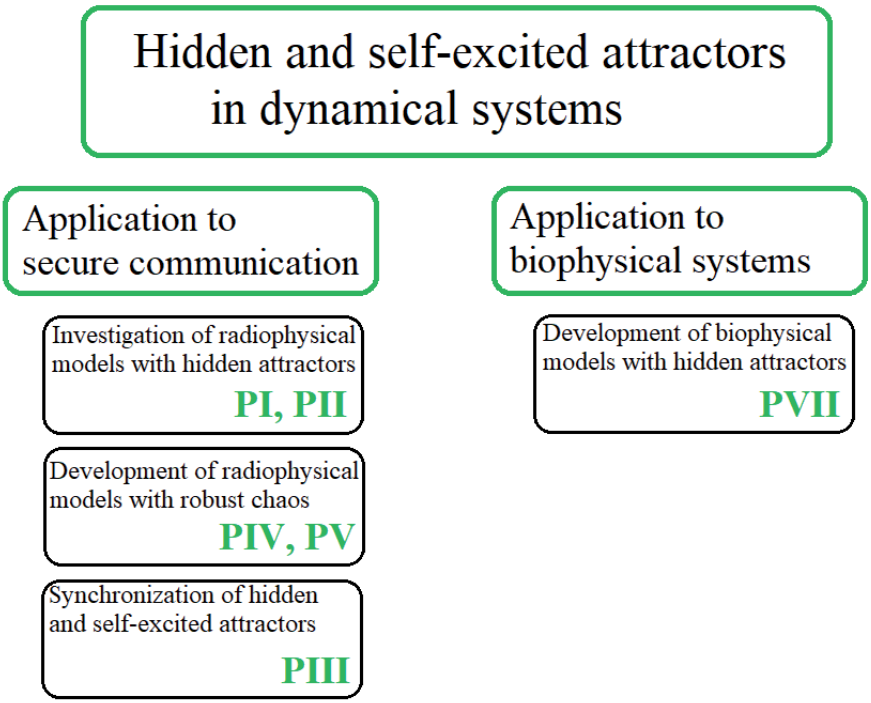

FIGURE 1 Structure of the work.

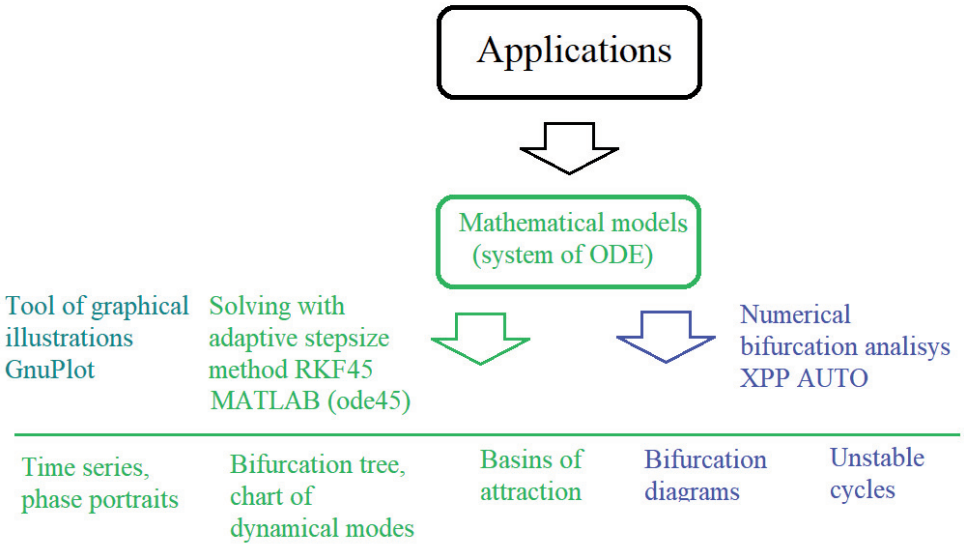

FIGURE 2 Algorithm of studying different models.

1.3 Included articles and author contribution

In **PI** and **PII**, the author applied numerical methods for studying the model of the Chua circuit to localize a new the existence region of hidden attractors and to study scenario when hidden attractors occur. In **PIII**, the author investigated synchronization between two coupled oscillators with hidden and self-excited attractors using numerical simulations. In **PIV**, the author considered generalized model, where the formation of self-excited chaotic attractors with property of robustness is possible. In **PV**, the author realized experiment with radiophysical circuits, which can demonstrate self-excited dynamics including quasiperiodic oscillations and chaos. In **PVI**, the author carried out an experiment with multi-contour generator where chaotic oscillations were observed. In **PVII**, the author proposed a modification of the well-known simplified model of the pancreatic beta-cell, where the existence of hidden attractors was observed.

Author contributions are in writing, numerical simulations, radiophysical experiments.

The biophysical results were discussed with Prof. E. Mosekilde from Denmark Technical Universuty. The author made scientific visit to DTU in 2012. In 2016 the author visited Max-Planck Institute for Molecular Physiology, where she discussed biological model with Dr. rer. nat. habil. Aneta Koseska.

The results of this work were presented at 20^{th} World Congress The International Federation of Automatic Control (IFAC-2017, Toulouse, France, 9-14 July 2017), at Conference "Understanding learning in the brain" (Jyväskylä, Finland, 13-14 June 2017), at IEEE Conference "Progress In Electromagnetics Research Symposium" (PIERS-2017, Saint-Petersburg, 22-25 May 2017), at International Symposium "Topical problems of Nonlinear wave physics" (NWP-2017, Moscow-St.Petersburg, 22-28 July 2017); at the seminars of the Department of Applied Cybernetics (St. Petersburg State University), and at the seminars of the Faculty of Information Technology (University of Jyväskylä).

2 PROBLEM STATEMENT AND MAIN RESULTS

In this section following to papers **PI-PVII**, the main content is presented.

2.1 Dynamical system: attractors and classification

A dynamical system is a mathematical abstraction designed to characterize and study systems whose time evolution is uniquely determined by the initial state and which describe some object, process, or phenomena. A phase space of a dynamical system is the set of all possible states. Thus, the dynamical system is characterized by its initial state and the law by which the system evolves from the initial state. Let us introduce some rigorous notions of a dynamical system and attractor and discuss the connection with the notions of self-excited and hidden attractors from a computational perspective.

An autonomous system can be described by the system of differential equations:

$$\dot{u} = f(u), f : U \subseteq \mathbb{R}^n \to \mathbb{R}^n, \tag{1}$$

where f is a continuously differentiable vector-function. Suppose that any solution $u(t, u_0)$ of (1) such that $u(0, u_0) = u_0 \in U$ exists for $t \in [0, \infty)$, it is unique and stays in U. Then the evolutionary operator $\varphi^t(u_0) = u(t, u_0)$ is continuously differentiable and satisfies the semigroup property:

$$\varphi^{t+s}(u_0) = \varphi^t(\varphi^s(u_0)), \varphi^0(u_0) = u_0 \ \ \forall\ t, s \geq 0, \forall u_0 \in U. \tag{2}$$

Thus, ${\varphi^t}_{t\geq 0}$ is a smooth *dynamical system* in the phase space $(U, \|\cdot\|) : ({\varphi^t}_{t\geq 0}, (U \subseteq \mathbb{R}^n, \|\ \cdot\ \|))$. Here $\|\ u\ \| = \sqrt{u_1^2 + ... + u_n^2}$ is Euclidean norm of the vector $u = (u_1, ..., u_n) \in \mathbb{R}^n$. Similarly, one can consider a dynamical system generated by the difference equation

$$u(t+1) = \varphi(u(t)), t = 0, 1, ... \tag{3}$$

where $\varphi : U \subseteq \mathbb{R}^n \to U$ is a continuously differentiable vector-function. Here $\varphi^t(u) = \underbrace{(\varphi \circ \varphi \circ \cdots \circ \varphi)(u)}_{t \text{ times}}, \varphi^0(u) = u$, and the existence and uniqueness (in the forward-time direction) take place for all $t \geq 0$.

The classical definitions of an attractor is connected with investigation of the limit behavior of the trajectories of dynamical systems.

Definition 1. A set K is said to be positively invariant for a dynamical system if

$$u(t, K) \subset K, \forall t \geq 0,$$

and to be invariant if

$$u(t, K) = K, \forall t \geq 0,$$

where $u(t, K) = \{u(t, u_0) \mid u_0 \in K, t \geq 0\}$.

Property 1. Invariant set K is said to be locally attractive for a dynamical system if, for a certain ε-neighborhood $K(\varepsilon)$ of set K,

$$\lim_{t \to +\infty} \rho(K, u(t, u_0)) = 0, \forall u_0 \in K(\varepsilon).$$

Here $\rho(K, u)$ is a distance from the point u to the set K, defined as

$$\rho(K, u) = \inf_{z \in K} \|z - u\|,$$

and $K(\varepsilon)$ is a set of points u for which $\rho(K, u) < \varepsilon$.

Property 2. Invariant set K is said to be globally attractive for a dynamical system if

$$\lim_{t \to +\infty} \rho(K, u(t, u_0)) = 0, \forall u_0 \in \mathbb{R}^n.$$

Property 3. Invariant set K is said to be uniformly locally attractive for a dynamical system if for a certain ε-neighborhood $K(\varepsilon)$, any number $\delta > 0$, and any bounded set B, there exists a number $t(\delta, B) > 0$ such that

$$u(t, B) \bigcap K(\varepsilon), \forall t \geq t(\delta, B).$$

Here

$$u(t, B \bigcap K(\varepsilon)) = \{u(t, u_0) \mid u_0 \in B \bigcap K(\varepsilon)\}.$$

Property 4. Invariant set K is said to be uniformly globally attractive for a dynamical system if, for any number $\delta > 0$ and any bounded set $B \subset \mathbb{R}^n$, there exists a number $t(\delta, B) > 0$ such that

$$u(t, B) \subset K(\delta), \forall t \geq t(\delta, B).$$

Definition 2. (Ladyzhenskaya, 1991; Babin and Vishik, 1992; Boichenko et al., 2005) For a dynamical system, a bounded closed invariant set K is:

1) *an attractor* if it is a locally attractive set (i.e., it satisfies *Property 1*);
2) *a global attractor* if it is a globally attractive set (i.e., it satisfies *Property 2*);
3) *a B-attractor* if it is a uniformly locally attractive set (i.e., it satisfies *Property 3*);
4) *a global B-attractor* if it is a uniformly globally attractive set (i.e., it satisfies *Property 4*).

Recently new classification of attractor was introduced.

Definition 3. (Leonov et al., 2011; Leonov and Kuznetsov, 2013; Leonov et al., 2015b; Kuznetsov, 2016). An attractor is called a *hidden* if its basin of attraction does not intersect with a neighborhood of stationary equilibria (states); otherwise, it is called a *self-excited* attractor.

For a *self-excited attractor*, its basin of attraction is connected with an unstable equilibrium and, therefore, self-excited attractors can be localized numerically by the *standard computational procedure* in which after a transient process a trajectory, started in a neighborhood of an unstable equilibrium (e.g., from a point of its unstable manifold), is attracted to the state of oscillation and then traces it. Thus, self-excited attractors can be easily visualized (e.g., the classical Lorenz, Rössler, and Hennon attractors can be visualized by a trajectory from a vicinity of unstable zero equilibrium).

For a hidden attractor, its basin of attraction is not connected with equilibria, and, thus, the search and visualization of hidden attractors in the phase space may be a challenging task. Hidden attractors are attractors in systems without equilibria (see, e.g. rotating electromechanical systems with Sommerfeld effect described in 1902 (Sommerfeld, 1902; Kiseleva et al., 2016)) and in systems with only one stable equilibrium (see, e.g. counterexamples (Leonov and Kuznetsov, 2011, 2013) to the Aizerman's (1949) and Kalman's (1957) conjectures on the monostability of nonlinear control systems (Aizerman, 1949; Kalman, 1957)). One of the first related problems is the second part of Hilbert's 16th problem (1900) (Hilbert, 1901-1902) on the number and mutual disposition of limit cycles in two-dimensional polynomial systems, where nested limit cycles (a special case of multistability and coexistence of attractors) exhibit hidden periodic oscillations (see, e.g., (Bautin, 1939; Kuznetsov et al., 2013; Leonov and Kuznetsov, 2013)).

The *classification of attractors as being hidden or self-excited* was introduced by G. Leonov and N. Kuznetsov in connection with the discovery of the first hidden Chua attractor (Leonov and Kuznetsov, 2009; Kuznetsov et al., 2010; Leonov et al., 2011; Bragin et al., 2011; Leonov et al., 2012; Kuznetsov et al., 2013; Leonov and Kuznetsov, 2013; Leonov et al., 2015) and has captured attention of scientists from around the world (see, e.g. (Burkin and Khien, 2014; Li and Sprott, 2014; Chen, 2015; Saha et al., 2015; Feng and Pan, 2017; Zhusubaliyev et al., 2015; Danca, 2016; Kuznetsov et al., 2015a; Chen et al., 2015; Pham et al., 2014; Ojoniyi and Njah, 2016; Rocha and Medrano-T, 2016; Borah and Roy, 2017; Danca et al., 2017; Wei et al., 2016; Pham et al., 2016; Jafari et al., 2016; Dudkowski et al., 2016; Singh and Roy, 2017; Zhang et al., 2017; Messias and Reinol, 2017; Brzeski et al., 2017; Wei et

al., 2017; Chaudhuri and Prasad, 2014; Jiang et al., 2016; Volos et al., 2017)).

Further study of the hidden Chua attractors and their observation in physical experiments can be found, e.g., in (Li et al., 2014; Chen et al., 2015; Bao et al., 2015; Chen et al., 2015a,b; Zelinka, 2016; Bao et al., 2016; Menacer et al., 2016; Chen et al., 2017; Hlavacka and Guzan, 2017). The synchronization of Chua circuits with hidden attractors is discussed, e.g. in (Kuznetsov and Leonov, 2014; Kuznetsov et al., 2016; Kiseleva et al., 2017). Some recent results on various modifications of Chua circuit can be found in (Rocha and Medrano-T, 2015; Bao et al., 2015; Semenov et al., 2015; Gribov et al., 2016; Kengne, 2017; Zhao et al., 2017; Chen et al., 2017; Corinto and Forti, 2017). Also hidden attractors were observed in other dynamical system (Kuznetsov et al., 2017; Danca and Kuznetsov, 2017a,b; Danca, 2017, 2016; Danca et al., 2017, 2016; Sharma et al., 2015a,b).

During the last five years different applications were found where presence of hidden attractors play the crucial role for operability of the system. Hidden periodic oscillations and hidden chaotic attractors have been studied in models such as phase-locked loops (Kuznetsov et al., 2015b, 2014), Costas loops (Best et al., 2015), drilling systems (Kiseleva et al., 2012) (Leonov et al., 2014), DC-DC converters (Zhusubaliyev and Mosekilde, 2015), aircraft control systems (Andrievsky et al., 2013a), launcher stabilization systems (Andrievsky et al., 2013b), convective fluid motion (Leonov et al., 2015a), and many others models. In the present work the role of hidden and self-excited attractors in the radiophysical (in application to the secure communication) and biophysical models is studied.

2.2 Application to secure communication

Nowadays, one of the areas of engineering where the theory of nonlinear oscillations and the theory of dynamical chaos get wide application is communications. In 2007, the method of direct chaotic communications (transfer by using chaotic pulses) was introduced into the Standard IEEE802.15.4a (Anon., 2007) ultra-broadband wireless personal communication. In 2012, ultra-wideband chaotic impulses were introduced in Standard IEEE 802.15.6- Wireless Body Area Networks - WBAN (Anon., 2012).

One of the promising directions of the practical applications of radiophysical generators of chaotic signals is to use them for secure communication systems (Cuomo and Oppenheim, 1993; Argyris et al., 2005; Kiani-B et al., 2009; Ponomarenko et al., 2013; Kaddoum, 2016; Xiong et al., 2016; Gutierrez and Gonzalez, 2016). This direction has been developing for quite a long time, however, there are a number of problems, preventing the use of these generators in applications. Such kind of problems can be concerned: the dependence of generation mode of chaotic signal from the parameters and initial conditions, sensitivity to noise, the problem of confidentiality of transmitted information, etc. In general all this problems are connected with different properties of chaotic attractors.

Most of the methods of secure communication based on synchronization of

chaos use primarily chaotic synchronization regimes (Pecora and Carroll, 1990) that imply a close identity of oscillators at opposite ends of the communication channel (See Fig. 3). The use of complete chaotic synchronization for secure information transmission implies the presence of at least two unidirectionally coupled identical chaotic oscillators.

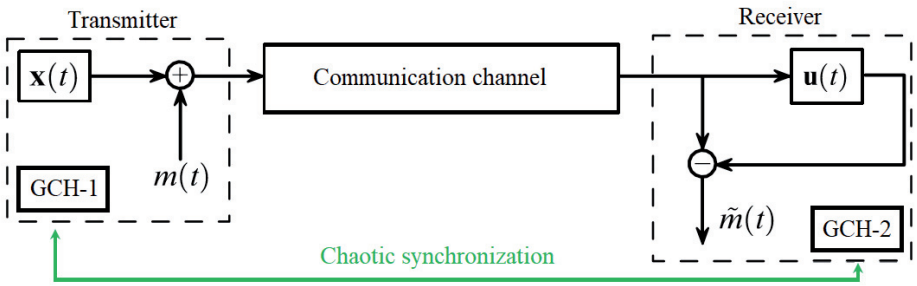

FIGURE 3 Principle scheme for secure communication system based on chaotic masking.

Chaotic masking is one of the first and simplest techniques for transmitting information in a secure fashion (Cuomo et al., 1993). A schematic diagram of this method is shown in Fig. 3. The information signal $m(t)$ is combined in the summator with a carrier generated by the chaotic system GCH-1 $x(t)$ for transmission through the communication channel. The received signal causes chaotic synchronization of the chaotic oscillator GCH-2 $u(t)$ in the receiver; as a result, the dynamics of the receiving oscillator becomes similar to that of the transmitting one. The detected signal $\tilde{m}(t)$ is produced after passing through the subtractor as a difference between the received signal and the synchronous response of chaotic oscillator in the receiver (see, e.g., Refs (Cuomo et al., 1993; Kiani-B et al., 2009)). Such a scheme of secure communication operates rather efficiently (in that it ensures high-quality transmission of information and its detection at the outlet) in the absence of noise in the channel (Downes, 1993). Given a noisy channel, the quality of transmitted information worsens considerably; this accounts for the high signal-to-noise ratio at which the system remains operative. Moreover, the introduction of a parameter mismatch between identical chaotic oscillators (located at the opposite ends of the communication channel) results in the appearance of additional desynchronization noises at the outlet and makes the transmission difficult to realize.

Then we can depict some problems of the secure communication system based on the chaotic synchronization connected with different dynamical properties of radiophysical generators of chaos (see Fig.4).

Hidden attractors were observed in different radiophysical generators, e.g. in mentioned above Chua circuit and in other generators, e.g., (Kuznetsov et al., 2015a). Nowadays, such kinds of chaotic electronic generators are used in various chaotic secure communication systems. If a generator has one global self-excited attractor, then it is easy enough to synchronize it. But generators can have several

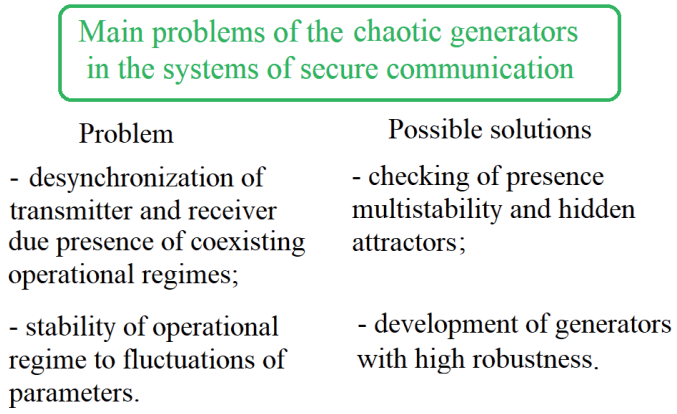

FIGURE 4 Problems of the scheme of the secure communications based on the chaotic synchronization.

coexisting attractors. In case when multistable attractors are hidden, it is difficult to find these attractors. Switching of operational regime on the hidden attractor can lead to desynchronization between receiver and transmitter, or inoperability of the whole system. Also additional attractors can appear in the systems with multistability as a result of interaction between coexisting attractors. In Sec.2.2.1. the problem of synchronization between two coupled Chua system is considered for two cases: when self-excited attractors and hidden attractors are observed in the subsystems.

One of the direction which can help to solve the second problem (see Fig. 4) is development of the generators of hyperbolic chaos [1], which provide stability of operational regime to variation of control parameters and initial conditions. Recently the radiophysical generators of hyperbolic chaos were realized in (Kuznetsov, 2005; Kuznetsov and Seleznev, 2006; Kuznetsov and Pikovsky, 2007). In the frame of this work such kind generators were studied. The main results in this direction are briefly described at the end of Sec.2.2.1.

2.2.1 Chua circuit: synchronization of hidden and self-excited attractors

The Chua circuit, invented in 1983 by Leon Chua (Matsumoto, 1984; Chua, 1992), is the simplest electronic circuit exhibiting chaos. In Fig. 5 Chua circuit with two resistors, one inductor, two capacitors (red) and one nonlinear resistor called Chua diode (green) is shown. The classical Chua circuit can be described by the following differential equations

$$\begin{aligned} \dot{x} &= \alpha(y - x) - \alpha f(x), \\ \dot{y} &= x - y + z, \\ \dot{z} &= -(\beta y + \gamma z), \end{aligned} \tag{4}$$

[1] See, e.g., (Anosov, 1967; Smale, 1967)

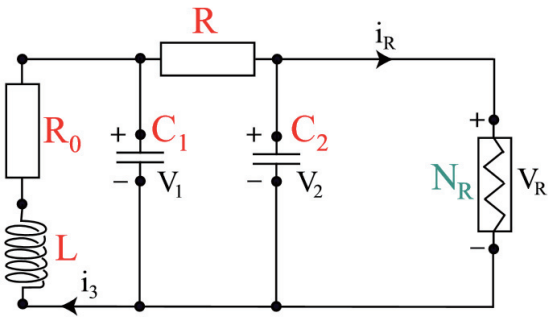

FIGURE 5 Scheme of Chua circuit

where $f(x) = m_1 x + \frac{1}{2}(m_0 - m_1)(|x+1| - |x-1|)$ is a piecewise linear voltage-current characteristic. Here x, y, z are dynamical variables; parameters m_0, m_1 characterize a piecewise linear characteristic of nonlinear element; parameters α, β, and γ characterize resistor, capacitors, and inductance, respectively. It is well known that model (4) is symmetric with respect to the origin and thereby it remains unchanged under the transformation $(x, y, z) \to (-x, -y, -z)$.

System (4) can be considered as a feedback control system in the Lur'e form

$$\dot{u} = Au + b\phi(c^* u), \quad u = (x, y, z) \in \mathbb{R}^3, \tag{5}$$

$$A = \begin{pmatrix} -\alpha(m_1+1) & \alpha & 0 \\ 1 & -1 & 1 \\ 0 & -\beta & -\gamma \end{pmatrix}, b = \begin{pmatrix} -\alpha \\ 0 \\ 0 \end{pmatrix}, c = \begin{pmatrix} 1 \\ 0 \\ 0 \end{pmatrix},$$

$\phi(x) = \frac{1}{2}(m_0 - m_1)(|x+1| - |x-1|)$.

The system (4) has tree equilibria: two symmetric equilibrium points $u_{\text{eq}}^{1,3}$ and one equilibrium in zero u_{eq}^2

$$u_{\text{eq}}^{1,3} = \pm(u_{\text{eq}}^x, u_{\text{eq}}^y, u_{\text{eq}}^z) = \pm\left(\frac{(\gamma+\beta)(m_0-m_1)}{\gamma m_1+\beta m_1+\beta}, \frac{\gamma(m_0-m_1)}{\gamma m_1+\beta m_1+\beta}, \frac{-\beta(m_0-m_1)}{\gamma m_1+\beta m_1+\beta}\right). \tag{6}$$

In **PI** the domains of the parameter plane (m_0, m_1), where exist hidden attractors in the Chua system (4), were defined [2]. In Fig.6 the chart of dynamical modes is shown. For each point in the parameter plane the dynamical regime was determined in Poincaré section by plane $z = 0$. In the right part of Fig.6 one can see the legends corresponding to the color palette and realizing dynamical regime. In fact, the chart in Fig.6 depends on the initial conditions. For the construction of this chart we take initial conditions on the surface of hidden attractor and use continuation method of changing initial condition by varying of controlling parameters. In Fig.6, line l_{H0} corresponds to the line of Hopf bifurcation, which happened with zero equilibrium point.

[2] In **PII** was discovered another domain in the parameter plane where new hidden attractors were observed.

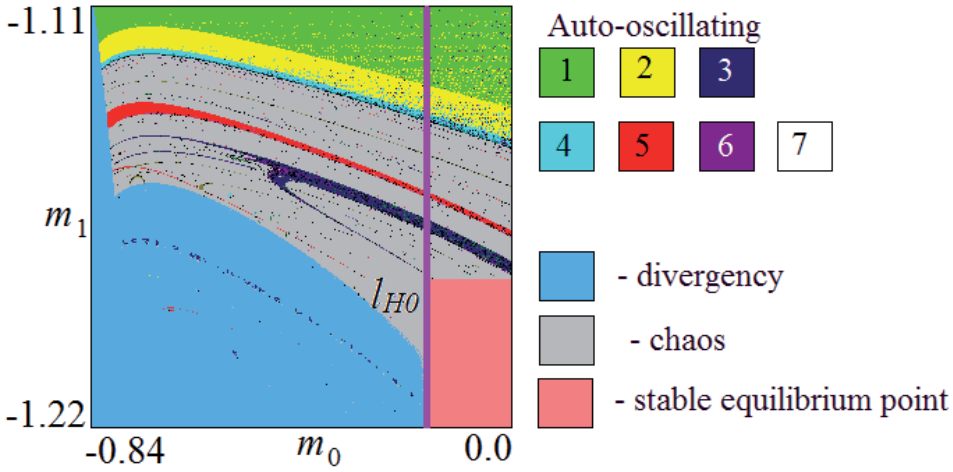

FIGURE 6 Chart of dynamical modes for the Chua system.

For $m_0 < l_{H0}$ ($l_{H0} \approx -0.1761$) in the phase space, there is a saddle-focus in zero and two saddle-foci corresponding to two symmetric equilibrium points (6). For $m_0 > -0.1761$ the zero equilibrium point becomes stable, but stability of symmetric saddle-foci does not change. Twin chaotic attractors exist for these parameters. In Fig. 6 one can see the development of chaotic dynamics. There is stable limit cycle at $m_1 = -1.11$ (green color on the chart). With decrease in the parameter m_1, bifurcation of symmetry broken happens. Then two symmetric limit cycles undergo cascade of period doubling bifurcations with transition to chaos. As a result, two symmetric twin chaotic attractors occur. This scenario develops in both cases: before and after the Hopf bifurcation for the zero equilibrium point. In the case of stable equilibrium point $m_0 < -0.1761$, we can talk about the existence of twin hidden attractors. If $m_0 > -0.1761$ then attractors are self-excited. Fig.7 a) shows a two-dimensional section of basins of attraction for different attractors at $m_0 = -0.121$, $m_1 = -1.143$. Blue color in Fig.7 a) corresponds to the regime of divergency, when phase trajectories get unlimited growing to infinity. It determines the boundary for the basin of attraction in the phase space. Light gray color corresponds to the existence of the twin chaotic attractors, different symmetric attractors are not distinguished in the basin (both attractors are marked by gray color). Red color corresponds to the area of the stable zero equilibrium point. Two-dimensional projections of twin hidden attractors (A_H^1, A_H^2), projections of the saddle-foci (EP_{S1}, EP_{S2}) and the zero equilibrium point (EP_0) are also shown in Fig.7 a). For the chosen parameters m_0 and m_1, the eigenvalues for the symmetric equilibriums points are: $\lambda_1 = 2.168$, $\lambda_{2,3} = -0.986 \pm 2.387i$, and for the zero equilibrium are: $\lambda_1 = -8.34$, $\lambda_{2,3} = -0.024 \pm 3.259i$. If we change parameter m_0, fix it, for example, $m_0 = -0.2$, then the zero equilibrium point becomes unstable saddle-focus. For this parameter value, eigenvalues for the zero equilibrium point equal $\lambda_1 = -7.734$, $\lambda_{2,3} = 0.0044 \pm 3.229i$, for the symmetric equilibrium points they are the same. In this case, self-excited twin chaotic attrac-

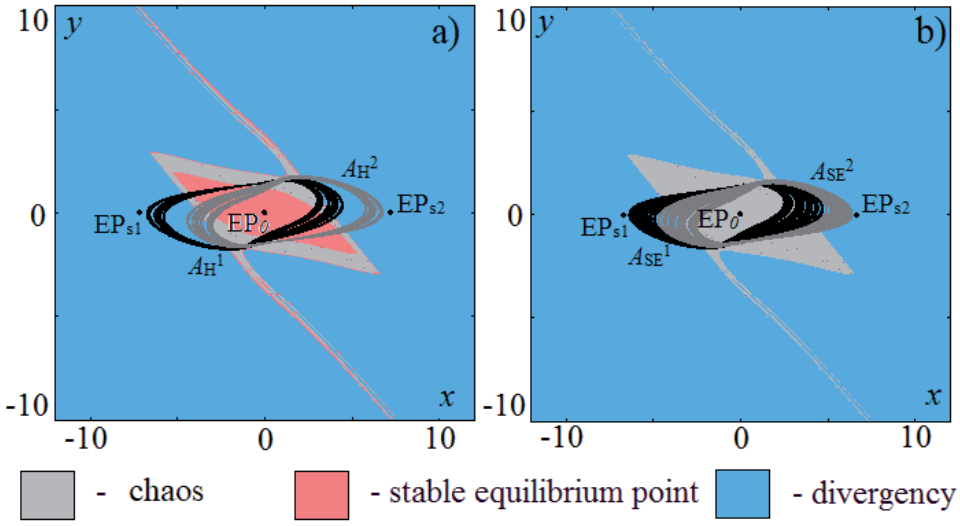

FIGURE 7 Basins of attraction and two-dimensional projection of chaotic attractors and equilibrium points for the Chua system.

tors are reached while starting from the vicinity of the zero equilibrium. These attractors are shown in Fig.7 b) (A^1_{SE}, A^2_{SE}) with the basins of attraction.

Following **PIII** let us turn to the study of synchronization between two Chua systems linearly coupled through the second equation by the y variables. The system of two coupled oscillators may be written in the form:

$$\begin{aligned}
\dot{x_1} &= \alpha(y_1 - x_1) - \alpha f(x_1),\\
\dot{y_1} &= x_1 - y_1 + z_1 + M_C(y_2 - y_1),\\
\dot{z_1} &= -(\beta y_1 + \gamma z_1),\\
\dot{x_2} &= \alpha(y_2 - x_2) - \alpha f(x_2),\\
\dot{y_2} &= x_2 - y_2 + z_2 + M_C(y_1 - y_2),\\
\dot{z_2} &= -(\beta y_2 + \gamma z_2).
\end{aligned} \tag{7}$$

Here M_C is the coupling strength. We analyze dynamics of the coupled system (7) by using the bifurcation diagrams dependence on the coupling parameter M_C.

Firstly, the dynamics of self-excited attractors is observed. The parameters of each individual model are chosen as in Fig.7 b) ($m_0 = -0.2$, $m_1 = -1.143$). We take different initial conditions in our numerical experiments and consider dynamics of the coupled system (7) at variation of the coupling strength M_C. We choose two kinds of initial conditions which are critical for detecting hidden and self-excited attractors. Firstly, we take the initial conditions on the surface of chaotic attractors. This situation is similar for both self-excited and hidden attractors. In Fig.8 a) the bifurcation diagram for case ($x^1_0 = 2.36$, $y^1_0 = 0.97$, $z^1_0 = -3.96$), ($x^2_0 = 2.361$, $y^2_0 = 0.971$, $z^2_0 = -3.961$) is shown. In order to see different possible regimes, we construct bifurcation diagrams using continuation

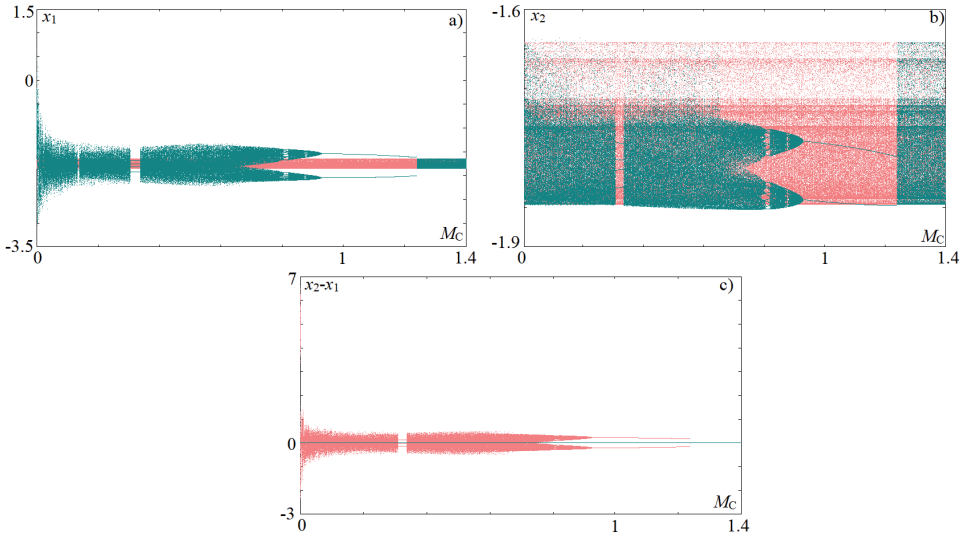

FIGURE 8 Bifurcation diagrams for the system of two coupled Chua models in the regime of self-excited attractors.

method of changing initial conditions by the varying parameter M_C. So the initial condition for each new value of the parameter is chosen as the final value in the previous step of integration. Red and green colors in Fig.8 correspond to different directions of the parameter variation: green from left to right, red from right to left. Fig.8 a) and b) show the dependences of the x-variable in the first and the second oscillators, respectively. Fig. 8 c) shows the difference between variables $x_2 - x_1$. As one can see in Fig.8 a) at small coupling starting from the chaotic attractors in individual oscillators, we can reach chaotic nonsynchronous oscillations in the coupled system. At some value of the parameter M_C, one can see windows of periodicity of period-2 and period-4. At $M_C \approx 1.2467$, a complete synchronization between oscillators takes place. The complete synchronization regime corresponds to regime when difference between variables of different oscillators is equal to zero (see Fig. 8 c)). Then we change direction of the parameter variation. Now one can see that synchronous regime co-exists with the chaotic non-synchronous regime.

For another initial conditions when one of the oscillators is in the vicinity of the zero equilibrium point ($x_0^1 = 0.01$, $y_0^1 = 0.00001$, $z_0^1 = 0.01$) and another is left on the surface of chaotic self-excited attractors ($x_0^2 = 2.361$, $y_0^2 = 0.971$, $z_0^2 = -3.961$).

The chaotic attractors are reached if we start near the equilibrium point for a self-excited attractor in an individual oscillator. Consequently, bifurcation diagram for coupled models (7) is exactly the same if we start near the zero equilibrium under such initial conditions for self-excited attractors.

Now let us turn to the case of the synchronization between hidden attractors. We fix parameters $m_0 = -0.121$, $m_1 = -1.143$ (phase portraits for these parameters are shown in Fig.6 b)) and consider the same two cases, when 1) the ini-

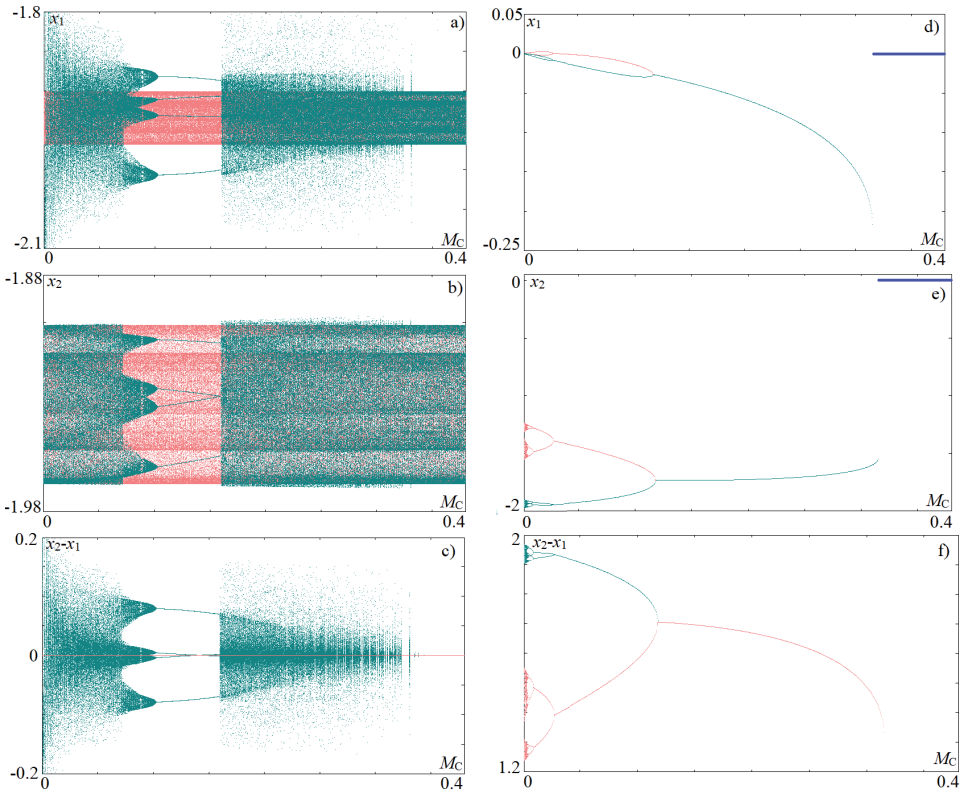

FIGURE 9 Bifurcation diagrams for the system of two coupled Chua models in the regime of hidden attractors.

tial conditions are chosen on the surface of chaotic attractors ($x_0^1 = 2.36$, $y_0^1 = 0.2$, $z_0^1 = -6.5$), ($x_0^2 = 2.361$, $y_0^2 = 0.21$, $z_0^2 = -6.51$); and 2) in the vicinity of the zero equilibrium point ($x_0^1 = 0.01$, $y_0^1 = -0.00001$, $z_0^1 = -0.01$) (this point is stable for hidden attractor and trajectories in the vicinity of equilibrium go into zero equilibrium point) and on the surface of hidden attractor ($x_0^2 = 2.361$, $y_0^2 = 0.21$, $z_0^2 = -6.51$). For this case of synchronization between hidden attractors, different choice of initial conditions leads to different results.

Fig. 9 shows bifurcation diagrams for hidden attractors. Figs. 9 a), b), c) correspond to initial conditions on the surface of chaotic hidden attractors. As one can see for this initial conditions, structure of the bifurcation diagrams is very similar to those in case of self-excited attractors. Bifurcation diagrams for small coupling demonstrate chaotic dynamics. With increase in the coupling strength, there is window of periodicity with period-4. At $M_C \approx 0.296$ we can observe complete mutual synchronization between oscillators (difference between variables of oscillators is equal to zero). For self-excited attractors with large coupling strength, synchronization is only observed, complex dynamics is suppressed. Fig. 9 c) illustrates the difference between dynamical variables, one can see that it can be equal to zero. It means that the complete synchronization is observed in the system.

If we change the initial conditions and fix one of them in the vicinity of the zero equilibrium point, the bifurcation diagrams undergo serious changes (see Figs. 9 d), e), f)). Stable equilibrium point is observed at large coupling (stabilization occurs at $M_C \approx 0.316$, blue line in Figs. 9 d), e)). Then it becomes unstable and we can see birth of limit cycle, which is divided into two limit cycles as a result of broken symmetry bifurcation. Then each of the cycles undergoes cascade of period doubling bifurcations. Thus, a complete synchronization can not be observed for chosen initial conditions. Also, the chaotic dynamics is destroyed in this case.

Thus, dynamics of two coupled Chua oscillators is considered with interaction of hidden and self-excited attractors. The possibility of complete synchronization for hidden and self-excited attractors is revealed. Stabilization of zero equilibrium point is discovered for interacting hidden attractors. Such kind of dynamics can lead to inoperability in the communication system.

Another aspect of dynamical behavior of radiophysics generators is considered in **PIV - PVII**. Generalized model for generator of chaos with property of robustness in respect to changing of the controlling parameters and initial conditions is suggested in **PIV**. The birth scenario is studied for such kind of behavior. Non-autonomous generator of chaos is suggested in **PV** and realized in an experiment. Another generator with chaotic dynamics is studied in **PVI**, where the formation of chaotic dynamics with several incommensurate frequencies and more wide power spectrum is described.

2.3 Application to biological models

Multistability, or coexistence of dynamical regimes, is a characteristic feature of many types of biological cells, neural networks, and other forms of oscillatory biophysical systems (Laurent and Kellershohn, 1999; Pmerening et al., 2003; Ozbudak et al., 2004; Koseska et al., 2009; Kelso, 2012; Pisarchik and Feudel, 2014; Wells et al., 2015). This feature is particularly significant in connection with the study of interacting ensembles of many, nearly identical subsystems. It is well-known, for instance, that a variety of unusual phenomena that emerge in ensembles of coupled oscillators can lead to major reconstructions of an oscillator population, or to its total collapse. It is broadly accepted, for instance, that synchronization plays an important role in the pathogenesis of neurological diseases such as Parkinson's disease and essential tremor (Buzsáki and Draguhn, 2004; Milton, 2010) and, more specifically, that Parkinson's disease is associated with asynchronous pacemaker activity involving a population of many thousands of neurons in the basal ganglia (Bergman et al., 1998; Sarnthein J. and D., 2003).

It is well-known that the electrical activity of pancreatic beta-cells and other biological cells relies on a number of different types of voltage- and ligand-gated ion channels that are permeable to inorganic ions such as sodium, potassium, chloride, and calcium. Thus, the dynamics of a cell can be described from the point of view of voltages and currents passing through membrane, this principle is called Hodgkin-Huxley formalism (Hodgkin and Huxley, 1952). Increasing evidence suggests that ion channels not only regulate membrane potential, ion homeostasis, and electrical signaling of these cells but also play an important role in cell proliferation, migration, apoptosis and differentiation. Recently, the role of ion channels in different oncogenic processes was demonstrated (Monteith et al., 2007) (Huang and Jan, 2014) (Litan and Langhans, 2015).

In **VII** we introduce a modified version of the Sherman pancreatic beta-cell model obtained by introducing a new type of potassium-like ion channel with a characteristic set of channel parameters selected in accordance with a standard Hodgkin-Huxley formalism. The suggested modification is designed to be local and small enough to allow for the existence of an attracting state inside the regime of stable bursting dynamics. This provides for the presence of multistability in the modified beta-cell model and, at the same time, serves as an example of a biophysical system that allows for the coexistence of a stable equilibrium point with large amplitude bursting. Let us consider it in detail.

2.3.1 Simplified pancreatic beta-cell model

As the starting point for our analysis, let us use the following simplified beta-cell model as suggested by Sherman et al. (Sherman et al., 1988):

$$\begin{aligned} &\tau\dot{V} = -I_{Ca}(V) - I_K(V,n) - I_S(V,S), \\ &\tau\dot{n} = \sigma(n_\infty(V) - n), \\ &\tau_S\dot{S} = S_\infty(S) - S. \end{aligned} \tag{8}$$

TABLE 1 Parameters of simplified beta-cell model.

τ	=	0.02 *sec*	τ_S	=	35 *sec*	σ	=	0.93
g_{Ca}	=	3.6	g_K	=	10.0	g_S	=	4.0
V_{Ca}	=	25.0 mV	V_K	=	-75.0 mV			
θ_m	=	12.0 mV	θ_n	=	5.6 mV	θ_S	=	10.0 mV
V_m	=	-20.0 mV	V_n	=	-16.0 mV	V_S	=	-35.0 mV

Here, V represents the membrane potential, n may be interpreted as the opening probability of the potassium channels, and S accounts for the presence of a slow variable in the system. The variables $I_{Ca}(V)$ and $I_K(V,n)$ are the calcium and potassium currents, g_{Ca} = 3.6 and g_K = 10.0 are the associated conductances, and V_{Ca} = 25 mV and V_K = - 75 mV are the respective Nernst (or reversal) potentials. Together with $I_S(V,S)$, the slow calcium current I_{Ca} and the potassium current I_K define the three transmembrane currents of our basic system:

$$I_{Ca}(V) = g_{Ca} m_\infty(V)(V - V_{Ca}), \tag{9}$$

$$I_K(V,n) = g_K n(V - V_K), \tag{10}$$

$$I_S(V,S) = g_S S(V - V_K), \tag{11}$$

with the gating variables for m, n and S representing the opening probabilities of the fast and slow potassium channels:

$$\omega_\infty(V) = \frac{1}{1 + \exp\frac{V_\omega - V}{\theta_\omega}}, \omega = m, n, S. \tag{12}$$

Table 1 below lists the parameter values corresponding to the observed bursting dynamics for model (8). In principle, the characteristic time constant for the membrane potential is determined by the membrane capacity and the corresponding electrical conductance. In accordance with the original formulation of the model (Sherman et al., 1988) there is no electrical capacitance in Eq. (8), and the conductances are all dimensionless. To eliminate the dependence on cell size, the conductances have thus been scaled relative to some appropriate conductance. With time constants of τ = 0.02 *sec* and τ_S = 35 *sec*, the ratio $k_S = \frac{\tau}{\tau_S}$ is quite small, and the model is numerically stiff.

Figs. 10 a) and b) show typical examples of the time series obtained for the fast variable V and slow variable S. Calcium functions as an essential part of a double-sided feedback loop that controls the bursting process and involves modulations of both electrical activity and hormonal secretion (Chay and Keizer, 1983). Calcium removal leads to depolarization and controls the silent phase through deactivation of calcium activated potassium channels. This depolarization activates both the voltage-gated calcium channels and the Hodgkin-Huxley like potassium channels until a renewed influx of calcium takes place and the spiking dynamics is initiated again.

Following (Izhikevich, 2000), the bursting attractor in the cell model (8) is born through simultaneous Hopf and saddle-node bifurcations. The parameter

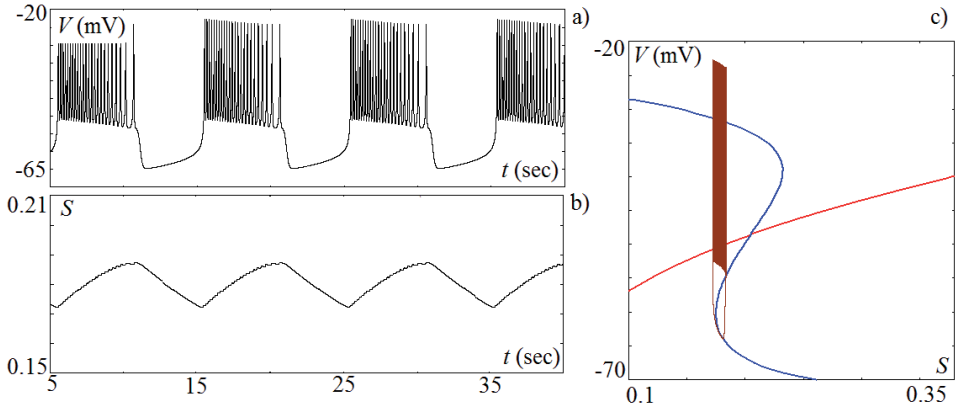

FIGURE 10 Time series of the a) fast and b) slow variables; c) fast (blue) and slow (red) manifolds together with a two-dimensional projection of phase portrait for the Sherman model.

V_S only controls the slow manifold, and with increasing values of this parameter, the slow manifold moves upwards relatively to the fast manifold. The bursting attractor is born in the vicinity of the equilibrium point, but after the bifurcation that occurs for increasing values of V_S, the equilibrium point moves far away from the bursting attractor.

2.3.2 Modification of pancreatic beta-cell model

An interesting feature of the biological bursting system is the large variation one often observes for the bursting period. We have already referred to this variability in relation to the discussion of slow and fast bursters. Besides variations associated with differences in clusters size, the most obvious reason for variations to occur is inhomogeneity in the cell clusters. This has inspired a number of authors (Chay and Keizer, 1983; Sherman et al., 1988) to propose the so-called phantom burster model that allows fast and slow bursting to occur simultaneously, i.e. by replacing the original equation for the slow potassium current with a set of two (or more) parallel potassium currents. The idea has been to use a multiple degree-of-freedom approach to generate a broader range of interacting bursting oscillators while maintaining the overall structure of the system. If the conductance is large, the bursting that results from this feedback will be fast. On the other hand, if the conductance is small, this feedback has little influence, and the bursting that results from it will be slow. In this way, it has been possible to account for a range of biomedical phenomena, including the ubiquitous tri-phase response to a step increase in glucose, the response to perturbations of intra-cellular Ca^{2+} stores, and different intracellular functions of potassium (Sherman et al., 1988; Heart and Smith, 2007).

Figure 10 c) shows the two-dimensional projection of the phase portrait (brown color) together with the fast and slow manifolds for V_S = -35 mV. For

these parameters, the (periodic) trajectories do not intersect in the neighborhood of the equilibrium point, but the bursting state terminates in a homoclinic bifurcation as the trajectory hits the slow manifold at some other point. Hence, it appears possible to reorganize the conditions around the equilibrium point in such a way that this point is stabilized while the bursting trajectory continues to exist. Between the stable equilibrium point and the bursting state we expect to find some rejecting structure and, under these conditions, the bursting state represents a hidden attractor. To achieve stabilization of the equilibrium point we propose a form of the voltage-dependent potassium current that varies strongly with the membrane potential right near this equilibrium point and, hence, its stability can exist without affecting the global flow in the model. The suggested form of the potassium current is specified by the equation:

$$I_{K2}(V) = g_{K2} p_\infty (V - V_K), \tag{13}$$

where the function

$$p_\infty(V) = \frac{1}{\exp \frac{V - V_p}{\theta_p} + \exp \frac{V_p - V}{\theta_p}}. \tag{14}$$

represents the opening probability for the suggested new type of potassium channel. The same probability functions for the normal channels are represented by sigmoidal function (12) (see Fig. 11 a), b)). When the membrane voltage reaches a threshold voltage, the potassium channel will open with probability $n_\infty(V)$=1.0. For the pathological channels, the opening function is never equal to 1.0. When the membrane voltage reaches a threshold voltage, the opening probability will equal only 0.5 (this probability function is presented on Fig. 11 c)). From the physiological point of view, such situation can be interpreted as blocking of potassium channel, or inactivation.

Thus, modified beta-cell model has form:

$$\begin{aligned} \tau \dot{V} &= -I_{Ca}(V) - I_K(V, n) - I_{K2}(V) - I_S(V, S), \\ \tau \dot{n} &= \sigma(n_\infty(V) - n), \\ \tau_S \dot{S} &= S_\infty(S) - S. \end{aligned} \tag{15}$$

with $I_{K2}(V)$ and $p_\infty(V)$ as given by (13) and (14).

All the parameters of the original model (8) still apply. However, the modified model has three additional parameters g_{K2}, V_p, θ_p that can be used to characterize the new ion channel. Fig. 11 e) shows the null-clines of the modified model (15). These curves illustrate how one can introduce new types of ion channels to the model, each leading to appearance of new pairs of extreme points (minima and maxima) on the fast manifold without affecting the slow manifold. By changing parameter V_p one can determine the extreme points or the range of voltage where the system is most sensitive. The parameter θ_p=1 controls the voltage range in which the new ion channel is active regarding the membrane potential V. In this situation, the equilibrium point can be stable, but bursting dynamics can develop on the same branch of the manifold as in the original model (8). Figure 11 d) illustrates the variation of Ca^{2+}-current (red) and of the sum of the

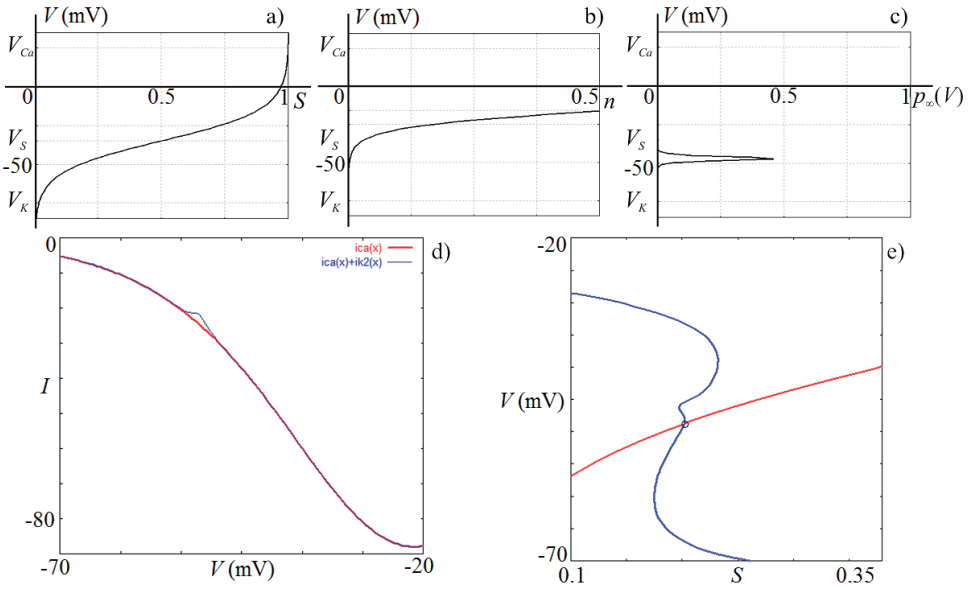

FIGURE 11 Dependence of the membrane potential on the different ions, a) calcium channel; b) potassium channel; c) probability function of new ion channel; d) current of Ca^{2+} and sum of current Ca^{2+} and current of new channel; e) fast and slow manifolds of the modified beta-cell model.

Ca^{2+}-currents and the current associated with new ion channel. One can see, however, that changing the current can only be local, very small, and without major changes of the system. Figure 11 e) shows the fast (blue) and slow (red) manifolds of the modified beta-cell model.

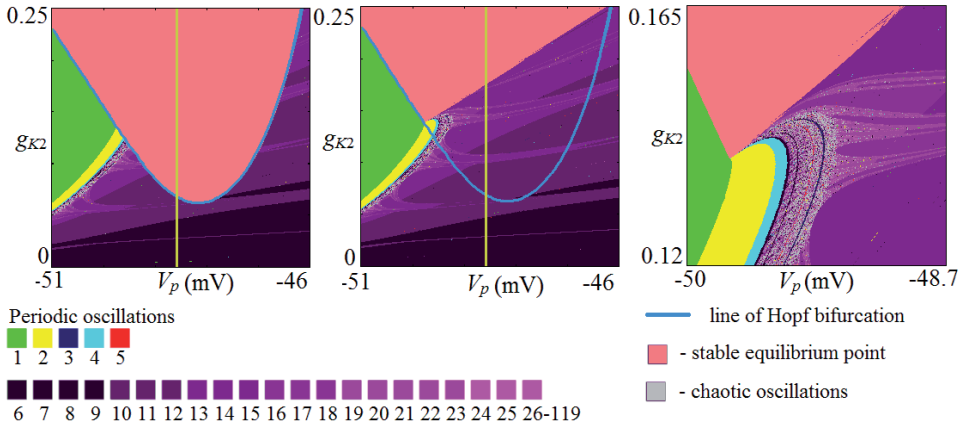

FIGURE 12 Charts of dynamical modes for the modified model for different initial conditions.

Let us now consider the mode distribution across a plane scanned by the parameters V_p and g_{K2} that characterize the new ion channel in the model. Fig.12

shows charts of dynamical modes for the modified system (15) with different initial conditions and different magnifications. These charts were constructed in the following way: using a standard Poincaré section technique, the parameter plane was scanned in small steps. The dynamical state was determined by using a sufficiently long transient for each point in the Poincaré section defined by n = 0.02. The distribution of points in the Poincaré section and the corresponding number/colors in Fig. 12 are shown below. If the number of points exceeded 120, the corresponding region was considered to represent a chaotic mode. Charts a) and b) were constructed with different initial conditions. Chart c) is a magnified part of chart b). In Figs. 12 a) and b) the line of Hopf bifurcation of the equilibrium point is indicated by blue color. This curve was obtained by the use of the software package XPP AUTO.

For control parameters we have used the parameter g_{K2} that characterizes the conductance of the new ion channel and the parameter V_p, that determines the point on the fast-slow manifold where the transition occurs. By varying V_p one can move the fast manifold relatively to the slow manifold, and in this way can shift equilibrium point. In the original model, the unstable equilibrium point falls in the point $EP_0(V_0, n_0, S_0)$ = (-48.578, 0.0029663, 0.2046). In the following, we will vary parameter V_p in the vicinity of V_0. In Fig. 12, the vertical green line is the line that corresponds to line $V_p = V_0$.

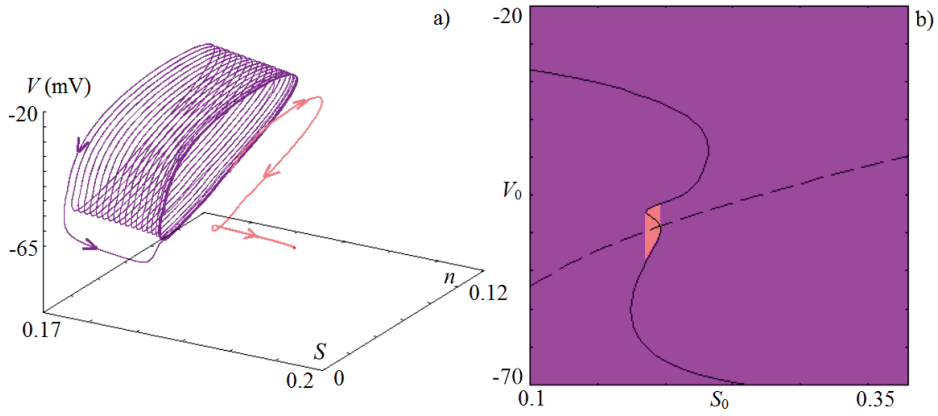

FIGURE 13 Co-existence of the bursting dynamics and the stable equilibrium point: a) three-dimensional phase portraits; b) basin of attraction for co-existing attractors.

Let us now focus on the coexistent regimes of bursting and of silence (stable equilibrium) as they appear in our modified beta-cell model. In the charts of dynamical modes, the red area, representing a region of stable equilibrium, and the purple area, representing a region bursting dynamics, overlap. Hence, depending on the initial conditions, either the stable equilibrium point or the bursting oscillator may be the final state.

In Fig. 13 a) we have plotted the trajectories for a pair of coexisting attracting states in three-dimensional phase space. The purple trajectory represents the

stable bursting attractor and the pink curve represents a phase space trajectory that goes to the silent regime. Hence, we conclude that the bursting oscillator (for a range of initial conditions) can operate with a stable equilibrium state in its middle.

Fig. 13 b) shows a two-dimensional section of the basin of attraction for the attractors depicted in Fig. 13 a). The section covers the (S_0, V_0) plane while the third variable n_0 was fixed near the equilibrium point at n_0=0.00275. The dynamical regimes were obtained by Poincaré section at the plane n_0=0.02. Red color represents initial conditions that lead to the stable equilibrium point and purple represents initial conditions that lead to the bursting state. The black curves on Fig.13 b) represent the lines of the fast and slow manifolds. In this way we can demonstrate that the basin of attraction for the bursting oscillator surrounds a three-dimensional region in which the dynamics is controlled by the stable equilibrium point. This island of stable equilibrium dynamics is located between two extrema of null-clines. This boundary is defined by the unstable limit cycle which occurs as a result of introducing the new ion channel via subcritical Hopf bifurcation. If we iterate modified model (15) starting from the vicinity of equilibrium we can not reach bursting attractor; this means that bursting attractor in this case is a hidden attractor.

3 CONCLUSIONS

This dissertation is devoted to the investigation of hidden and self-excited attractors in different models which have applications in radiophysics and biophysics.

The present work considers features of radiophysical generators, which can be used for systems of secure communication based on the dynamical chaos. Using the Chua circuit as an example, the problem of synchronization between two coupled generators is investigated in case when the realized regimes represent hidden and self-excited attractors in the system. It is shown that desynchronization of coupled subsystems is possible in case of hidden attractors under certain initial conditions, which can lead the system of secure communication to an inoperative state. Alternative radiophysical generators with self-excited attractors are also proposed. For these generators, dynamical chaos is stable to the variation of parameters, initial conditions and fluctuations.

The present work proposes a modification of simplified beta-cell based on the Hodgkin-Huxley formalism model to demonstrate the coexistence of bursting and silent regimes. For the considered modification of the cell model, this type of bistability occurs at the introduction of an additional voltage-dependent potassium current that is activated in the region around the original unstable equilibrium point. The mechanism of bistability is associated with the birth of an unstable cycle as a result of the subcritical Hopf-bifurcation inside the bursting attractor. From the point of view of hidden attractors, the bursting regime is a hidden attractor that can not be reached from initial conditions in the vicinity of the equilibrium point. This model can be used to describe the formation of various pathological states of cells, for example, such as cancer cells.

YHTEENVETO (FINNISH SUMMARY)

Piilevät ja itseherätteiset attraktorit radiofysiikan ja biofysiikan malleissa

Tämä väitöstyö tutkii piilevän ja itseherätteisen kaaoksen syntymistä erilaisissa radiofysiikan ja biofysiikan sovelluksissa. Tutkielma käsittelee radiofysikaalisten generaattorien piirteitä joita voidaan käyttää dynaamiseen kaaokseen perustuvan systeemien turvalliseen viestintään. Kahden kytketyn, Chuan piirien avulla mallinnetun, kaoottisen generaattorin synkronisointia tarkastellaan tapauksessa, jossa järjestelmän toiminta-alueet sisältävät sekä piilotettuja että itseherätteisiä attraktoreita. Tutkimuksessa osoitetaan, että piilotetut attraktorit on tietyin ehdoin mahdollista desynkronoida tavalla, joka voi mahdollistaa turvallisen kommunikaation osajärjestelmien välissä. Lisäksi työssä esitellään vaihtoehtoisia itseherätteisiä kaaos-generaattoreita, joilla dynaaminen kaaos on stabiili parametrien muutoksille ja alkuehdoille.

Biofysiikan osuudessa esitetään modifikaatio yksinkertaistettuun, Hodgkin-Huxley, beta-solumalliin. Muokatussa solumallissa ns. hiljaiset alueet ja kaoottiset alueet voivat esiintyä samanaikaisesti. Biofysikaalisesti tämä kaksoisstabiilisuuden mahdollistava mekanismi perustuu, jänniteriippuvaan Kaliumvuohon, joka aktivoituu epästabiilin tasa-painopisteen ympärille. Matemaattisesti kaksoisstabiiliuden mekanismi yhdistyy epästabiilin syklin syntymiseen sub-kriittisessä Hopf-bifurkaatiossa attraktorin sisällä. Piilotettujen attraktorien näkökulmasta, kaootista aluetta ei voida yhdistää epästabiiliin tasapainopisteeseen. Laadullisesti mallia voidaan käyttää kuvaamaan solujen tilan patologista muutosta, kuten esimerkiksi terveen solun muuttumista syöpäsoluksi.

REFERENCES

Aizerman, M. A. 1949. On a problem concerning the stability in the large of dynamical systems. Uspekhi Mat. Nauk (in Russian) 4, 187-188.

Andrievsky, B., Kuznetsov, N., Leonov, G. & Pogromsky, A. 2013a. Hidden oscillations in aircraft flight control system with input saturation. IFAC Proceedings Volumes 46 (12), 75-79. doi:10.3182/20130703-3-FR-4039.00026.

Andrievsky, B., Kuznetsov, N., Leonov, G. & Seledzhi, S. 2013b. Hidden oscillations in stabilization system of flexible launcher with saturating actuators. IFAC Proceedings Volumes 46 (19), 37-41. doi:10.3182/20130902-5-DE-2040.00040.

Anon. 2007. IEEE 802.15.4a-2007 IEEE Standard for Information technology– Local and metropolitan area networks– Specific requirements– Part 15.4: Wireless Medium Access Control (MAC) and Physical Layer (PHY) Specifications for Low-Rate Wireless Personal Area Networks (WPANs): Amendment 1: Add Alternate PHYs.

Anon. 2012. IEEE 802.15.6-2012 IEEE Standard for Local and metropolitan area networks - Part 15.6: Wireless Body Area Networks.

Anosov, D. 1967. Geodesic flows on closed riemannian manifolds of negative curvature. Trudy Matematicheskogo Instituta Imeni VA Steklova 90, 3-210.

Argyris, A., Syvridis, D., Larger, L., Annovazzi-Lodi, V., Colet, P., Fischer, I., Garcéa-Ojalvo, J., Mirasso, C., Pesquera, L. & Shore, K. 2005. Chaos-based communications at high bit rates using commercial fibre-optic links. Nature 437, 343-346.

Babin, A. V. & Vishik, M. I. 1992. Attractors of Evolution Equations. Amsterdam: North-Holland.

Bao, B., Jiang, P., Wu, H. & Hu, F. 2015. Complex transient dynamics in periodically forced memristive Chua's circuit. Nonlinear Dynamics 79, 2333-2343.

Bao, B. C., Li, Q. D., Wang, N. & Xu, Q. 2016. Multistability in Chua's circuit with two stable node-foci. Chaos: An Interdisciplinary Journal of Nonlinear Science 26 (4). (art. num. 043111).

Bao, B., Hu, F., Chen, M., Xu, Q. & Yu, Y. 2015. Self-excited and hidden attractors found simultaneously in a modified Chua's circuit. International Journal of Bifurcation and Chaos 25 (05). doi:10.1142/S0218127415500753. (art. num. 1550075).

Bautin, N. N. 1939. On the number of limit cycles generated on varying the coefficients from a focus or centre type equilibrium state. Doklady Akademii Nauk SSSR (in Russian) 24 (7), 668-671.

Bergman, H., Feingold, A., Nini, A., Raz, A., Slovin, H., Abeles, M., & Vaadia, E. 1998. Physiological aspects of information processing in the basal ganglia of normal and parkinsonian primates. Trends in neurosciences 21, 32-38.

Best, R., Kuznetsov, N., Kuznetsova, O., Leonov, G., Yuldashev, M. & Yuldashev, R. 2015. A short survey on nonlinear models of the classic Costas loop: rigorous derivation and limitations of the classic analysis. In Proceedings of the American Control Conference. IEEE, 1296–1302. doi:10.1109/ACC.2015.7170912. (art. num. 7170912).

Boichenko, V. A., Leonov, G. A. & Reitmann, V. 2005. Dimension Theory for Ordinary Differential Equations. Stuttgart: Teubner.

Borah, M. & Roy, B. K. 2017. Hidden attractor dynamics of a novel non-equilibrium fractional-order chaotic system and its synchronisation control. In 2017 Indian Control Conference (ICC), 450-455.

Bragin, V., Vagaitsev, V., Kuznetsov, N. & Leonov, G. 2011. Algorithms for finding hidden oscillations in nonlinear systems. The Aizerman and Kalman conjectures and Chua's circuits. Journal of Computer and Systems Sciences International 50 (4), 511-543. doi:10.1134/S106423071104006X.

Brzeski, P., Wojewoda, J., Kapitaniak, T., Kurths, J. & Perlikowski, P. 2017. Sample-based approach can outperform the classical dynamical analysis - experimental confirmation of the basin stability method. Scientific Reports 7. (art. num. 6121).

Burkin, I. & Khien, N. 2014. Analytical-numerical methods of finding hidden oscillations in multidimensional dynamical systems. Differential Equations 50 (13), 1695-1717.

Buzsáki, G. & Draguhn, A. 2004. Neuronal oscillations in cortical networks. Scienc 304, 1926-1929.

Chaudhuri, U. & Prasad, A. 2014. Complicated basins and the phenomenon of amplitude death in coupled hidden attractors. Physics Letters A 378 (9), 713-718.

Chay, T. & Keizer, J. 1983. Minimal model for membrane oscillations in the pancreatic beta-cell. Biophysical journal 42, 181-189.

Chen, G., Kuznetsov, N., Leonov, G. & Mokaev, T. 2017. Hidden attractors on one path: Glukhovsky-Dolzhansky, Lorenz, and Rabinovich systems. International Journal of Bifurcation and Chaos 27 (8). (art. num. 1750115).

Chen, G. 2015. Chaotic systems with any number of equilibria and their hidden attractors. In 4th IFAC Conference on Analysis and Control of Chaotic Systems (plenary lecture). (http://www.ee.cityu.edu.hk/~gchen/pdf/CHEN_IFAC2015.pdf).

Chen, M., Li, M., Yu, Q., Bao, B., Xu, Q. & Wang, J. 2015. Dynamics of self-excited attractors and hidden attractors in generalized memristor-based Chua's circuit. Nonlinear Dynamics 81, 215-226.

Chen, M., Xu, Q., Lin, Y. & Bao, B. 2017. Multistability induced by two symmetric stable node-foci in modified canonical Chua's circuit. Nonlinear Dynamics 87 (2), 789-802.

Chen, M., Yu, J. & Bao, B.-C. 2015a. Finding hidden attractors in improved memristor-based Chua's circuit. Electronics Letters 51, 462-464.

Chen, M., Yu, J. & Bao, B.-C. 2015b. Hidden dynamics and multi-stability in an improved third-order Chua's circuit. The Journal of Engineering. (doi: 10.1049/joe.2015.0149).

Chua, L. 1992. The genesis of Chua's circuit. International Journal of Electronics and Communications 46 (4), 250–257.

Corinto, F. & Forti, M. 2017. Memristor circuits: bifurcations without parameters. IEEE Transactions on Circuits and Systems I: Regular Papers 64 (6), 1540-1551.

Cuomo, K., Oppenheim, A. & Strogatz, S. 1993. Synchronization of lorenz-based chaotic circuits with applications to communications. IEEE Transactions on circuits and systems II: Analog and digital signal processing 40 (10), 626-633.

Cuomo, K. & Oppenheim, A. 1993. Circuit implementation of synchronized chaos with applications to communications. Phys.Rev.Lett. 71, 65-68.

Danca, M.-F., Feckan, M., Kuznetsov, N. & Chen, G. 2016. Looking more closely at the Rabinovich–Fabrikant system. International Journal of Bifurcation and Chaos 26 (02). doi:10.1142/S0218127416500383. (art. num. 1650038).

Danca, M.-F. & Kuznetsov, N. 2017a. Hidden chaotic sets in a Hopfield neural system. Chaos, Solitons & Fractals 103, 144-150. doi:https://doi.org/10.1016/j.chaos.2017.06.002.

Danca, M.-F. & Kuznetsov, N. 2017b. Parameter switching synchronization. Applied Mathematics and Computation 313, 94-102. doi:http://dx.doi.org/10.1016/j.amc.2017.05.075.

Danca, M.-F., Kuznetsov, N. & Chen, G. 2017. Unusual dynamics and hidden attractors of the Rabinovich–Fabrikant system. Nonlinear Dynamics 88, 791-805. doi:10.1007/s11071-016-3276-1.

Danca, M.-F. 2016. Hidden transient chaotic attractors of Rabinovich–Fabrikant system. Nonlinear Dynamics 86 (2), 1263–1270.

Danca, M.-F. 2017. Hidden chaotic attractors in fractional-order systems. Nonlinear Dynamics 89 (1), 577–586.

De Rossi, A., Conti, C. & Trillo, S. 1998. Stability, multistability, and wobbling of optical gap solitons. Phys. Rev. Lett. 81, 85–88. doi:10.1103/PhysRevLett.81.85. ⟨URL:https://link.aps.org/doi/10.1103/PhysRevLett.81.85⟩.

Downes, P. 1993. Secure communication using chaotic synchronization. SPEE Chaos Commun, 227-233.

Dudkowski, D., Jafari, S., Kapitaniak, T., Kuznetsov, N., Leonov, G. & Prasad, A. 2016. Hidden attractors in dynamical systems. Physics Reports 637, 1-50. doi:10.1016/j.physrep.2016.05.002.

Ermentrout, G., B. 2002. Simulating, Analyzing, and Animating Dynamical Systems: A Guide to XPPAUT for Researchers and Students. Philadelphia: SIAM.

Feng, Y. & Pan, W. 2017. Hidden attractors without equilibrium and adaptive reduced-order function projective synchronization from hyperchaotic Rikitake system. Pramana 88 (4), 62.

Gribov, A., Kanatnikov, A. & Krishchenko, A. 2016. Localization method of compact invariant sets with application to the Chua system. International Journal of Bifurcation and Chaos 26. (art. num. 1650073).

Gutierrez, D. G. & Gonzalez, R. D. L. G. 2016. System for steering a drill string. US Patent 9,438,422.

Heart, E. & Smith, P. 2007. Rhythm of the β-cell oscillator is not governed by a single regulator: multiple systems contribute to oscillatory behavior. American Journal of Physiology-Endocrinology and Metabolism 292, e1295-e1300.

Hilbert, D. 1901-1902. Mathematical problems. Bull. Amer. Math. Soc. 8, 437-479.

Hlavacka, M. & Guzan, M. 2017. Hidden attractor and regions of attraction. In 2017 27th International Conference Radioelektronika, 1-4. doi:10.1109/RADIOELEK.2017.7936651.

Hodgkin, A. L. & Huxley, A. F. 1952. A quantitative description of membrane current and its application to conduction and excitation in nerve. The Journal of physiology 117, 500-544.

Huang, X. & Jan, L. 2014. Targeting potassium channels in cancer. J. Cell Biol 206, 151-162.

Izhikevich, E. 2000. Neural excitability, spiking and bursting. International Journal of Bifurcation and Chaos 10, 1171-1266.

Jafari, S., Pham, V.-T., Golpayegani, S., Moghtadaei, M. & Kingni, S. 2016. The relationship between chaotic maps and some chaotic systems with hidden attractors. Int. J. Bifurcat. Chaos 26 (13). (art. num. 1650211).

Jiang, H., Liu, Y., Wei, Z. & Zhang, L. 2016. Hidden chaotic attractors in a class of two-dimensional maps. Nonlinear Dynamics 85 (4), 2719–2727.

Joshi, A. & Xiao, M. 2003. Optical multistability in three-level atoms inside an optical ring cavity. Phys. Rev. Lett. 91, 143904.

Kaddoum, G. 2016. Wireless chaos-based communication systems: A comprehensive survey. IEEE Access 4, 2621-2648.

Kalman, R. E. 1957. Physical and mathematical mechanisms of instability in nonlinear automatic control systems. Transactions of ASME 79 (3), 553-566.

Kelso, J. 2012. Multistability and metastability: understanding dynamic coordination in the brain. Phil. Trans. R. Soc. B 367, 906-918.

Kengne, J. 2017. On the dynamics of Chua's oscillator with a smooth cubic nonlinearity: occurrence of multiple attractors. Nonlinear Dynamics 87 (1), 363-375.

Kiani-B, A., Kia, F., Naser, P. & L., H. 2009. A chaotic secure communication scheme using fractional chaotic systems based on an extended fractional kalman filter. Communications in Nonlinear Science and Numerical Simulation 14, 863-879.

Kiseleva, M., Kudryashova, E., Kuznetsov, N., Kuznetsova, O., Leonov, G., Yuldashev, M. & Yuldashev, R. 2017. Hidden and self-excited attractors in Chua circuit: synchronization and SPICE simulation. International Journal of Parallel, Emergent and Distributed Systems. (doi:10.1080/17445760.2017.1334776).

Kiseleva, M., Kuznetsov, N., Leonov, G. & Neittaanmäki, P. 2012. Drilling systems failures and hidden oscillations. In IEEE 4th International Conference on Nonlinear Science and Complexity, NSC 2012 - Proceedings, 109-112. doi: 10.1109/NSC.2012.6304736.

Kiseleva, M., Kuznetsov, N. & Leonov, G. 2016. Hidden attractors in electromechanical systems with and without equilibria. IFAC-PapersOnLine 49 (14), 51-55. doi:10.1016/j.ifacol.2016.07.975.

Koseska, A., Zaikin, A., Kurths, J. & García-Ojalvo 2009. Timing cellular decision making under noise via cell- cell communication. PLoS ONE 4, e4872.

Kuznetsov, A., Kuznetsov, S., Mosekilde, E. & Stankevich, N. 2015a. Co-existing hidden attractors in a radio-physical oscillator system. Journal of Physics A: Mathematical and Theoretical 48, 125101.

Kuznetsov, N., Kuznetsova, O., Leonov, G., Neittaanmaki, P., Yuldashev, M. & Yuldashev, R. 2015b. Limitations of the classical phase-locked loop analysis. Proceedings - IEEE International Symposium on Circuits and Systems 2015-July, 533-536. doi:10.1109/ISCAS.2015.7168688.

Kuznetsov, N., Kuznetsova, O. & Leonov, G. 2013. Visualization of four normal size limit cycles in two-dimensional polynomial quadratic system. Differential equations and dynamical systems 21 (1-2), 29-34. doi:10.1007/s12591-012-0118-6.

Kuznetsov, N., Leonov, G., Mokaev, T. & Seledzhi, S. 2016. Hidden attractor in the Rabinovich system, Chua circuits and PLL. AIP Conference Proceedings 1738 (1). (art. num. 210008).

Kuznetsov, N., Leonov, G. & Vagaitsev, V. 2010. Analytical-numerical method for attractor localization of generalized Chua's system. IFAC Proceedings Volumes 43 (11), 29-33. doi:10.3182/20100826-3-TR-4016.00009.

Kuznetsov, N., Leonov, G., Yuldashev, M. & Yuldashev, R. 2014. Nonlinear analysis of classical phase-locked loops in signal's phase space. IFAC Proceedings Volumes (IFAC-PapersOnline) 19, 8253-8258. doi:10.3182/20140824-6-ZA-1003.02772.

Kuznetsov, N., Leonov, G., Yuldashev, M. & Yuldashev, R. 2017. Hidden attractors in dynamical models of phase-locked loop circuits: limitations of simulation in MATLAB and SPICE. Commun Nonlinear Sci Numer Simulat 51, 39-49. doi: 10.1016/j.cnsns.2017.03.010.

Kuznetsov, N. & Leonov, G. 2014. Hidden attractors in dynamical systems: systems with no equilibria, multistability and coexisting attractors. IFAC Proceedings Volumes 47, 5445-5454. doi:10.3182/20140824-6-ZA-1003.02501.

Kuznetsov, N. 2016. Hidden attractors in fundamental problems and engineering models. A short survey. Lecture Notes in Electrical Engineering 371, 13-25. doi:10.1007/978-3-319-27247-4_2. ((Plenary lecture at International Conference on Advanced Engineering Theory and Applications 2015)).

Kuznetsov, N., Kuznetsova, O., Leonov, G. & Vagaitsev, V. 2013. Analytical-numerical localization of hidden attractor in electrical Chua's circuit. Lecture Notes in Electrical Engineering 174 (4), 149-158. doi:10.1007/978-3-642-31353-0_11.

Kuznetsov, S. & Pikovsky, A. 2007. Autonomous coupled oscillators with hyperbolic strange attractors. Phys. D 232 (2), 87–102.

Kuznetsov, S. & Seleznev, E. 2006. Strange attractor of Smale-Williams type in the chaotic dynamics of a physical system. J. Exp. Theor. Phys. 102 (2), 355–364.

Kuznetsov, S. 2005. Example of a physical system with a hyperbolic attractor of the Smale-Williams type. Phys. Rev. Lett. 95 (14). (art. num. 144101).

Ladyzhenskaya, O. A. 1991. Attractors for semi-groups and evolution equations. Cambridge University Press.

Laurent, M. & Kellershohn, N. 1999. Multistability: a major means of differentiation and evolution in biological systems. Trends in Biochemical Science 24, 418-422.

Leonov, G., Kiseleva, M., Kuznetsov, N. & Kuznetsova, O. 2015. Discontinuous differential equations: comparison of solution definitions and localization of hidden Chua attractors. IFAC-PapersOnLine 48 (11), 408-413. doi:10.1016/j.ifacol.2015.09.220.

Leonov, G., Kuznetsov, N., Kiseleva, M., Solovyeva, E. & Zaretskiy, A. 2014. Hidden oscillations in mathematical model of drilling system actuated by induction motor with a wound rotor. Nonlinear Dynamics 77 (1-2), 277-288. doi:10.1007/s11071-014-1292-6.

Leonov, G., Kuznetsov, N. & Mokaev, T. 2015a. Hidden attractor and homoclinic orbit in Lorenz-like system describing convective fluid motion in rotating cavity. Communications in Nonlinear Science and Numerical Simulation 28, 166-174. doi:10.1016/j.cnsns.2015.04.007.

Leonov, G., Kuznetsov, N. & Mokaev, T. 2015b. Homoclinic orbits, and self-excited and hidden attractors in a Lorenz-like system describing convective fluid motion. Eur. Phys. J. Special Topics 224 (8), 1421-1458. doi:10.1140/epjst/e2015-02470-3.

Leonov, G., Kuznetsov, N. & Vagaitsev, V. 2011. Localization of hidden Chua's attractors. Physics Letters A 375 (23), 2230-2233. doi:10.1016/j.physleta.2011.04.037.

Leonov, G., Kuznetsov, N. & Vagaitsev, V. 2012. Hidden attractor in smooth Chua systems. Physica D: Nonlinear Phenomena 241 (18), 1482-1486. doi:10.1016/j.physd.2012.05.016.

Leonov, G. & Kuznetsov, N. 2009. Localization of hidden oscillations in dynamical systems (plenary lecture). In 4th International Scientific Conference on Physics and Control. ⟨URL:http://www.math.spbu.ru/user/leonov/publications/2009-PhysCon-Leonov-plenary-hidden-oscillations.pdf\#page=21⟩.

Leonov, G. & Kuznetsov, N. 2011. Algorithms for searching for hidden oscillations in the Aizerman and Kalman problems. Doklady Mathematics 84 (1), 475-481. doi:10.1134/S1064562411040120.

Leonov, G. & Kuznetsov, N. 2013. Hidden attractors in dynamical systems. From hidden oscillations in Hilbert-Kolmogorov, Aizerman, and Kalman problems to hidden chaotic attractors in Chua circuits. International Journal of Bifurcation and Chaos 23 (1). doi:10.1142/S0218127413300024. (art. no. 1330002).

Li, C. & Sprott, J. C. 2014. Coexisting hidden attractors in a 4-D simplified Lorenz system. International Journal of Bifurcation and Chaos 24 (03). doi:10.1142/S0218127414500345. (art. num. 1450034).

Li, Q., Zeng, H. & Yang, X.-S. 2014. On hidden twin attractors and bifurcation in the Chua's circuit. Nonlinear Dynamics 77 (1-2), 255-266.

Litan, A. & Langhans, S. 2015. Cancer as a channelopathy: ion channels and pumps in tumor development and progression. Frontiers in cellular neuroscience 9, 86.

Marquardt, F., Harris, J. G. E. & Girvin, S. M. 2006. Dynamical multistability induced by radiation pressure in high-finesse micromechanical optical cavities. Phys. Rev. Lett. 96, 103901.

Matsumoto, T. 1984. A chaotic attractor from Chua's circuit. IEEE Transaction on Circuits and Systems 31, 1055-1058.

Menacer, T., Lozi, R. & Chua, L. 2016. Hidden bifurcations in the multispiral Chua attractor. International Journal of Bifurcation and Chaos 26 (14). (art. num. 1630039).

Messias, M. & Reinol, A. 2017. On the formation of hidden chaotic attractors and nested invariant tori in the Sprott A system. Nonlinear Dynamics 88 (2), 807–821.

Milton, J. 2010. Epilepsy as a dynamic disease: a tutorial of the past with an eye to the future. Epilepsy & behavior 18, 33-44.

Monteith, G., McAndrew, D., Faddy, H. & Roberts-Thomson, S. 2007. Calcium and cancer: targeting ca2+ transport. Nature Reviews Cancer 7, 519-530.

Ojoniyi, O. S. & Njah, A. N. 2016. A 5D hyperchaotic Sprott B system with coexisting hidden attractors. Chaos, Solitons & Fractals 87, 172 - 181.

Ozbudak, E. M., Thattai, M., Lim, H. N., Shraiman, B. I. & van Oudenaarden, A. 2004. Multistability in the lactose utilization network of escherichia coli. Nature 427, 737-740.

Paraïso, T., Wouters, M., Léger, E., Morier-Genoud, F. & Deveaud-Plédran, B. 2010. Multistability of a coherent spin ensemble in a semiconductor microcavity. Nature Materials 9, 655-660.

Pecora, L. & Carroll, T. 1990. Synchronization in chaotic systems. Physical Review Letters 64 (8), 821-824.

Pham, V.-T., Rahma, F., Frasca, M. & Fortuna, L. 2014. Dynamics and synchronization of a novel hyperchaotic system without equilibrium. International Journal of Bifurcation and Chaos 24 (06). (art. num. 1450087).

Pham, V.-T., Volos, C., Jafari, S., Vaidyanathan, S., Kapitaniak, T. & Wang, X. 2016. A chaotic system with different families of hidden attractors. International Journal of Bifurcation and Chaos 26 (08), 1650139.

Pisarchik, A. & Feudel, U. 2014. Control of multistability. Physics Reports 540 (4), 167–218. doi:10.1016/j.physrep.2014.02.007.

Pmerening, J., Sontag, E. & Ferrell, J. 2003. Building a cell cycle oscillator: hysteresis and bistability in the activation of cdc2. Nature cell biology 5 (4), 346-351.

Ponomarenko, V., Prokhorov, M., Karavaev, A. & Kulminskiy, D. 2013. An experimental digital communication scheme based on chaotic time-delay system. Nonlinear dynamics 74, 1013-1020.

Rocha, R. & Medrano-T, R.-O. 2015. Stablity analysis and mapping of multiple dynamics of Chua's circuit in full-four parameter space. International Journal of Bifurcation and Chaos 25, 1530037.

Rocha, R. & Medrano-T, R. O. 2016. Finding hidden oscillations in the operation of nonlinear electronic circuits. Electronics Letters 52 (12), 1010-1011.

Saha, P., Saha, D., Ray, A. & Chowdhury, A. 2015. Memristive non-linear system and hidden attractor. European Physical Journal: Special Topics 224 (8), 1563-1574.

Sarnthein J., Morel A., V. S. A. & D., J. 2003. Thalamic theta field potentials and eeg: high thalamocortical coherence in patients with neurogenic pain, epilepsy and movement disorders. Thalamus & Related Systems 2, 231-238.

Semenov, V., Korneev, I., Arinushkin, P., Strelkova, G., Vadivasova, T. & Anishchenko, V. 2015. Numerical and experimental studies of attractors in memristor-based Chua's oscillator with a line of equilibria. Noise-induced effects. European Physical Journal: Special Topics 224 (8), 1553-1561.

Sharma, P., Shrimali, M., Prasad, A., Kuznetsov, N. & Leonov, G. 2015a. Control of multistability in hidden attractors. Eur. Phys. J. Special Topics 224 (8), 1485-1491.

Sharma, P., Shrimali, M., Prasad, A., Kuznetsov, N. & Leonov, G. 2015b. Controlling dynamics of hidden attractors. International Journal of Bifurcation and Chaos 25 (04). doi:10.1142/S0218127415500613. (art. num. 1550061).

Sherman, A., Rinzel, J. & Keizer, J. 1988. Emergence of organized bursting in clusters of pancreatic beta-cells by channel sharing. Biophysical journal 54, 411-425.

Singh, J. & Roy, B. 2017. Multistability and hidden chaotic attractors in a new simple 4-D chaotic system with chaotic 2-torus behaviour. International Journal of Dynamics and Control. (doi: 10.1007/s40435-017-0332-8).

Smale, S. 1967. Differentiable dynamical systems. Bulletin of the American mathematical Society 73, 747-817.

Sommerfeld, A. 1902. Beitrage zum dynamischen ausbau der festigkeitslehre. Zeitschrift des Vereins deutscher Ingenieure 46, 391-394.

Volos, C., Pham, V.-T., Zambrano-Serrano, E., Munoz-Pacheco, J. M., Vaidyanathan, S. & Tlelo-Cuautle, E. 2017. Advances in Memristors, Memristive Devices and Systems.

Wei, Z., Moroz, I., Sprott, J., Akgul, A. & Zhang, W. 2017. Hidden hyperchaos and electronic circuit application in a 5D self-exciting homopolar disc dynamo. Chaos 27 (3). (art. num. 033101).

Wei, Z., Pham, V.-T., Kapitaniak, T. & Wang, Z. 2016. Bifurcation analysis and circuit realization for multiple-delayed Wang–Chen system with hidden chaotic attractors. Nonlinear Dynamics 85 (3), 1635–1650.

Wells, D., Kath, W. & Motter, A. 2015. Control of stochastic and induced switching in biophysical networks. Phys. Rev. X 5, 031036.

Xiong, L., Lu, Y.-J., Zhang, Y.-F., Zhang, X.-G. & Gupta, P. 2016. Design and hardware implementation of a new chaotic secure communication technique. PLoS ONE 11 (8), e0158348.

Zelinka, I. 2016. Evolutionary identification of hidden chaotic attractors. Engineering Applications of Artificial Intelligence 50, 159-167.

Zhang, G., Wu, F., Wang, C. & Ma, J. 2017. Synchronization behaviors of coupled systems composed of hidden attractors. International Journal of Modern Physics B 31. (art. num. 1750180).

Zhao, H., Lin, Y. & Dai, Y. 2017. Hopf bifurcation and hidden attractor of a modified Chua's equation. Nonlinear Dynamics. (doi:10.1007/s11071-017-3777-6).

Zhusubaliyev, Z., Mosekilde, E., Churilov, A. & Medvedev, A. 2015. Multistability and hidden attractors in an impulsive Goodwin oscillator with time delay. European Physical Journal: Special Topics 224 (8), 1519-1539.

Zhusubaliyev, Z. & Mosekilde, E. 2015. Multistability and hidden attractors in a multilevel DC/DC converter. Mathematics and Computers in Simulation 109, 32-45.

ORIGINAL PAPERS

PI

SCENARIO OF THE BIRTH OF HIDDEN ATTRACTORS IN THE CHUA CIRCUIT

by

N. V. Stankevich, N. V. Kuznetsov, G. A. Leonov, L. Chua 2017

International Journal of Bifurcation and Chaos, Vol.27, Issue 12, 1730038(18 pages)

International Journal of Bifurcation and Chaos

Scenario of the Birth of Hidden Attractors in the Chua Circuit

Nataliya V. Stankevich
Saint-Petersburg State University, Russia;
Yuri Gagarin State Technical University of Saratov, Russia;
University of Jyväskylä, Finland;
stankevichnv@mail.ru

Nikolay V. Kuznetsov
Saint-Petersburg State University, Russia;
University of Jyväskylä, Finland;
nkuznetsov239@gmail.com

Gennady A. Leonov
Saint-Petersburg State University, Russia
g.leonov@spbu.ru

Leon O. Chua
University of California, USA
chua@eecs.berkeley.edu

Received (to be inserted by publisher)

Recently it was shown that in the dynamical model of Chua circuit both the classical self-excited and hidden chaotic attractors can be found. In this paper the dynamics of the Chua circuit is revisited. The scenario of the chaotic dynamics development and the birth of self-excited and hidden attractors is studied. It is shown a pitchfork bifurcation in which a pair of symmetric attractors coexists and merges into one symmetric attractor through an attractor-merging bifurcation and a splitting of a single attractor into two attractors. The scenario relating the subcritical Hopf bifurcation near equilibrium points and the birth of hidden attractors is discussed.

Keywords: hidden Chua attractor; Chua circuit; classification of attractors as being hidden or self-excited; subcritical Hopf bifurcation; pitchfork bifurcation; basin of attraction.

1. Introduction

The Chua circuit is one of the well-known and well-studied nonlinear dynamical models [Chua, 1992a,b; Kuznetsov *et al.*, 1993; Belykh & Chua, 1993; Nekorkin & Chua, 1993; Lozi & Ushiki, 1993; Shilnikov *et al.*, 2001; Bilotta & Pantano, 2008]. To date in the Chua circuit it has been found chaotic attractors of various shapes (see, e.g. a gallery of Chua attractors in [Bilotta & Pantano, 2008]). Until recently, all the known Chua attractors were self-excited attractors, which can be numerically visualized by a trajectory starting from a point in small neighborhood of an unstable equilibrium.

Definition. [Leonov *et al.*, 2011; Leonov & Kuznetsov, 2013; Leonov *et al.*, 2015b; Kuznetsov, 2016] *An attractor is* hidden *if its basin of attraction does not intersect with a neighborhood of all equilibria*

(stationary points); otherwise, it is called a self-excited *attractor.*

For a *self-excited attractor*, its basin of attraction is connected with an unstable equilibrium and, therefore, self-excited attractors can be localized numerically by the *standard computational procedure* in which after a transient process a trajectory, started in a neighborhood of an unstable equilibrium (e.g., from a point of its unstable manifold), is attracted to a state of oscillation and then traces it. Thus, self-excited attractors can be easily visualized (e.g., the classical Lorenz, Rössler, and Hennon attractors can be visualized by a trajectory from a vicinity of unstable zero equilibrium).

For a hidden attractor, its basin of attraction is not connected with equilibria, and, thus, the search and visualization of hidden attractors in the phase space may be a challenging task. Hidden attractors are attractors in systems without equilibria (see, e.g. rotating electromechanical systems with Sommerfeld effect described in 1902 [Sommerfeld, 1902; Kiseleva *et al.*, 2016]) and in systems with only one stable equilibrium (see, e.g. counterexamples [Leonov & Kuznetsov, 2011, 2013] to the Aizerman's (1949) and Kalman's (1957) conjectures on the monostability of nonlinear control systems [Aizerman, 1949; Kalman, 1957]). One of the first related problems is the second part of Hilbert's 16th problem (1900) [Hilbert, 1901-1902] on the number and mutual disposition of limit cycles in two-dimensional polynomial systems, where nested limit cycles (a special case of multistability and coexistence of attractors) exhibit hidden periodic oscillations (see, e.g., [Bautin, 1939; Kuznetsov *et al.*, 2013a; Leonov & Kuznetsov, 2013]).

The *classification of attractors as being hidden or self-excited* was introduced by G. Leonov and N. Kuznetsov in connection with the discovery of the first hidden Chua attractor [Leonov & Kuznetsov, 2009; Kuznetsov *et al.*, 2010; Leonov *et al.*, 2011; Bragin *et al.*, 2011; Leonov *et al.*, 2012; Kuznetsov *et al.*, 2013b; Leonov & Kuznetsov, 2013; Leonov *et al.*, 2015a] and has captured attention of scientists from around the world (see, e.g. [Burkin & Khien, 2014; Li & Sprott, 2014; Chen, 2015; Saha *et al.*, 2015; Feng & Pan, 2017; Zhusubaliyev *et al.*, 2015; Danca, 2016; Kuznetsov *et al.*, 2015; Chen *et al.*, 2015a; Pham *et al.*, 2014; Ojoniyi & Njah, 2016; Rocha & Medrano-T, 2016; Borah & Roy, 2017; Danca *et al.*, 2017; Wei *et al.*, 2016; Pham *et al.*, 2016; Jafari *et al.*, 2016; Dudkowski *et al.*, 2016; Singh & Roy, 2017; Zhang *et al.*, 2017; Messias & Reinol, 2017; Brzeski *et al.*, 2017; Wei *et al.*, 2017; Chaudhuri & Prasad, 2014; Jiang *et al.*, 2016; Volos *et al.*, 2017]).

Further study of the hidden Chua attractors and their observation in physical experiments can be found, e.g. in [Li *et al.*, 2014; Chen *et al.*, 2015a; Bao *et al.*, 2015a; Chen *et al.*, 2015c,b; Zelinka, 2016; Bao *et al.*, 2016; Menacer *et al.*, 2016; Chen *et al.*, 2017a; Rocha *et al.*, 2017; Hlavacka & Guzan, 2017]. The synchronization of Chua circuits with hidden attractors is discussed, e.g. in [Kuznetsov & Leonov, 2014; Kuznetsov *et al.*, 2016, 2017b; Kiseleva *et al.*, 2017]. Also some recent results on various modifications of Chua circuit can be found in [Rocha & Medrano-T, 2015; Bao *et al.*, 2015b; Semenov *et al.*, 2015; Gribov *et al.*, 2016; Kengne, 2017; Zhao *et al.*, 2017; Chen *et al.*, 2017b; Corinto & Forti, 2017].

In this work the scenario of the chaotic dynamics development and the birth of self-excited and hidden Chua attractors is studied. It is shown a pitchfork bifurcation in which a pair of symmetric attractors coexists and merges into one symmetric attractor through an attractor-merging bifurcation and a splitting bifurcation of a single attractor into two attractors. It is presented the scenario of the birth of hidden attractor connected with a subcritical Hopf bifurcation near equilibrium points and a saddle-node bifurcation of a limit cycles. In general, the *conjecture is that for a globally bounded autonomous system of ordinary differential equations with unique equilibrium point, which is asymptotically stable, the subcritical Hopf bifurcation leads to the birth of a hidden attractor.*[1]

2. Dynamical regimes of the Chua circuit

The Chua circuit, invented in 1983 by Leon Chua [Chua, 1992a,b], is the simplest electronic circuit exhibiting chaos. The classical Chua circuit can be described by the following differential equations

$$\begin{aligned} \dot{x} &= \alpha(y - x) - \alpha f(x), \\ \dot{y} &= x - y + z, \\ \dot{z} &= -(\beta y + \gamma z), \end{aligned} \tag{1}$$

[1]The conjecture was formulated in 2012 by L. Chua in private communication with N. Kuznetsov and G. Leonov.

where $f(x) = m_1 x + \frac{1}{2}(m_0 - m_1)(|x+1| - |x-1|)$ is a piecewise linear voltage-current characteristic. Here x, y, z are dynamical variables; parameters m_0, m_1 characterize a piecewise linear characteristic of nonlinear element; parameters α, β, and γ characterize a resistor, a capacitors, and an inductance. It is well known that model (1) is symmetric with respect to the origin and remains unchanged under the transformation $(x, y, z) \to (-x, -y, -z)$.

System (1) can be considered as a feedback control system in the Lur'e form

$$\begin{aligned} &\dot{u} = Pu + q\phi(r^* u), \quad u = (x, y, z) \in \mathbb{R}^3, \\ &P = \begin{pmatrix} -\alpha(m_1+1) & \alpha & 0 \\ 1 & -1 & 1 \\ 0 & -\beta & -\gamma \end{pmatrix}, \; q = \begin{pmatrix} -\alpha \\ 0 \\ 0 \end{pmatrix}, \; r = \begin{pmatrix} 1 \\ 0 \\ 0 \end{pmatrix}, \\ &\phi(x) = (m_0 - m_1)\,\mathrm{sat}(x) = \frac{1}{2}(m_0 - m_1)(|x+1| - |x-1|). \end{aligned} \tag{2}$$

2.1. *Local analysis of equilibrium points*

Suppose that

$$\begin{aligned} &(\beta \neq -\gamma) \text{ and } \Big(\big(m_0 < -\tfrac{\beta}{\gamma+\beta} \text{ and } m_1 > -\tfrac{\beta}{\gamma+\beta}\big) \text{ or } \big(m_1 < \tfrac{1}{2}(m_0 - \tfrac{\beta}{\gamma+\beta}) \text{ and } m_1 > -\tfrac{\beta}{\gamma+\beta}\big) \text{ or } \\ &\big(m_0 > -\tfrac{\beta}{\gamma+\beta} \text{ and } m_1 < -\tfrac{\beta}{\gamma+\beta}\big) \text{ or } \big(m_1 > \tfrac{1}{2}(m_0 - \tfrac{\beta}{\gamma+\beta}) \text{ and } m_1 < -\tfrac{\beta}{\gamma+\beta}\big)\Big). \end{aligned} \tag{3}$$

Then two symmetric equilibrium points:

$$u_{\mathrm{eq}}^{1,3} = \pm(u_{\mathrm{eq}}^x, u_{\mathrm{eq}}^y, u_{\mathrm{eq}}^z) = \pm\big(\tfrac{(\gamma+\beta)(m_0-m_1)}{\gamma m_1+\beta m_1+\beta}, \tfrac{\gamma(m_0-m_1)}{\gamma m_1+\beta m_1+\beta}, \tfrac{-\beta(m_0-m_1)}{\gamma m_1+\beta m_1+\beta}\big), \tag{4}$$

exist and the corresponding linearizations have the form:

$$J(u_{\mathrm{eq}}^{1,3}) = \begin{pmatrix} -\alpha(m_1+1) & \alpha & 0 \\ 1 & -1 & 1 \\ 0 & -\beta & -\gamma \end{pmatrix}. \tag{5}$$

For the zero equilibrium $u_{\mathrm{eq}}^2 = \big(0, 0, 0\big)$ we have the following matrix of linearization

$$J(u_{\mathrm{eq}}^2) = \begin{pmatrix} -\alpha(m_0+1) & \alpha & 0 \\ 1 & -1 & 1 \\ 0 & -\beta & -\gamma \end{pmatrix}. \tag{6}$$

Remark that for $(m_0, m_1) \to (m_1, m_0)$ we have $\big(J(u_{\mathrm{eq}}^{1,3}), J(u_{\mathrm{eq}}^2)\big) \to \big(J(u_{\mathrm{eq}}^2), J(u_{\mathrm{eq}}^{1,3})\big)$. It means that the local bifurcations, which occur at the symmetric equilibria $u_{\mathrm{eq}}^{1,3}$ and at the zero equilibrium u_{eq}^2, are the same. For the symmetric equilibria, the bifurcations occur, when the parameter m_1 is varying, for the zero equilibrium, when the parameter m_0 is varying. The stability of equilibria depends on m_0 and m_1 and is determined by the eigenvalues (λ_1, λ_2, λ_3) of the corresponding linearization matrices.

Consider the following values of parameters

$$\alpha = 8.4, \beta = 12, \gamma = -0.005, \tag{7}$$

which are close to the values, considered in [Leonov *et al.*, 2011] and are used for the construction of a hidden attractor. Then for all equilibrium points, one of the eigenvalues, λ_1 is always real and can be positive or negative. Two other eigenvalues λ_2 and λ_3 are complex-conjugated and their real parts can be also positive or negative. Therefore we consider the following types of equilibria:

- F is a stable focus, $\lambda_1 < 0$, $Re(\lambda_{2,3}) < 0$;
- SF-I is a saddle-focus of the first type: there are an unstable one-dimensional manifold and a stable two-dimensional manifold, $\lambda_1 > 0$, $Re(\lambda_{2,3}) < 0$;
- SF-II is a saddle-focus of the second type: there are a stable one-dimensional manifold and an unstable two-dimensional manifold, $\lambda_1 < 0$, $Re(\lambda_{2,3}) > 0$.

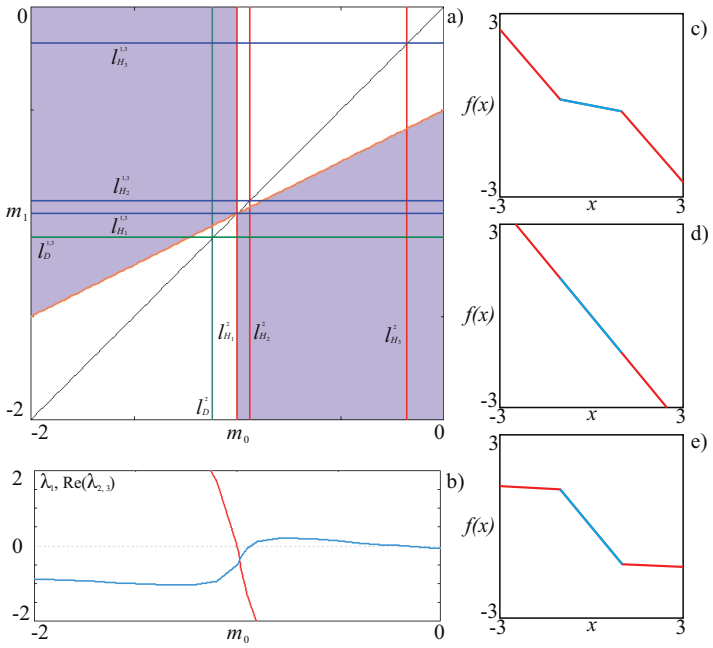

Fig. 1. a) Bifurcation lines of equilibrium points on the parameter plane (m_0, m_1) for $\alpha = 8.4$, $\beta = 12$, $\gamma = -0.005$, the red lines correspond to u^2_{eq} and the blue lines to $u^{1,3}_{\text{eq}}$, the areas of existence of the equilibria $u^{1,3}_{\text{eq}}$ are filled by violet color; b) the dependence of the real eigenvalue (red color) and the real part of the complex conjugate eigenvalues (blue color) on the parameter m_1; c) - e), the examples of the voltage-current characteristics, c) $m_0 = -0.2$, $m_1 = -1.15$; d) $m_0 = -1.2$, $m_1 = -1.2$; e) $m_0 = -1.2$, $m_1 = -0.05$.

In Fig. 1(a) is shown the plane of parameters (m_0, m_1) with the bifurcation curves: blue color denotes the bifurcation curves of the symmetric equilibrium stability, red color denotes the bifurcation curves of the zero equilibrium stability. Areas, filled by violet color, denote the areas of existence of the symmetric equilibria $u^{1,3}_{\text{eq}}$. The domains filled by white color correspond to the existence of the only one equilibrium (see conditions (3)). In Fig. 1(b) are shown the plots of λ_1 (red color) and real part of $\lambda_{2,3}$ (blue color) versus the parameter m_0 for the equilibrium u^2_{eq}, where one can see the changes of the eigenvalues sign caused by a Hopf bifurcation.

In Fig. 1(a) the following symbols are used for $u^{1,3}_{\text{eq}}$ and u^2_{eq}:

- $l^{1,3}_{H_1}$ $(m_1 \approx -1.0004)$, $l^2_{H_1}$ $(m_0 \approx -1.0004)$ are the lines of the Hopf bifurcation corresponding to the transition from the saddle-focus of the first type $(SF\text{-}I)$ to the stable focus (F);
- $l^{1,3}_{H_2}$ $(m_1 \approx -0.939)$, $l^2_{H_2}$ $(m_0 \approx -0.939)$ are the lines of the Hopf bifurcation corresponding to the transition from the stable focus (F) to the saddle-focus of the second type $(SF\text{-}II)$;
- $l^{1,3}_{H_3}$ $(m_1 \approx -0.1761)$, $l^2_{H_3}$ $(m_0 \approx -0.1761)$ are the lines of the Hopf bifurcation corresponding to transition from the saddle-focus of the second type $(SF\text{-}II)$ to the stable focus (F).

As mentioned above, the parameters m_0, m_1 are characterized by the slopes of piecewise linear characteristic. In Fig. 1(c)-(e) are shown examples of voltage-current characteristic for the Chua system (1) for different points of the parameter plane.

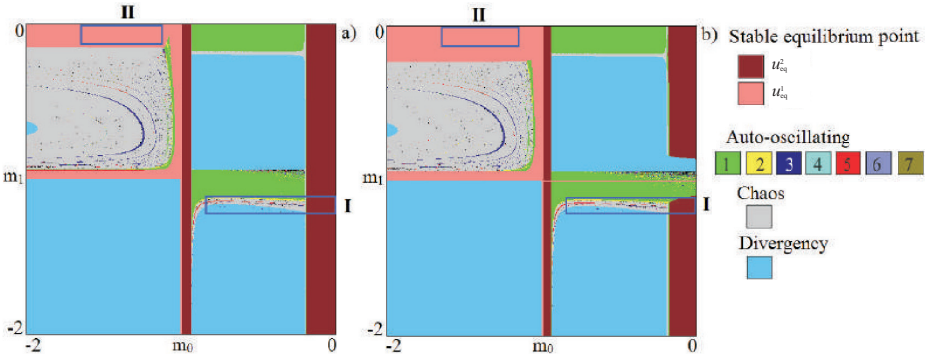

Fig. 2. Dynamics of the Chua system, $\alpha = 8.4$, $\beta = 12$, $\gamma = -0.005$, and initial conditions: a) in the vicinity of the zero equilibrium $u^2_{\rm eq}$, $x_0 = y_0 = z_0 = 0.0001$; b) in the vicinity of one of the symmetric equilibrium points $u^1_{\rm eq}$, $x_0 = u^x_{\rm eq} + 0.0001$, $y_0 = u^y_{\rm eq} + 0.0001$, $z_0 = u^z_{\rm eq} + 0.0001$.

2.2. *Numerical study of the parameter plane. Bifurcation scenario of the hidden attractors transformations*

Consider numerically the dynamics and the qualitative behavior of the Chua system (1) in terms of parameters m_0, m_1.

In Fig. 2 the charts of dynamical regimes are shown on the parameter plane (m_0, m_1). These charts are constructed in the following way. The parameter plane (m_0, m_1) is scanned with a small step. The dynamical regime, corresponding to a point on the plane, is determined according to the number of different points in the Poincaré section, defined by $z = 0$ after a long enough transition process. Initial conditions are the same for each value of parameters: for the chart in Fig. 2(a) we take initial condition (x_0, y_0, z_0)=(0.0001, 0.0001, 0.0001) in the vicinity of the zero equilibrium $u^2_{\rm eq}$. For the chart in Fig. 2(b) we choose initial condition (x_0, y_0, z_0)= ($u^x_{\rm eq}$+0.0001, $u^y_{\rm eq}$+0.0001, $u^z_{\rm eq}$+0.0001) in the vicinity of $u^1_{\rm eq}$ (one of the symmetric equilibria, see (4)). Thus, we expect that the dynamical regimes, which are visualized on these charts, are self-excited. On the charts the symmetric stable equilibrium points $u^{1,3}_{\rm eq}$ are marked by pink color, the zero stable equilibrium point $u^2_{\rm eq}$ by maroon color, the regime of divergency[2] by blue color, the chaotic dynamics[3] by gray color. The periodic oscillations with different periods are distinguished: the green color for cycles of period-1, the yellow color for cycles of period-2, the dark-blue for cycles of period-3, the blue color for cycles of period-4 and so on (see the color legend in Fig. 2).

We reveal that the complex dynamics of system (1) is developed only in the case that three equilibria coexist. Most of the areas where there is only one equilibrium (see white domains in Fig. 1), belongs to the regime of divergency (see the corresponding domains in Fig. 2). The exceptions are the bands, corresponding to the stable zero equilibrium $u^2_{\rm eq}$ for

$$m_0 > -0.1761 \text{ and } m_1 < \frac{1}{2}(m_0 - \frac{\beta}{\beta+\gamma}),$$

and the periodic oscillations, associated with the Hopf bifurcation of the zero equilibrium $u^2_{\rm eq}$, for

$$m_1 > -0.1761 \text{ and } m_0 > -\frac{\beta}{\beta+\gamma}.$$

In the case of coexistence of three equilibria the self-excited chaotic attractors are found (gray color). However besides self-excited attractors, here it is possible to find hidden attractors.

[2]Regime of divergency corresponds to the regime, when the dynamical variables numerically grow to infinity, the detection of this regime is realized under the condition $\sqrt{x^2+y^2+z^2} > 10000$.

[3]Chaotic regime is determined roughly: if the number of discrete points in the Poincaré section is more than 120.

In Fig. 2 the blue rectangle (**I**) is the area of the parameter plane where a hidden chaotic attractor was discovered for the first time [Leonov *et al.*, 2011]. For $m_0 < -0.1761$ (see, the line $l^2_{H_3}$ of the Hopf bifurcation for the zero equilibrium), all the observed attractors are self-excited. In Fig. 3(a) is shown an example of self-excited Chua attractor from this area of parameters. For $m_0 > -0.1761$, all dynamical regimes coexist with stable zero equilibrium point. For $m_0 > -0.1761$, hidden attractors are observed (an example of hidden Chua attractor is in Fig. 3(b), but in some small part of parameter plane a self-excited attractor is found: the phase trajectories, starting from a small neighborhood of the zero equilibrium $u^2_{\rm eq}$, tend to the zero stable equilibrium, but the phase trajectories, starting from the vicinity of the symmetric equilibria $u^{1,3}_{\rm eq}$, tend to an attractor (a limit cycle of period-1), in which case the attractors are not hidden. We consider this case in details in Section 3.1.

As mentioned in Section 2.1, the Chua system (1) has symmetry with respect to the parameters m_0, m_1. This means that the replacement $(m_0, m_1) \to (m_1, m_0)$ in the Chua system (1) leads to the replacement of stability of the equilibria: $u^2_{\rm eq} \to u^{1,3}_{\rm eq}$. Thus, we can consider another area of possible existence of hidden attractors, which is situated below the line $l^{1,3}_{H_3}$ in Fig. 1(a), i.e. before the Hopf bifurcation at the symmetric equilibria. This area is denoted by the blue rectangle (**II**) in Fig. 2. For $m_1 > -0.1761$ ($l^{1,3}_{H_3}$) there are hidden attractors which cannot be visualized from the initial conditions in a small vicinity of the equilibria.

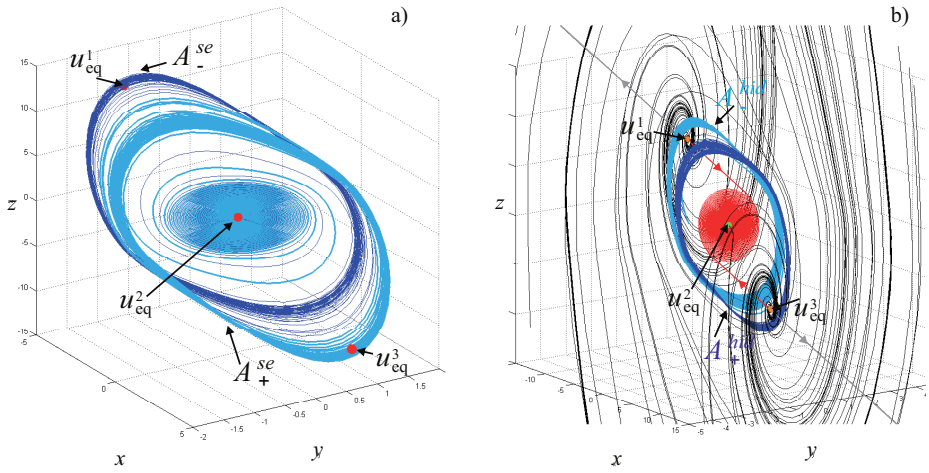

Fig. 3. Self-excited and hidden attractors in the Chua system (1) with parameters $\alpha = 8.4$, $\beta = 12$, $\gamma = -0.005$: a) two symmetric self-excited Chua attractors (cyan and blue domains $A^{se}_{\pm}$) excited from unstable zero equilibrium (parameters $m_0 = -0.3$, $m_1 = -1.12$); b) two symmetric hidden chaotic Chua attractors (cyan and blue domains $A^{hid}_{\pm}$). Red and gray trajectories from unstable manifold of the symmetric saddle-focuses equilibria $u^{1,3}_{\rm eq}$ (orange dots) are attracted to locally stable equilibrium $u^2_{\rm eq}$ (green dot) and infinity, respectively. Black trajectories are stable manifolds of $u^{1,3}_{\rm eq}$ (parameters $m_0 = -0.121$, $m_1 = -1.143$).

3. Hidden twin attractors

3.1. *Merged twin attractors*

Now we consider the dynamics of the Chua system (1) with the parameters corresponding to the rectangle (**I**) in Fig. 2, the zoom of which is shown in Fig. 4(a). For this area, for each point of parameter plane the initial conditions are the same as in the vicinity of equilibrium $u^1_{\rm eq}$. In Fig. 4(b) the same fragment of the chart is constructed by the so-called continuation method for choosing initial conditions, i.e., for each new

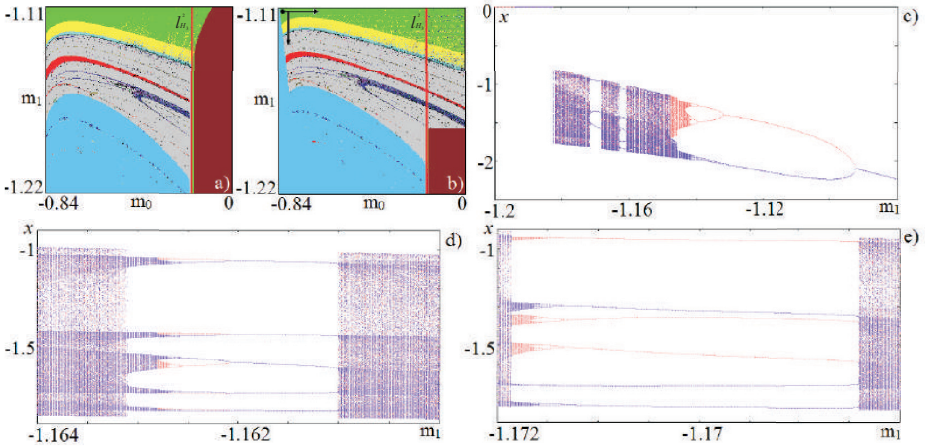

Fig. 4. a), b) magnified fragment (**I**) of the chart of dynamical regimes for different initial conditions, $\alpha = 8.4$, $\beta = 12$, $\gamma = -0.005$; c) bifurcation diagram: red and violet colors correspond to different initial conditions, $m_0 = -0.121$; d), e) magnified fragments of bifurcation diagram.

value of parameter as initial point, the same value is chosen as the final point (obtained from the previous value of the parameter). We use this method to identify the area where hidden attractors exist. In Fig. 4(b) we mark a point in which we start our calculations, and the arrows show the direction of scanning.

The analysis of stability of the equilibrium points in this area (see Fig. 1(a)) shows that for $m_0 = 0$ three equilibrium points exist: two symmetric saddle-focus SF-I and one stable focus F (zero equilibrium). In Fig. 4(a) and (b) is shown the bifurcation line of the loss of stability of the zero equilibrium for $m_0 \approx -0.1761$ ($l^2_{H_3}$). In the area colored in the maroon, the zero equilibrium point is characterized by one negative real number and two complex conjugate numbers with negative real part; after crossing the bifurcation line ($l^2_{H_3}$) the real parts of the conjugate-complex eigenvalues become positive, and a stable focus is transformed into a saddle-focus with a two-dimensional unstable manifold. For the same parameters there exist also two symmetric equilibria, which are characterized by one positive real number and two complex-conjugate eigenvalues with a negative real part.

In the chart of dynamical regimes in Figs. 4(a) and (b), for fixed parameter m_0 and decreasing parameter m_1, one can observe a transition from a limit cycle of period-1 to a chaotic attractor. This transition corresponds to the Feigenbaum scenario (the cascade of period-doubling bifurcations) and it occurs in both the self-excited and the hidden attractors.

To analyze the birth of bifurcations, we construct a bifurcation diagram versus parameter m_1. In Fig. 4 are shown bifurcation diagram (c) and its magnified fragments (d, e). In Figs. 4(c)-(e) is shown the dependence of the variable x, in the Poincaré section by the plane $z = 0$ (for $m_0 = -0.1210$), on the parameter m_1. In the diagram in Fig. 4(c), we identify the value of the parameter $m_1^* \approx -1.1247$ corresponding to the transition from a self-excited attractor to a hidden attractor. For $-1.0929 < m_1 < -1.0800$ the system exhibits one limit cycle with period-1 in Fig. 4(c). For $m_1 \approx -1.0929$, the limit cycle is split into two different period-1 limit cycles via a pitchfork bifurcation. The pitchfork bifurcation is typical in the Chua system since this system exhibits an inner symmetry. For $-1.1317 < m_1 < -1.0929$ two limit cycles of period-1 coexist, these cycles are symmetric to each other. Notice that for $m_1 \approx -1.1247$ these two period-1 limit cycles become hidden. For $m_1 \approx -1.1317$ both limit cycles become limit cycles of period-2 via a period doubling bifurcation. By continuous decreasing the parameter m_1, after the sequence of period-doubling bifurcations, as shown in Fig. 4(c), the two limit cycles are transformed into two different hidden chaotic attractors, respectively. In this case these attractors coexist with a symmetric twin-attractor, and a stable zero equilibrium point. For $m_1 \approx -1.1483$ the twin-attractors are merged into one, which by further

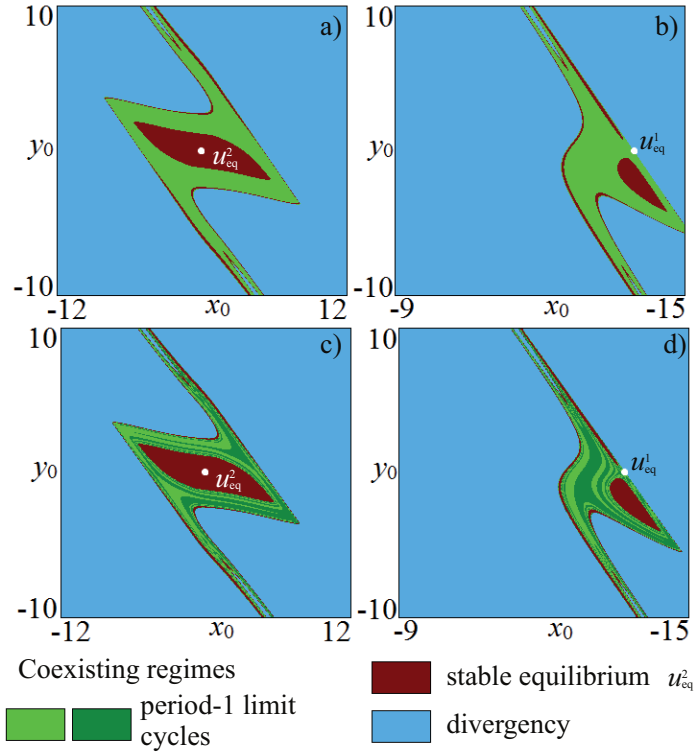

Fig. 5. Basins of attraction of coexisting self-excited attractors of the Chua system with $\alpha = 8.4$, $\beta = 12$, $\gamma = -0.005$, $m_0 = -0.121$: a) limit cycle of period-1 before pitchfork bifurcation $m_1 = -1.09$, in the section defined by the plane $z_0 = 0.00001$; b) in the section defined by the plane $z_0 = u^z_{eq}$; c) period-1 limit cycles after pitchfork bifurcation at $m_1 = -1.1$, in the section defined by the plane $z_0 = 0.00001$; d) in the section defined by the plane $z_0 = u^z_{eq}$.

decreasing the parameter m_1, forms an increasingly larger chaotic set. For $m_1 \approx -1.1609$, a periodic window of period-5 emerges (in Fig. 4(d) is shown a magnified fragment near the periodic window of period-5). The same scenario takes place for the period-5 cycle. For $m_1 \approx -1.1621$ the period-5 limit cycle is split into two symmetric period-5 limit cycles via a pitchfork bifurcation. For $-1.1626 < m_1 < -1.1621$ two limit cycles of period-5 coexist. For $m_1 \approx -1.1621$ both limit cycles bifurcate into two limit cycles of period-10 via a period-doubling bifurcation. Upon further decreasing the parameter m_1, after a sequence of period-doubling bifurcations, two hidden chaotic attractors emerge. Then they merged at $m_1 \approx -1.1628$, and collapse with the chaotic set of the previous attractor at $m_1 \approx -1.1631$.

Upon a further decrease of the parameter m_1, a periodic window of period-3 emerges (Fig. 4(e) shows a magnified fragment near a period-3 window). In this case there is no pitchfork bifurcation, and for $-1.1714 < m_1 < -1.1684$ two symmetric hidden cycles of period-3 coexist. For $m_1 \approx -1.1714$ both period-3 cycles become a pair period-6 limit cycles via a period doubling bifurcation. Further decrease of the parameter m_1 gives rise to a cascades of period-doubling bifurcations. In this case we can not see the merging of two chaotic attractors, but for $m_1 \approx -1.1719$ two hidden symmetric attractors merge into a chaotic set.

To analyze localization of hidden attractors in the phase space, and transition from self-excited to hidden attractors, we consider the basins of attraction under varying parameter. Firstly, we consider the

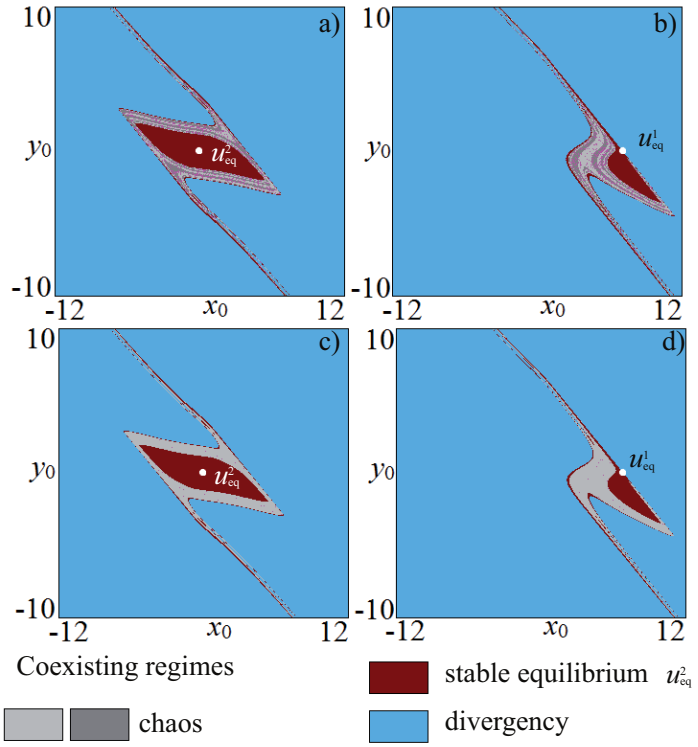

Fig. 6. Basins of attraction of coexisting hidden attractors of the Chua system with $\alpha = 8.4$, $\beta = 12$, $\gamma = -0.005$, $m_0 = -0.121$: a) twin hidden chaotic attractors for $m_1 = -1.143$, in the section defined by the plane $z_0 = 0.0001$; b) in the section defined by the plane $z_0 = u^z_{eq}$; c) merged hidden chaotic attractors for $m_1 = -1.15$, in the section defined by the plane $z_0 = 0.0001$; d) in the section defined by the plane $z_0 = u^z_{eq}$.

case that a self-excited attractor is realized: $m_0 = -0.121$, $m_1 = -1.09$. Since its basin of attraction in three-dimensional phase space is difficult to analyze, we analyze two-dimensional sections of this volume at various planes, which correspond to two-dimensional planes of initial conditions. To distinguish between hidden and self-excited attractors, the dynamical behavior of the model in the vicinity of equilibria is crucial. That is why we consider two sections of phase volume: in the vicinity of the zero equilibrium u^2_{eq} and in the vicinity of one of the symmetric equilibria u^1_{eq} (for the other symmetric equilibrium u^3_{eq}, the structure of the basin is similar).

In Fig. 5 is shown the two-dimensional plane of initial conditions for vicinities of equilibria points and for different values of parameter m_1. The regime of divergency is marked by blue color, the area of attraction of the stable zero equilibrium is marked by maroon color. The areas of attraction regimes of different period-1 limit cycles are denoted by two different green colors. The location of the equilibrium points in the plane is identified by white dots. In Fig. 5(a) is shown a two-dimensional plane of initial conditions for fixed $z_0 = 0.0001$ in the vicinity of the zero equilibrium u^2_{eq} (stable focus F). For $m_1 = -1.09$ in system (1) the coexistence of a period-1 limit cycle, before the pitchfork bifurcation, and the stable zero equilibrium is observed. In Fig. 5(a) is shown the structure of the basins of attraction of two coexisting regimes. There is a rather large basin of attraction surrounding the stable zero equilibrium (maroon color), and a large area of divergency. Between these two areas we have an area of stable periodic oscillations, which represents the

basin of attraction of a period-1 limit cycle. The boundary between the areas of divergency and self-excited limit cycle is indicated by a thick line, which corresponds to the stable zero equilibrium. In Fig. 5(b) is shown a vicinity of one of the symmetric points $z_0 = u^z_{\rm eq}$ (saddle-focuses *SF-I*). The symmetric equilibrium state is located on the boundary between the basin of attraction of the stable limit cycle and the area of divergency. In this case we cannot affirm that the limit cycle is a hidden attractor because if we start to iterate a trajectory, with a randomly chosen initial state in the vicinity of symmetric equilibrium points, it can either diverge from the initial state, or tend to the limit cycle.

After the pitchfork bifurcation ($m_0 = -1.1$) two symmetric limit cycles occur. In Figs. 5(c),(d) are shown two planes of initial conditions with basins of attraction of symmetric limit cycles in the vicinity of the two equilibria for fixed third initial conditions $z_0 = 0.00001$ and $z_0 = u^z_{\rm eq}$, in which case, the two different green colors correspond to the basins of attraction of the two symmetric limit cycles ($m_1 = -1.1$). In this case after the pitchfork bifurcation, the basin of attraction of original limit cycle is split into two basins of attraction of the two symmetric period-1 limit cycles. These basins have a complex but symmetric structure. In this case the equilibrium $u^1_{\rm eq}$ is also situated on the boundary of the basins of attraction of the two limit cycles, implying that the limit cycles are self-excited for $m_1 > m^*_1$.

Next, we decrease parameter m_1 such that it becomes less then m^*_1. In this case the attractors become hidden, while bifurcating into chaotic dynamics, and we observe the corresponding changes in the structure in the plane of initial conditions. In Fig. 4 is shown that hidden twin chaotic attractors exist, for instance, at $m_1 \approx -1.141$, and with decreasing parameter m_1 these two attractors merged (for $m_1 \approx -1.147$). In Fig. 6 are shown the planes of initial conditions for the twin chaotic attractors (a) and (b), and the merged chaotic attractor (c) and (d). In Figs. 6(a),(b) the basins of attraction of the two different chaotic attractors are identified by different shaded gray colors. The composition of the basins in the plane of initial states near the vicinity of the zero equilibrium point is the same as in the case of self-excited limit cycle. We observe the basins of attraction of the twin chaotic attractors and the basin of attraction of zero stable equilibrium point in the center. But the structure of the plane of initial states in the section near the vicinity of the symmetric equilibrium points has a significant distinction. The basin of attraction of the stable zero equilibrium $u^2_{\rm eq}$ at the center is combined with the another part of the basin of attraction of the stable zero equilibrium point $u^2_{\rm eq}$ on the boundary of the area of divergency, and a saddle equilibrium $u^1_{\rm eq}$ is located on the boundary between the basin of attraction of the stable zero equilibrium point and the area of divergency. Consequently, a twin chaotic attractor becomes hidden because if we choose initial states near one of the equilibrium points, then we cannot reach the chaotic attractors.

In Figs. 6(c) and d are shown the same illustrations for merged hidden chaotic attractor. In this case one can see that the basin of attraction of the merged hidden attractor represents the combining of the areas of attraction of each twin-hidden attractors. In the vicinity of the saddle equilibrium we also see only two possible regimes: the stable zero equilibrium and the divergency. It follows that the merged attractor is the hidden one.

3.2. *Separated twin-attractors*

Now we consider the dynamics of the Chua system (1) and the features of hidden attractors in another area of the parameter plane, which is marked by the blue rectangles (**II**) in Fig. 2. In Fig. 7(a) is shown the zoom of fragment (**II**). For the continuation method of changing initial conditions, the starting point is denoted on the parameter plane, and we scan the plane of parameters in different directions in accordance with the arrows in this figure.

The analysis of stability of equilibria (Fig. 1(a)) shows that in this area there are two symmetric stable focuses (F_1, F_2) and one saddle-focus of the first type (*SF-I*) at the zero equilibrium point.

By numerical integration the trajectories starting from the vicinity of any equilibrium point in rectangle (**II**) can reach only one of the symmetric equilibrium points (Fig. 2). But we can see in Fig. 7(a) that for some special initial conditions it is possible to observe hidden attractors. In particular, the bifurcation scenario associated with the hidden attractors from the area of the parameter plane (**II**) is the same as that in the area (**I**): one can observe chaotic dynamics resulting from of a cascade of period-doubling bifurcations.

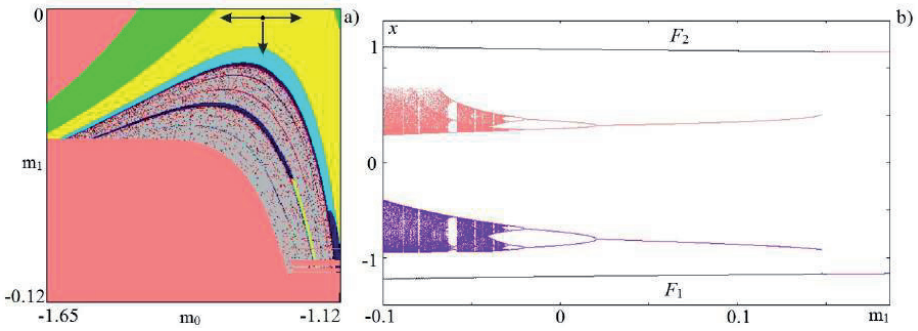

Fig. 7. a) the magnified fragment (**II**) of the chart of dynamical regimes for continuation method of changing initial conditions, $\alpha = 8.4$, $\beta = 12$, $\gamma = -0.005$; b) bifurcations diagram: black, red, and violet colors correspond to different initial conditions, $m_0 = -1.2$.

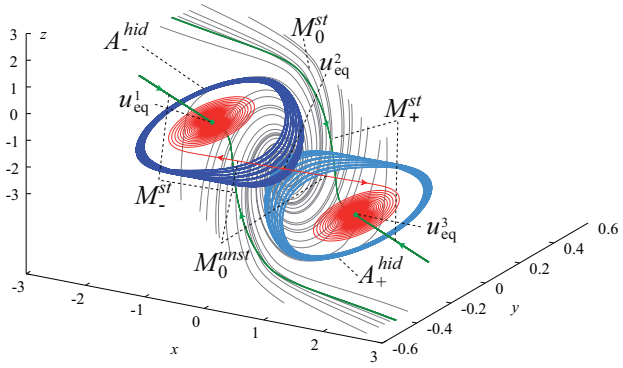

Fig. 8. Example of two symmetric hidden chaotic Chua attractors (blue and cyan domains $\mathcal{A}_{\pm}^{\rm hid}$), $m_1 = -0.05$. Red trajectories from unstable manifold $\mathrm{M}_0^{\rm unst}$ of the zero saddle-focus equilibrium $u_{\rm eq}^2$ (orange dot) are attracted to locally stable equilibria $u_{\rm eq}^{1,3}$ (green dots); gray trajectories are stable manifold $\mathrm{M}_0^{\rm st}$ of $u_{\rm eq}^2$; green trajectories are stable manifolds $\mathrm{M}_{\pm}^{\rm st}$ of $u_{\rm eq}^{1,3}$.

To analyze the bifurcations and transformations in this case, let us consider a bifurcation diagram. In Fig. 7(b) are shown diagrams for different initial conditions for $m_0 = -1.2$, as a function of the parameter m_1 in the Poincaré section by the plane $z = 0$. The black lines correspond to initial condition near the symmetric equilibrium points (the scanning of parameter m_1 was realized by the continuation method to choose initial conditions), and these lines mark the coexisting stable focuses (F_1 and F_2). For the red and violet bifurcation diagrams the initial conditions are chosen in the following way: $x_0 = \mp 1.2$, $y_0 = \mp 0.0005$, $z_0 = 0$, respectively. For these initial conditions for $m_1 = 0$ we have two symmetric period-2 limit cycles, and from these points we scan the parameter intervals m_1 $[-0.2, 0.1]$ in two directions (to the right and to the left).

For $m_1 = 0.2$ there are two symmetric stable equilibrium points. If the parameter m_1 decreases, then

at $m_1 \approx 0.15$ a limit cycle emerges near each symmetric equilibrium point. In the bifurcation diagram one can see the hard birth of the cycles, because of the form of nonlinearity (piecewise-linear characteristic of the Chua circuit). As m_1 decreases, we see stable focuses and two coexisting limit cycles, undergoing a period-doubling bifurcation and transition to chaos. However, for this area of parameter plane there is no a pitchfork bifurcation of limit cycles and a merging of chaotic attractors. In this case two bifurcation diagrams in Fig. 7 (b) do not cross each other and are separated by the saddle point at the zero equilibrium. In Fig. 8 the example of two symmetric hidden chaotic Chua attractors are shown for $m_1 = -0.05$. By red, gray and green colors in Fig. 8 are shown the stable and unstable manifolds in the vicinity of equilibrium points. Gray and green trajectories were constructed by integration in inverse time for initial conditions in the vicinity of equilibrium points (gray lines are near saddle-focus, green lines are near stable focuses). Red trajectories tend to the symmetric equilibria and are obtained by the integration in forward time near the zero equilibrium.

To analyze the structure of the phase space and the localization of hidden attractors in the phase space, we consider two-dimensional planes of initial conditions. Then we can study the basins of attraction of coexisting attractors. As in the previous case we consider two-dimensional sections of the three-dimensional phase space of initial states in the vicinity of one of the stable symmetric equilibria u^1_{eq}, and in the vicinity of the zero equilibrium u^2_{eq}. In Fig. 9 is shown the structure of areas of attraction for different parameters of m_1 and $m_0 = -1.2$, and for different cross-section of the phase space. In Fig. 9(a) and (b) are shown the basins of attraction of coexisting attractors for $m_1 = 0.1$ in the vicinity of one stable focus F_1 (a) and in the vicinity of the zero saddle equilibrium (b), the location of equilibrium points are marked in the plane by black dots. In this case in the bifurcation diagram one can see two coexisting symmetric equilibrium points and two symmetric cycles of period-1. Also it is observed a new period-1 limit cycle, surrounding all regimes described above, and the dynamics near the equilibria is developed inside this limit cycle of sufficiently large radius. So, for this area of parameters we have five coexisting attractors. We shaded the areas of attraction of different symmetric period-1 limit cycles by green color. The area of attraction of the outside limit cycle is marked on the plane by light green color. We use the pink and red colors to denote the basins of attraction of the two symmetric equilibria u^1_{eq} and u^3_{eq}, respectively.

Firstly, we consider a vicinity of the stable equilibrium (Fig. 9(a)). In the vicinity of the stable equilibrium one can see a basin of attraction of one of the symmetric stable equilibrium points. Also, there are the basin of attraction of another symmetric stable equilibrium point, and the symmetric basins of attraction of two symmetric limit cycles. The complex structure of their basins is represented by the area of attractions in the form of bands, which are spiralled together, and their boundaries have self-similar patterns, i.e., fractal structures. Also, there is a basin of attraction of the external limit cycle, which surround all other basins of attraction.

Then we consider a plane of initial conditions and the basins of attraction of different attractors in the vicinity of the saddle equilibrium point (Fig. 9(b)). We can see that the phase trajectories, starting from the vicinity of the saddle point, can reach one of the stable symmetric equilibria only. The zero equilibrium point u^2_{eq} is located on a boundary between the attracting areas of different symmetric stable equilibria. The areas of attraction are symmetric to each other, and a boundary between these areas represents the stable manifold of the zero saddle-focus. Consequently, if we choose initial conditions in the vicinity of any equilibrium point, we will reach one of the stable equilibrium points and, thus, all of the limit cycles are hidden attractors.

Let us decrease the parameter m_1 so that chaotic dynamics emerges, and consider the basins of attraction of the coexisting stable symmetric equilibria, the chaotic attractors, and the external limit cycle. In Fig. 9(c) and (d) are shown two planes of initial conditions in the vicinity of the equilibrium points for $m_1 = -0.05$. By two shades of gray color we identify the basins of attraction of the coexisting twin-chaotic attractors. It is rather easy to distinguish the basins of attraction for these chaotic attractors because the attractors in the phase space are separated by the zero saddle equilibrium. For decreasing parameter m_1 the structure of the basin of attraction persists. In place of the areas of two symmetric period-1 limit cycles one sees the basins of attraction of the symmetric chaotic attractors. In this case the order of alternation of the basin of attraction of different attractors remains the same. The structure of the basin of attraction in the vicinity of the saddle equilibrium point persists: the saddle point is located on the boundary of

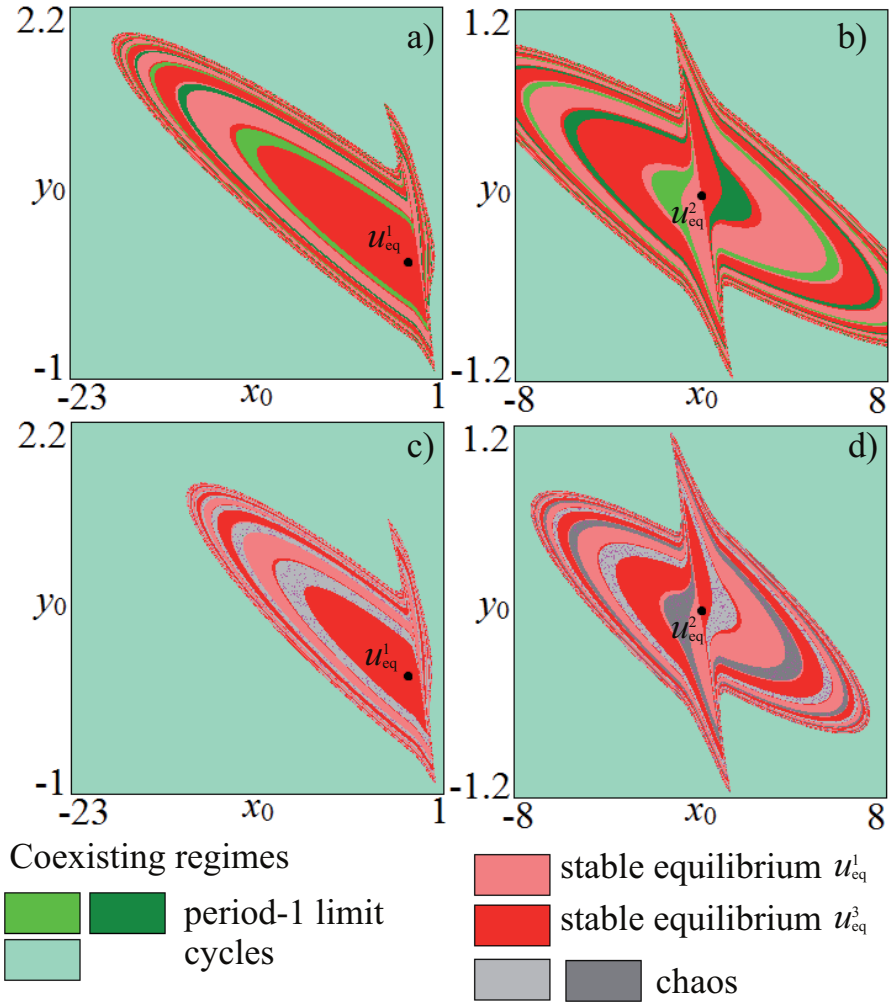

Fig. 9. Basins of attraction of coexisting attractors of the Chua system (1) $\alpha = 8.4$, $\beta = 12$, $\gamma = -0.005$, $m_0 = -1.2$: a) twin hidden period-1 attractors with $m_1 = 0.1$, and cross-section by the plane $z_0 = u^z_{eq}$; b) cross-section by the plane $z_0 = 0.0001$; c) twin hidden chaotic attractors with $m_1 = -0.05$, cross-section by the plane $z_0 = u^z_{eq}$; d) cross-section by the plane $z_0 = 0.0001$.

the basins of attraction of two symmetric equilibrium points, and the boundary corresponds to an stable manifold of the saddle point.

In Fig. 10 (a),(b) is shown a structure of the phase space in the above case, where we see a coexisting large stable limit cycle (orange color in Fig. 10 (a)) and two separated hidden chaotic Chua attractors (blue and cyan domains Fig. 10 (b)) from Fig. 8. The basins of attraction of periodic and chaotic attractors do not intersect with small neighborhood of the equilibria, thus, the attractors are hidden. Therefore in this case there are 5 coexisting attractors: two stable equilibria, one hidden limit cycle, and two hidden "twin" attractors.

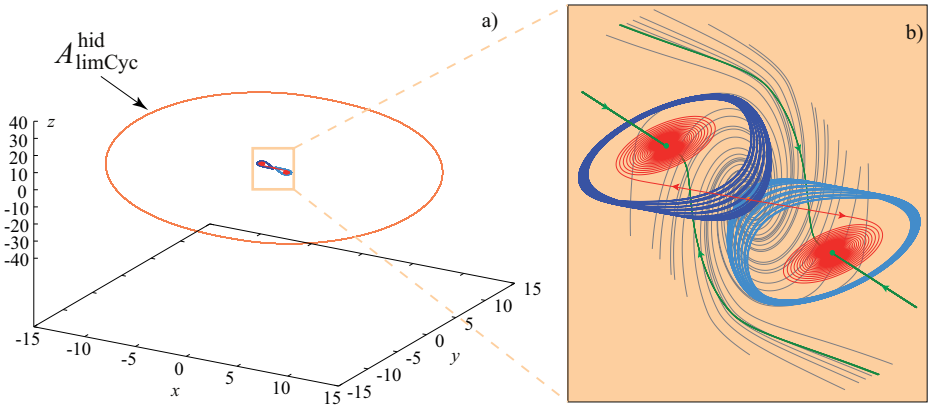

Fig. 10. Multistability with 5 coexisting attractors in the Chua system (1) with $\alpha = 8.4$, $\beta = 12$, $\gamma = -0.005$, $m_0 = -1.2$, $m_1 = -0.05$. Coexistence of hidden periodic attractor (orange trajectory $\mathcal{A}^{\text{hid}}_{\text{limCyc}}$ is a stable limit cycle) and two symmetric hidden chaotic Chua attractors (blue and cyan domains). Here the basins of attraction of the periodic and the two symmetric Chua attractors do not intersect with a small neighborhood of the equilibria, thus, the attractors are hidden.

Thus, we reveal two area on the parameter plane $(m_0,\ m_1)$, where we observe hidden attractors. Observe that for the physical realization of the Chua circuit and observation of hidden attractors we need nonnegative parameters α, β, γ. For example, both configurations of hidden attractors cited above are observed for the case $\gamma = 0$ in [Rocha & Medrano-T, 2015, 2016]; and for the positive γ one may consider, for example, the following two sets of parameters: $\alpha = 8.4562, \beta = 12.0732, \gamma = 0.0052, m_0 = -0.1768, m_1 = -1.1468$ and $\alpha = 8.4, \beta = 12, \gamma = 0.005, m_0 = -0.12, m_1 = -1.143$.

Note that the existence of hidden attractors in the Chua system can be effectively predicted by the describing function method (DFM) [Leonov *et al.*, 2011; Rocha & Medrano-T, 2015; Kuznetsov *et al.*, 2017a]. The classical DFM (see, e.g. [Krylov & Bogolyubov, 1947; Khalil, 2002]) is only an approximate method which gives the information on the frequency and amplitude of periodic orbits. However DFM may lead to wrong conclusions[4] about the existence of periodic orbits and does not provide initial data for the localization of periodic orbits. But for the systems of special type with a small parameter, DFM can be rigorously justified. For this purpose, following references [Leonov *et al.*, 2011; Leonov & Kuznetsov, 2013], we introduce a coefficient k and represent the linear part and nonlinearity in (2) as follows:

$$P_0 = P + kqr^* = \begin{pmatrix} -\alpha(m_1+1+k) & \alpha & 0 \\ 1 & -1 & 1 \\ 0 & -\beta & -\gamma \end{pmatrix}, \qquad (8)$$
$$\psi(\sigma) = \phi(\sigma) - k\sigma = (m_0 - m_1)\,\mathrm{sat}(\sigma) - k\sigma,$$

where $\lambda^{P_0}_{1,2} = \pm i\omega_0$, $\lambda^{P_0}_3 = -d < 0$. Then we consider a small parameter ε, change $\psi(\cdot)$ by $\varepsilon\psi(\cdot)$, and reduce

[4]Well-known Aizerman's and Kalman's conjectures on the absolute stability of nonlinear control systems are valid from the standpoint of DFM which may explain why these conjectures were put forward. Nowadays, various counterexamples to these conjectures (nonlinear systems, where the only equilibrium, which is stable, coexists with a hidden periodic oscillation) are known (see, e.g. [Pliss, 1958; Fitts, 1966; Barabanov, 1988; Bernat & Llibre, 1996; Leonov *et al.*, 2010; Leonov & Kuznetsov, 2011] and surveys [Bragin *et al.*, 2011; Leonov & Kuznetsov, 2013]; the corresponding discrete examples are considered in [Alli-Oke *et al.*, 2012; Heath *et al.*, 2015]).

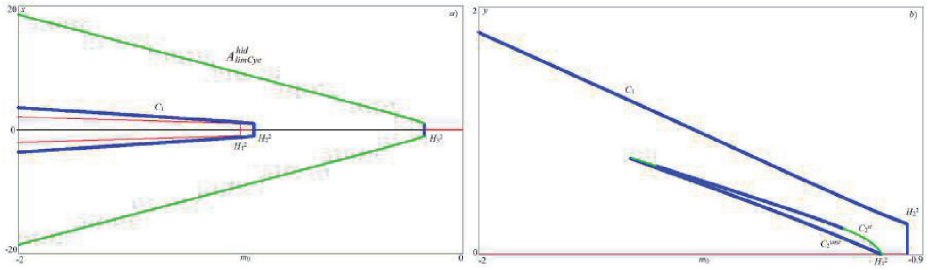

Fig. 11. Bifurcation diagram of the Chua system (1), $\alpha = 8.4$, $\beta = 12$, $\gamma = -0.005$, $m_1 = -0.05$.

by a non-singular linear transformation $w = Su$ system (8) to the following form

$$\dot{w} = Aw + b\varepsilon\psi(u^* y),$$
$$A = \begin{pmatrix} 0 & -\omega_0 & 0 \\ \omega_0 & 0 & 0 \\ 0 & 0 & -d \end{pmatrix}, \; b = \begin{pmatrix} b_1 \\ b_2 \\ b_3 \end{pmatrix}, \; c = \begin{pmatrix} 1 \\ 0 \\ -h \end{pmatrix}. \tag{9}$$

Theorem [Leonov *et al.*, 2011; Leonov & Kuznetsov, 2013; Kuznetsov *et al.*, 2017a] *Consider the describing function* $\Phi(a) = \int_0^{2\pi/\omega_0} \psi(a\cos(\omega_0 t))\cos(\omega_0 t)dt$. *If there exists a positive* a_0 *such that* $\Phi(a_0) = 0$, $b_1\Phi'(a_0) < 0$, *then system* (9) *has a stable*[5] *periodic solution with the initial data* $w_0 = \big(a_0 + O(\varepsilon), 0, O(\varepsilon)\big)$ *and period* $T = \frac{2\pi}{\omega_0} + O(\varepsilon)$.

This theorem gives an initial point for the numerical computation of periodic solution (starting attractor) in the system with small parameter. Then, using the method of numerical continuation and gradually increasing ε, one can numerically follow the transformation of the starting attractor.

It turns out that for the numerical localization of the considered hidden attractors we can skip the multistep procedure based on numerical continuation and use the initial data $u_0 = S^{-1}w_0$ for the localization of hidden attractors in the initial system (). For the parameters $\alpha = 8.4, \beta = 12, \gamma = -0.005, m_0 = -1.2, m_1 = -0.05$ we get: a) $k = -0.8890, \omega_0 = 2.0260, a_0 = 1.5187$ and the corresponding initial data $\pm(1.5187, 0.0926, -2.1682)$ allows us to visualize two symmetric hidden chaotic attractors; b) $k = -0.1244, \omega_0 = 3.2396, a_0 = 11.7546$ and the corresponding initial data $(11.7546, 9.7044, -16.7367)$ allows us to localize the hidden periodic attractor (see Fig. 10). For the parameters $\alpha = 8.4, \beta = 12, \gamma = -0.005, m_0 = -0.121, m_1 = -1.143$ we get $k = 0.2040, \omega_0 = 2.0260, a_0 = 6.3526$ and the corresponding initial data $\pm(6.3526, 0.3874, -9.0694)$ allows us to visualize two symmetric hidden chaotic attractors (see Fig. 3(b)).

4. Scenario of the birth of hidden attractors

In Sections 3.1 and 3.2 we have shown the opportunity of existence of hidden attractors in different areas of the parameter plane. In order to study the scenario of the emergence of hidden attractors we use numerical bifurcation analysis by the software package XPP AUTO [Ermentrout, 2002].

4.1. *Formation of separated hidden attractors*

Firstly we consider hidden attractors from the area (**II**) in the parameter plane (m_0, m_1) (Fig. 2). In Fig. 11(a) is shown the bifurcation diagram of the Chua system (1) for parameters (7) and $m_1 = -0.05$. In the diagram red and black color denote stable and unstable equilibrium points, green and blue colors denote stable and unstable limit cycles, respectively. At $m_0 \approx -0.1761$ the Hopf bifurcation (H_3^2) takes place, that is in a good agreement with the results obtained by linear analysis in Section 2.1 and by numerical

[5]See detailed discussion in [Leonov & Kuznetsov, 2013].

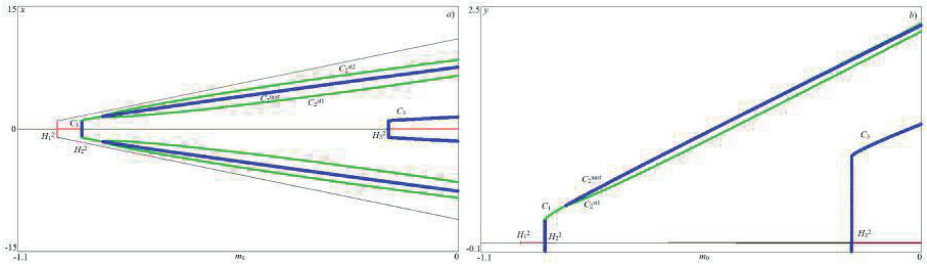

Fig. 12. Bifurcation diagram for the Chua system (1) with $\alpha = 8.4$, $\beta = 12$, $\gamma = -0.005$, $m_1 = -1.11$.

simulations in Section 3.2. In this case the supercritical Hopf bifurcation occurs: the zero equilibrium point loses stability and a limit cycle A^{hid}_{limCyc} is born. With decreasing of parameter m_0 the radius of limit cycle is increased. At $m_0 \approx -0.939$ a second Hopf bifurcation (H_2^2) emerges, where the zero equilibrium becomes stable, which is accompanied by the hard birth of an unstable limit cycle C_1. The radius of the internal unstable cycle C_1 surrounding the zero equilibrium increases initially according to square root of 2, upon a further decrease of the parameter m_0. At $m_0 \approx -1.0004$ occurs a third Hopf bifurcation (H_1^2), which is a pitchfork bifurcation of the zero equilibrium, in which case two stable symmetric equilibria are born, and the zero equilibrium become unstable. In this case the limit cycle C_1 surrounds all equilibria, splits the limit cycle A^{hid}_{limCyc} and equilibria in the phase space, and forms the boundary of the basin of attraction of the limit cycle A^{hid}_{limCyc}. The pitchfork bifurcation (H_1^2) is accompanied by the occurrence of two symmetric pairs of limit cycles C_2^{st} and C_2^{unst}, which are denoted in the magnified fragment of the diagram in Fig. 11(b). The birth of the limit cycles is a result of a saddle-node bifurcation, i.e. a pair of limit cycles (stable and unstable) are born, along with its identical symmetric pair. Thus, the stable limit cycle C_2^{st} is surrounded by the unstable limit cycle C_1 on the one side, and by the unstable limit cycle C_2^{unst} on the other side, making it unreachable from the vicinity of stable equilibria points and also from the vicinity of unstable equilibrium points. Thus, the limit cycles C_2^{st}, and the chaotic attractor, which occur on the base of this limit cycle are hidden.

4.2. *Formation of merged hidden attractors*

Formation of hidden attractors in the area (**I**) in the parameter plane (m_0, m_1) is as follows. In Fig. 12 the corresponding bifurcation diagrams are shown. In this case it is better to exam the bifurcation diagrams by increasing the parameter m_0. At $m_0 \approx -1.0004$ the Hopf bifurcation (H_1^2) occurs, where the unstable zero equilibrium point becomes stable, simultaneously with pitchfork bifurcation, and as a result of which two unstable equilibria are born. At $m_0 \approx -0.939$ the zero equilibrium point undergoes a supercritical Hopf bifurcation (H_2^2), and as a result the zero equilibrium point loses stability and a stable limit cycle C_1 is born, where it is situated between two symmetric unstable equilibria in projections onto the x and z variables, where it surrounds all equilibria in a projection of y-variable. Upon increasing the parameter m_0, the limit cycle undergoes a symmetry breaking bifurcation (it is the same as a pitchfork bifurcation), and splits into two stable symmetric limit cycles C_2^{st1}, C_2^{st2} and one unstable limit cycle C_2^{unst}. At $m_0 \approx -0.1761$ (H_3^2) the zero equilibrium point changes stability again. In this case the bifurcation is subcritical, and as a result the unstable limit cycle C_3 is born. The limit cycle C_3 forms boundaries of the basin of attraction of the zero stable equilibrium point. In Fig. 12(b) is shown the projection of the y-variable. Thus, for $m_0 > -0.1761$ (H_3^2) the limit cycles C_2^{st1} and C_2^{st2} are isolated from all equilibria by the unstable limit cycle C_3, and these symmetric limit cycles C_2^{st1} and C_2^{st2} and chaotic attractors, which occur on the base of these cycles for another set of parameters, are hidden.

5. Conclusion

The dynamics of the Chua circuit gives a complex picture in the space of controlling parameters. The areas with similar behavior exist, and the detailed study of the dynamics of the Chua system in these areas allows one to reveal new hidden attractors. It is shown that the formation of hidden attractors is connected with the subcritical Hopf bifurcations of equilibrium points and the saddle-node bifurcations of the limit cycles. In general, the conjecture is that for a globally bounded autonomous system of ODE with asymptotically stable equilibrium point, the subcritical Hopf bifurcation leads to the birth of a hidden attractor. In two different areas of parameter plane it was found two types of hidden attractors, namely, merged and separated attractors. These features of hidden attractors are connected with the location of stable and unstable equilibria and with the associated with them unstable limit cycles in the phase space. The open questions are what is the maximum number of coexisting attractors[6] that can be exhibited in the Chua system (1) and how many of the coexisting attractors can be hidden.

Acknowledgments

This work was supported by the Russian Science Foundation project 14-21-00041 (sections 2.2-4). L.Chua's research is supported by grant no. AFOSR FA 9550-13-1-0136.

References

Aizerman, M. A. [1949] "On a problem concerning the stability in the large of dynamical systems," *Uspekhi Mat. Nauk (in Russian)* **4**, 187–188.

Alli-Oke, R., Carrasco, J., Heath, W. & Lanzon, A. [2012] "A robust Kalman conjecture for first-order plants," *IFAC Proceedings Volumes (IFAC-PapersOnline)* **7**, 27–32,

Bao, B., Hu, F., Chen, M., Xu, Q. & Yu, Y. [2015a] "Self-excited and hidden attractors found simultaneously in a modified Chua's circuit," *International Journal of Bifurcation and Chaos* **25**, art. num. 1550075.

Bao, B., Jiang, P., Wu, H. & Hu, F. [2015b] "Complex transient dynamics in periodically forced memristive Chua's circuit," *Nonlinear Dynamics* **79**, 2333–2343.

Bao, B. C., Li, Q. D., Wang, N. & Xu, Q. [2016] "Multistability in Chua's circuit with two stable node-foci," *Chaos: An Interdisciplinary Journal of Nonlinear Science* **26**, art. num. 043111.

Barabanov, N. E. [1988] "On the Kalman problem," *Sib. Math. J.* **29**, 333–341.

Bautin, N. N. [1939] "On the number of limit cycles generated on varying the coefficients from a focus or centre type equilibrium state," *Doklady Akademii Nauk SSSR (in Russian)* **24**, 668–671.

Belykh, V. & Chua, L. [1993] "A new type of strange attractor related to the Chua's circuit," *J. Circuits Syst. Comput.* **3**, 361–374.

Bernat, J. & Llibre, J. [1996] "Counterexample to Kalman and Markus-Yamabe conjectures in dimension larger than 3," *Dynamics of Continuous, Discrete and Impulsive Systems* **2**, 337–379.

Bilotta, E. & Pantano, P. [2008] *A gallery of Chua attractors*, Vol. Series A. 61 (World Scientific).

Borah, M. & Roy, B. K. [2017] "Hidden attractor dynamics of a novel non-equilibrium fractional-order chaotic system and its synchronisation control," *2017 Indian Control Conference (ICC)*, pp. 450–455.

Bragin, V., Vagaitsev, V., Kuznetsov, N. & Leonov, G. [2011] "Algorithms for finding hidden oscillations in nonlinear systems. The Aizerman and Kalman conjectures and Chua's circuits," *Journal of Computer and Systems Sciences International* **50**, 511–543.

Brzeski, P., Wojewoda, J., Kapitaniak, T., Kurths, J. & Perlikowski, P. [2017] "Sample-based approach can outperform the classical dynamical analysis - experimental confirmation of the basin stability method," *Scientific Reports* **7**, art. num. 6121.

[6]This question is related to the "chaotic" generalization [Leonov & Kuznetsov, 2015] of the second part of Hilbert's 16th problem *on the number and mutual disposition of attractors and repellers in the chaotic multidimensional dynamical systems and, in particular, their dependence on the degree of polynomials in the model*; see corresponding discussion, e.g. in [Sprott *et al.*, 2017; Zhang & Chen, 2017].

Burkin, I. & Khien, N. [2014] "Analytical-numerical methods of finding hidden oscillations in multidimensional dynamical systems," *Differential Equations* **50**, 1695–1717.

Chaudhuri, U. & Prasad, A. [2014] "Complicated basins and the phenomenon of amplitude death in coupled hidden attractors," *Physics Letters A* **378**, 713–718.

Chen, G. [2015] "Chaotic systems with any number of equilibria and their hidden attractors," *4th IFAC Conference on Analysis and Control of Chaotic Systems (plenary lecture)*, http://www.ee.cityu.edu.hk/~gchen/pdf/CHEN_IFAC2015.pdf.

Chen, G., Kuznetsov, N., Leonov, G. & Mokaev, T. [2017a] "Hidden attractors on one path: Glukhovsky-Dolzhansky, Lorenz, and Rabinovich systems," *International Journal of Bifurcation and Chaos* **27**, art. num. 1750115.

Chen, M., Li, M., Yu, Q., Bao, B., Xu, Q. & Wang, J. [2015a] "Dynamics of self-excited attractors and hidden attractors in generalized memristor-based Chua's circuit," *Nonlinear Dynamics* **81**, 215–226.

Chen, M., Xu, Q., Lin, Y. & Bao, B. [2017b] "Multistability induced by two symmetric stable node-foci in modified canonical Chua's circuit," *Nonlinear Dynamics* **87**, 789–802.

Chen, M., Yu, J. & Bao, B.-C. [2015b] "Finding hidden attractors in improved memristor-based Chua's circuit," *Electronics Letters* **51**, 462–464.

Chen, M., Yu, J. & Bao, B.-C. [2015c] "Hidden dynamics and multi-stability in an improved third-order Chua's circuit," *The Journal of Engineering*.

Chua, L. [1992a] "The genesis of Chua's circuit," *International Journal of Electronics and Communications* **46**, 250–257.

Chua, L. [1992b] "A zoo of strange attractors from the canonical Chua's circuits," *Proceedings of the IEEE 35th Midwest Symposium on Circuits and Systems (Cat. No.92CH3099-9)* **2**, 916–926.

Corinto, F. & Forti, M. [2017] "Memristor circuits: bifurcations without parameters," *IEEE Transactions on Circuits and Systems I: Regular Papers* **64**, 1540–1551.

Danca, M.-F. [2016] "Hidden transient chaotic attractors of Rabinovich–Fabrikant system," *Nonlinear Dynamics* **86**, 1263–1270.

Danca, M.-F., Kuznetsov, N. & Chen, G. [2017] "Unusual dynamics and hidden attractors of the Rabinovich–Fabrikant system," *Nonlinear Dynamics* **88**, 791–805.

Dudkowski, D., Jafari, S., Kapitaniak, T., Kuznetsov, N., Leonov, G. & Prasad, A. [2016] "Hidden attractors in dynamical systems," *Physics Reports* **637**, 1–50.

Ermentrout, B., G. [2002] *Simulating, Analyzing, and Animating Dynamical Systems: A Guide to XPPAUT for Researchers and Students* (SIAM, Philadelphia).

Feng, Y. & Pan, W. [2017] "Hidden attractors without equilibrium and adaptive reduced-order function projective synchronization from hyperchaotic Rikitake system," *Pramana* **88**, 62.

Fitts, R. E. [1966] "Two counterexamples to Aizerman's conjecture," *Trans. IEEE* **AC-11**, 553–556.

Gribov, A., Kanatnikov, A. & Krishchenko, A. [2016] "Localization method of compact invariant sets with application to the Chua system," *International Journal of Bifurcation and Chaos* **26**, art. num. 1650073.

Heath, W. P., Carrasco, J. & de la Sen, M. [2015] "Second-order counterexamples to the discrete-time Kalman conjecture," *Automatica* **60**, 140 – 144.

Hilbert, D. [1901-1902] "Mathematical problems." *Bull. Amer. Math. Soc.* , 437–479.

Hlavacka, M. & Guzan, M. [2017] "Hidden attractor and regions of attraction," *2017 27th International Conference Radioelektronika*, pp. 1–4.

Jafari, S., Pham, V.-T., Golpayegani, S., Moghtadaei, M. & Kingni, S. [2016] "The relationship between chaotic maps and some chaotic systems with hidden attractors," *Int. J. Bifurcat. Chaos* **26**, art. num. 1650211.

Jiang, H., Liu, Y., Wei, Z. & Zhang, L. [2016] "Hidden chaotic attractors in a class of two-dimensional maps," *Nonlinear Dynamics* **85**, 2719–2727.

Kalman, R. E. [1957] "Physical and mathematical mechanisms of instability in nonlinear automatic control systems," *Transactions of ASME* **79**, 553–566.

Kengne, J. [2017] "On the dynamics of Chua's oscillator with a smooth cubic nonlinearity: occurrence of multiple attractors," *Nonlinear Dynamics* **87**, 363–375.

Khalil, H. K. [2002] *Nonlinear Systems* (Prentice Hall, N.J).

Kiseleva, M., Kudryashova, E., Kuznetsov, N., Kuznetsova, O., Leonov, G., Yuldashev, M. & Yuldashev, R. [2017] "Hidden and self-excited attractors in Chua circuit: synchronization and SPICE simulation," *International Journal of Parallel, Emergent and Distributed Systems*.

Kiseleva, M., Kuznetsov, N. & Leonov, G. [2016] "Hidden attractors in electromechanical systems with and without equilibria," *IFAC-PapersOnLine* **49**, 51–55.

Krylov, N. & Bogolyubov, N. [1947] *Introduction to non-linear mechanics* (Princeton Univ. Press, Princeton).

Kuznetsov, A., Kuznetsov, S., Mosekilde, E. & Stankevich, N. [2015] "Co-existing hidden attractors in a radio-physical oscillator system," *Journal of Physics A: Mathematical and Theoretical* **48**, 125101.

Kuznetsov, A., Kuznetsov, S., Sataev, I. & Chua, L. [1993] "Two-parameter study of transition to chaos in Chua's circuit: renormalization group, universality and scaling," *International Journal of Bifurcation and Chaos* **3**, 943–962.

Kuznetsov, N. [2016] "Hidden attractors in fundamental problems and engineering models. A short survey," *Lecture Notes in Electrical Engineering* **371**, 13–25, (Plenary lecture at International Conference on Advanced Engineering Theory and Applications 2015).

Kuznetsov, N., Kuznetsova, O. & Leonov, G. [2013a] "Visualization of four normal size limit cycles in two-dimensional polynomial quadratic system," *Differential equations and dynamical systems* **21**, 29–34.

Kuznetsov, N., Kuznetsova, O., Leonov, G., Mokaev, T. & Stankevich, N. [2017a] "Hidden attractors localization in Chua circuit via the describing function method," *IFAC-PapersOnLine* Preprints of the 20th World Congress The International Federation of Automatic Control.

Kuznetsov, N., Kuznetsova, O., Leonov, G. & Vagaitsev, V. [2013b] "Analytical-numerical localization of hidden attractor in electrical Chua's circuit," *Lecture Notes in Electrical Engineering* **174**, 149–158.

Kuznetsov, N. & Leonov, G. [2014] "Hidden attractors in dynamical systems: systems with no equilibria, multistability and coexisting attractors," *IFAC Proceedings Volumes* **47**, 5445–5454.

Kuznetsov, N., Leonov, G., Mokaev, T. & Seledzhi, S. [2016] "Hidden attractor in the Rabinovich system, Chua circuits and PLL," *AIP Conference Proceedings* **1738**, art. num. 210008.

Kuznetsov, N., Leonov, G. & Stankevich, N. [2017b] "Synchronization of hidden chaotic attractors on the example of radiophysical oscillators," *IEEE* Progress In Electromagnetics Research Symposium (PIERS 2017). Preprints.

Kuznetsov, N., Leonov, G. & Vagaitsev, V. [2010] "Analytical-numerical method for attractor localization of generalized Chua's system," *IFAC Proceedings Volumes* **43**, 29–33, doi:10.3182/20100826-3-TR-4016.00009.

Leonov, G., Bragin, V. & Kuznetsov, N. [2010] "Algorithm for constructing counterexamples to the Kalman problem," *Doklady Mathematics* **82**, 540–542.

Leonov, G., Kiseleva, M., Kuznetsov, N. & Kuznetsova, O. [2015a] "Discontinuous differential equations: comparison of solution definitions and localization of hidden Chua attractors," *IFAC-PapersOnLine* **48**, 408–413.

Leonov, G. & Kuznetsov, N. [2009] "Localization of hidden oscillations in dynamical systems (plenary lecture)," *4th International Scientific Conference on Physics and Control*, URL http://www.math.spbu.ru/user/leonov/publications/2009-PhysCon-Leonov-plenary-hidden-oscillations.pdf\#page=21.

Leonov, G. & Kuznetsov, N. [2011] "Algorithms for searching for hidden oscillations in the Aizerman and Kalman problems," *Doklady Mathematics* **84**, 475–481.

Leonov, G. & Kuznetsov, N. [2013] "Hidden attractors in dynamical systems. From hidden oscillations in Hilbert-Kolmogorov, Aizerman, and Kalman problems to hidden chaotic attractors in Chua circuits," *International Journal of Bifurcation and Chaos* **23**, art. no. 1330002.

Leonov, G. & Kuznetsov, N. [2015] "On differences and similarities in the analysis of Lorenz, Chen, and Lu systems," *Applied Mathematics and Computation* **256**, 334–343.

Leonov, G., Kuznetsov, N. & Mokaev, T. [2015b] "Homoclinic orbits, and self-excited and hidden attractors in a Lorenz-like system describing convective fluid motion," *Eur. Phys. J. Special Topics* **224**, 1421–1458.

Leonov, G., Kuznetsov, N. & Vagaitsev, V. [2011] "Localization of hidden Chua's attractors," *Physics*

Letters A **375**, 2230–2233.

Leonov, G., Kuznetsov, N. & Vagaitsev, V. [2012] "Hidden attractor in smooth Chua systems," *Physica D: Nonlinear Phenomena* **241**, 1482–1486.

Li, C. & Sprott, J. C. [2014] "Coexisting hidden attractors in a 4-D simplified Lorenz system," *International Journal of Bifurcation and Chaos* **24**, art. num. 1450034.

Li, Q., Zeng, H. & Yang, X.-S. [2014] "On hidden twin attractors and bifurcation in the Chua's circuit," *Nonlinear Dynamics* **77**, 255–266.

Lozi, R. & Ushiki, S. [1993] "The theory of confinors in Chua's circuit: accurate analysis of bifurcations and attractors," *International Journal of Bifurcation and chaos* **3**, 333–361.

Menacer, T., Lozi, R. & Chua, L. [2016] "Hidden bifurcations in the multispiral Chua attractor," *International Journal of Bifurcation and Chaos* **26**, art. num. 1630039.

Messias, M. & Reinol, A. [2017] "On the formation of hidden chaotic attractors and nested invariant tori in the Sprott A system," *Nonlinear Dynamics* **88**, 807–821.

Nekorkin, V. & Chua, L. [1993] "Spatial disorder and wave fronts in a chain of coupled Chua's circuits," *International Journal of Bifurcation and Chaos* **03**, 1281–1291.

Ojoniyi, O. S. & Njah, A. N. [2016] "A 5D hyperchaotic Sprott B system with coexisting hidden attractors," *Chaos, Solitons & Fractals* **87**, 172 – 181.

Pham, V.-T., Rahma, F., Frasca, M. & Fortuna, L. [2014] "Dynamics and synchronization of a novel hyperchaotic system without equilibrium," *International Journal of Bifurcation and Chaos* **24**, art. num. 1450087.

Pham, V.-T., Volos, C., Jafari, S., Vaidyanathan, S., Kapitaniak, T. & Wang, X. [2016] "A chaotic system with different families of hidden attractors," *International Journal of Bifurcation and Chaos* **26**, 1650139.

Pliss, V. A. [1958] *Some Problems in the Theory of the Stability of Motion (in Russian)* (Izd LGU, Leningrad).

Rocha, R. & Medrano-T, R.-O. [2015] "Stablity analysis and mapping of multiple dynamics of Chua's circuit in full-four parameter space," *International Journal of Bifurcation and Chaos* **25**, 1530037.

Rocha, R. & Medrano-T, R. O. [2016] "Finding hidden oscillations in the operation of nonlinear electronic circuits," *Electronics Letters* **52**, 1010–1011.

Rocha, R., Ruthiramoorthy, J. & Kathamuthu, T. [2017] "Memristive oscillator based on Chua's circuit: stability analysis and hidden dynamics," *Nonlinear Dynamics* **88**, 25772587.

Saha, P., Saha, D., Ray, A. & Chowdhury, A. [2015] "Memristive non-linear system and hidden attractor," *European Physical Journal: Special Topics* **224**, 1563–1574.

Semenov, V., Korneev, I., Arinushkin, P., Strelkova, G., Vadivasova, T. & Anishchenko, V. [2015] "Numerical and experimental studies of attractors in memristor-based Chua's oscillator with a line of equilibria. Noise-induced effects," *European Physical Journal: Special Topics* **224**, 1553–1561.

Shilnikov, L., Shilnikov, A., Turaev, D. & Chua, L. [2001] *Methods of Qualitative Theory in Nonlinear Dynamics: Part 2* (World Scientific).

Singh, J. & Roy, B. [2017] "Second order adaptive time varying sliding mode control for synchronization of hidden chaotic orbits in a new uncertain 4-D conservative chaotic system," *Transactions of the Institute of Measurement and Control*.

Sommerfeld, A. [1902] "Beitrage zum dynamischen ausbau der festigkeitslehre," *Zeitschrift des Vereins deutscher Ingenieure* **46**, 391–394.

Sprott, J. C., Jafari, S., Khalaf, A. & Kapitaniak, T. [2017] "Megastability: Coexistence of a countable infinity of nested attractors in a periodically-forced oscillator with spatially-periodic damping," *The European Physical Journal Special Topics* **226**, 1979–1985.

Volos, C., Pham, V.-T., Zambrano-Serrano, E., Munoz-Pacheco, J. M., Vaidyanathan, S. & Tlelo-Cuautle, E. [2017] "Analysis of a 4-D hyperchaotic fractional-order memristive system with hidden attractors," *Advances in Memristors, Memristive Devices and Systems* (Springer), pp. 207–235.

Wei, Z., Moroz, I., Sprott, J., Akgul, A. & Zhang, W. [2017] "Hidden hyperchaos and electronic circuit application in a 5D self-exciting homopolar disc dynamo," *Chaos* **27**, art. num. 033101.

Wei, Z., Pham, V.-T., Kapitaniak, T. & Wang, Z. [2016] "Bifurcation analysis and circuit realization

for multiple-delayed Wang–Chen system with hidden chaotic attractors," *Nonlinear Dynamics* **85**, 1635–1650.

Zelinka, I. [2016] "Evolutionary identification of hidden chaotic attractors," *Engineering Applications of Artificial Intelligence* **50**, 159–167.

Zhang, G., Wu, F., Wang, C. & Ma, J. [2017] "Synchronization behaviors of coupled systems composed of hidden attractors," *International Journal of Modern Physics B* **31**, art. num. 1750180.

Zhang, X. & Chen, G. [2017] "Constructing an autonomous system with infinitely many chaotic attractors," *Chaos: An Interdisciplinary Journal of Nonlinear Science* **27**, art. num. 071101.

Zhao, H., Lin, Y. & Dai, Y. [2017] "Hopf bifurcation and hidden attractor of a modified Chua's equation," *Nonlinear Dynamics*. doi: 10.1007/s11071-017-3777-6.

Zhusubaliyev, Z., Mosekilde, E., Churilov, A. & Medvedev, A. [2015] "Multistability and hidden attractors in an impulsive Goodwin oscillator with time delay," *European Physical Journal: Special Topics* **224**, 1519–1539.

PII

HIDDEN ATTRACTORS LOCALIZATION IN CHUA CIRCUIT VIA THE DESCRIBING FUNCTION METHOD

by

N. V. Kuznetsov, O. A. Kuznetsova, G. A. Leonov, T. N. Mokaev,
N. V. Stankevich 2017

IFAC PapersOnLine, Vol.50, Issue 1, pp.2651-2656

Available online at www.sciencedirect.com

ScienceDirect

IFAC PapersOnLine 50-1 (2017) 2651–2656

IFAC Papers Online
CONFERENCE PAPER ARCHIVE

Hidden attractors localization in Chua circuit via the describing function method

N.V. Kuznetsov [*,***], **O.A. Kuznetsova** [*], **G.A. Leonov** [*,**], **T.N. Mokaev** [*], **N.V. Stankevich** [***,****]

[*] *Faculty of Mathematics and Mechanics, St. Petersburg State University, Russia*
[**] *Institute of Problems of Mechanical Engineering RAS, Russia*
[***] *Dept. of Mathematical Information Technology, University of Jyväskylä, Finland*
[****] *Faculty of Electronics and Instrumentation, Saratov State Technical University, Russia*

Abstract: In this paper the Chua circuit with five linear elements and saturation non-linearity is studied. Numerical localization of self-excited attractor in the Chua circuit model can be done by computation of trajectory with initial data in a vicinity of an unstable equilibrium. For a hidden attractor its basin of attraction does not overlap with a small vicinity of equilibria, so it is difficult to find the corresponding initial data for localization. This survey is devoted to the application of describing function method for localization of hidden periodic and chaotic attractors in the Chua model. We use a rigorous justification of the describing function method, based on the method of small parameter, to get the initial data for the visualization of the hidden attractors. A new configuration of hidden Chua attractors is presented.

Keywords: Chua circuit, hidden attractor, self-excited attractor, describing function method

1. INTRODUCTION

In the initial period of the development of the theory of nonlinear oscillations (first half of the XX century) main attention of researchers was paid to analysis and synthesis of oscillating systems for which the oscillation existence problem can be solved relatively easily. The structure of many applied systems considered was such that the existence of oscillations was "almost obvious" - the oscillation was excited from an unstable equilibrium (so called *self-excited oscillation*). From a computational point of view this allows one to use a *standard computational procedure*, in which after a transient process a trajectory, started from a point of unstable manifold in a neighborhood of equilibrium, reaches a state of oscillation, therefore one can easily identify it. The use of the term *self-excited oscillation* or *self-oscillations* can be traced back to the works of H.G. Barkhausen and A.A. Andronov, where it describes the generation and maintenance of a periodic motion in mechanical and electrical models by a source of power that lacks any corresponding periodicity (e.g., a stable limit cycle in the van der Pol oscillator) (Andronov et al., 1966; Jenkins, 2013).

Attractor is called a *self-excited attractor* if its basin of attraction intersects any arbitrarily small open neighborhood of an equilibrium, otherwise it is called a *hidden attractor* (Leonov et al., 2011, 2012; Leonov and Kuznetsov, 2013; Leonov et al., 2015; Kuznetsov, 2016). We use the notion "self-excited" for attractors of dynamical systems to describe the existence of transient process from a small vicinity of an unstable equilibrium to an attractor.

If there is no such a transient process for an attractor, it is called a hidden attractor. For example, hidden attractors are attractors in systems without equilibria or with only one stable equilibrium (a special case of multistability and coexistence of attractors). Some examples of hidden attractors can be found in Shahzad et al. (2015); Brezetskyi et al. (2015); Jafari et al. (2015); Zhusubaliyev et al. (2015); Saha et al. (2015); Semenov et al. (2015); Feng and Wei (2015); Li et al. (2015); Feng et al. (2015); Sprott (2015); Pham et al. (2015); Vaidyanathan et al. (2015); Danca (2016); Zelinka (2016); Dudkowski et al. (2016); Kuznetsov et al. (2017); Danca et al. (2017); Kiseleva et al. (2016).

The *self-excited and hidden classification of attractors* was introduced by Leonov and Kuznetsov in connection with the discovery of hidden chaotic attractor in the Chua system (Kuznetsov et al., 2010; Leonov et al., 2011; Kuznetsov et al., 2013):

$$\begin{aligned} \dot{x} &= \alpha(y - x(m_1 + 1)) - \alpha\psi(x), \\ \dot{y} &= x - y + z, \\ \dot{z} &= -(\beta y + \gamma z), \\ \psi(x) &= (m_0 - m_1)\,\mathrm{sat}(x) = \\ &= \frac{1}{2}(m_0 - m_1)(|x+1| - |x-1|), \end{aligned} \tag{1}$$

where α, β, γ, m_0, m_1 are parameters. This system provides a mathematical model, describing the behavior of the Chua circuit (Chua and Lin, 1990; Chua, 1992, 1995) with five linear elements and saturation non-linearity (see Fig. 1). Until this discovery only self-excited chaotic attractors had been found in Chua circuits (see Fig. 2

2405-8963
Peer review under responsibility of International Federation of Automatic Control.
10.1016/j.ifacol.2017.08.470

and, e.g. works (Matsumoto, 1990; Lozi and Ushiki, 1993; Bilotta and Pantano, 2008)). Note that L. Chua himself, analyzing various cases of attractors existence in Chua circuit, does not admit the existence of hidden attractor in his circuits (Chua, 1992).

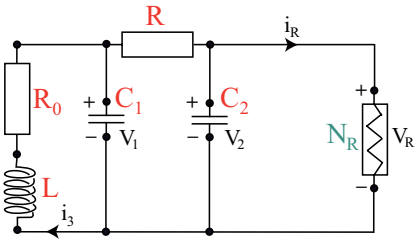

Fig. 1. Chua circuit with two resistors, one inductor, two capacitors (red) and one nonlinear resistor called "Chua diode" (green).

We consider only one type of the Chua circuits, while there are known various modifications of Chua circuit (see, e.g. (Banerjee, 2012; Semenov et al., 2015)) where hidden oscillations can also be localized (Chen et al., 2015b; Bao et al., 2015; Chen et al., 2015a; Menacer et al., 2016).

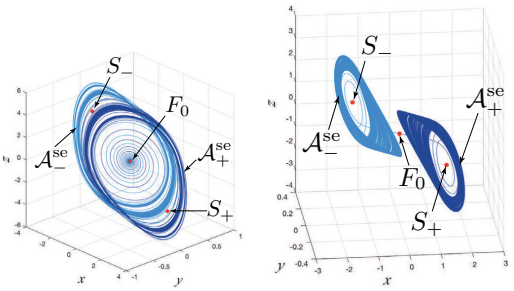

(a) Parameters $\alpha = 15$, $\beta = 28$, $\gamma = 0$, $m_0 = -5/7$, $m_1 = -8/7$. **(b)** Parameters $\alpha = 8.5$, $\beta = 14.28$, $\gamma = 0$, $m_0 = -8/7$, $m_1 = -5/7$.

Fig. 2. Self-excited attractors in Chua system (1): (2a) – two symmetric spiral attractors, (2b) – two symmetric Rössler-like attractors.

2. HIDDEN ATTRACTORS LOCALIZATION VIA DESCRIBING FUNCTION METHOD

In this section an effective analytical-numerical approach for hidden oscillations localization, based on the describing function method (DFM), the method of small parameter and continuation method, is demonstrated.

2.1 Describing function method

The describing function method (DFM) is a searching method for oscillations which are close to the harmonic periodic oscillations of nonlinear systems of automatic control. This method is *not strictly mathematically justified* and is one of approximate methods of analysis of control systems (see, e.g. (Krylov and Bogolyubov, 1947; Khalil, 2002)). One of the first examples, where the describing function method gives untrue results, is due to Tsypkin (1984). Remark that well-known Aizerman's and Kalman's conjectures on the absolute stability of nonlinear control systems are valid from the standpoint of the describing function method (what explains why these conjectures were put forward). Nowadays various counterexamples to these conjectures (nonlinear systems where the only equilibrium, which is stable, coexists with a hidden periodic oscillation) are known (see, e.g. Pliss (1958); Fitts (1966); Barabanov (1988); Bernat and Llibre (1996); Leonov et al. (2010); Bragin et al. (2011); Leonov and Kuznetsov (2011, 2013); the corresponding discrete examples are considered in Alli-Oke et al. (2012); Heath et al. (2015)).

Let us recall a classical way of applying the DFM. Consider a system with one scalar non-linearity in the Lur'e form

$$\frac{d\mathbf{x}}{dt} = \mathbf{P}\mathbf{x} + \mathbf{q}\psi(\mathbf{r}^*\mathbf{x}), \quad \mathbf{x} \in \mathbb{R}^n \tag{2}$$

where $\mathbf{P}$ is a constant $(n \times n)$-matrix, $\mathbf{q}, \mathbf{r}$ are constant n-dimensional vectors, * denotes transpose operation, $\psi(\sigma)$ is a continuous piecewise-differentiable scalar function, and $\psi(0) = 0$.

In order to find a periodic oscillation, a certain coefficient of harmonic linearization k (assume that such k exists) is introduced in such a way that the matrix $\mathbf{P}_0 = \mathbf{P} + k\mathbf{q}\mathbf{r}^*$ of the linear system

$$\frac{d\mathbf{x}}{dt} = \mathbf{P}_0\mathbf{x}, \quad \mathbf{x} \in \mathbb{R}^n$$

has a pair of pure-imaginary eigenvalues $\pm i\omega_0 (\omega_0 > 0)$, and the rest eigenvalues have negative real parts.

Introduce a transfer function

$$W(p) = \mathbf{r}^*\big(\mathbf{P} - p\mathbf{I}\big)^{-1}\mathbf{q}, \tag{3}$$

where p is a complex variable, $\mathbf{I}$ is a unit matrix. Transfer function $W(p)$ is applied to define the values of k and ω_0. The number $\omega_0 > 0$ is defined from the equation

$$\operatorname{Im} W(i\,\omega_0) = 0 \tag{4}$$

and k is defined by the formula

$$k = -\big(\operatorname{Re} W(i\,\omega_0)\big)^{-1}. \tag{5}$$

If such ω_0 and k exist, then system (2) has a periodic solution $\mathbf{x}(t)$ for which

$$\sigma(t) = \mathbf{r}^*\mathbf{x}(t) \approx a\cos\omega_0 t.$$

Following the DFM, the amplitude a can be obtained from the equation

$$\int_0^{2\pi/\omega_0} \big(\psi(a\cos\omega_0 t)a\cos\omega_0 t - k(a\cos\omega_0 t)^2\big)dt = 0.$$

Rewrite system (2) as follows

$$\frac{d\mathbf{x}}{dt} = \mathbf{P_0}\mathbf{x} + \mathbf{q}\varphi(\mathbf{r}^*\mathbf{x}), \tag{6}$$

where $\varphi(\sigma) = \psi(\sigma) - k\sigma$. As it is mentioned above classical DFM is not strictly mathematically justified and can lead to untrue results, however for the systems with a small parameter it can be rigorously justified. For that let us change $\varphi(\sigma)$ by $\varepsilon\varphi(\sigma)$ and consider the existence of a periodic solution for system

$$\frac{d\mathbf{x}}{dt} = \mathbf{P_0}\mathbf{x} + \varepsilon\mathbf{q}\varphi^0(\mathbf{r}^*\mathbf{x}). \tag{7}$$

To define the initial data $\mathbf{x}^0(0)$ of the periodic solution, system (7) is transformed by a linear non-singular transformation $\mathbf{x} = \mathbf{S}\mathbf{y}$ to the form [1]

$$\begin{aligned} \dot{y}_1 &= -\omega_0 y_2 + \varepsilon b_1 \varphi(y_1 + \mathbf{c}_3^* \mathbf{y}_3), \\ \dot{y}_2 &= \omega_0 y_1 + \varepsilon b_2 \varphi(y_1 + \mathbf{c}_3^* \mathbf{y}_3), \\ \dot{\mathbf{y}}_3 &= \mathbf{A}_3 \mathbf{y}_3 + \varepsilon \mathbf{b}_3 \varphi(y_1 + \mathbf{c}_3^* \mathbf{y}_3), \end{aligned} \tag{8}$$

where y_1, y_2 are scalars, $\mathbf{y}_3$, $\mathbf{b}_3$ and $\mathbf{c}_3$ are $(n-2)$-dimensional vectors, b_1 and b_2 are real numbers; $\mathbf{A}_3$ is a constant $((n-2)\times(n-2))$ matrix all eigenvalues of which have negative real parts. Without loss of generality, it can be assumed that for the matrix $\mathbf{A}_3$ there exists a positive number $d > 0$, such that $\mathbf{y}_3^*(\mathbf{A}_3 + \mathbf{A}_3^*)\mathbf{y}_3 \le -2d|\mathbf{y}_3|^2$, $\forall\, \mathbf{y}_3 \in \mathbb{R}^{n-2}$.

Introduce the describing function

$$\Phi(a) = \int_0^{2\pi/\omega_0} \varphi(\cos(\omega_0 t)a)\cos(\omega_0 t)dt \tag{9}$$

and assume the existence of its derivative.

Theorem 1. [Leonov and Kuznetsov (2013)] If there exists a positive number a_0 such that

$$\Phi(a_0) = 0, \quad b_1 \frac{d\Phi(a)}{da}\bigg|_{a=a_0} < 0, \tag{10}$$

then system (7) has a stable periodic solution with initial data

$$\mathbf{x}^0(0) = \mathbf{S}\left(y_1(0),\, y_2(0),\, y_3(0)\right)^*,$$

where $y_1(0) = a_0 + O(\varepsilon)$, $y_2(0) = 0$, $\mathbf{y}_3 = \mathbf{O}_{n-2}(\varepsilon)$ and with the period $T = \frac{2\pi}{\omega_0} + O(\varepsilon)$.

3. HIDDEN ATTRACTORS LOCALIZATION IN CHUA CIRCUIT VIA THE DESCRIBING FUNCTION METHOD

In this section we apply the above approach for hidden attractors localization in Chua circuit. Let us write Chua system (1) in the Lur'e form (2) (see, e.g. (Leonov et al., 2011)) with

$$\begin{aligned} &\mathbf{P} = \begin{pmatrix} -\alpha(m_1+1) & \alpha & 0 \\ 1 & -1 & 1 \\ 0 & -\beta & -\gamma \end{pmatrix}, \mathbf{q} = \begin{pmatrix} -\alpha \\ 0 \\ 0 \end{pmatrix}, \\ &\mathbf{r} = \begin{pmatrix} 1 \\ 0 \\ 0 \end{pmatrix}, \quad \psi(\sigma) = (m_0 - m_1)\,\mathrm{sat}(\sigma). \end{aligned} \tag{11}$$

Introduce a coefficient k and a small parameter ε, and represent (11) in the form (7) with

$$\begin{aligned} &\mathbf{P_0} = \mathbf{P} + k\mathbf{q}\mathbf{r}^* = \begin{pmatrix} -\alpha(m_1+1+k) & \alpha & 0 \\ 1 & -1 & 1 \\ 0 & -\beta & -\gamma \end{pmatrix}, \\ &\varphi(\sigma) = \psi(\sigma) - k\sigma = (m_0 - m_1)\,\mathrm{sat}(\sigma) - k\sigma, \end{aligned} \tag{12}$$

and $\lambda_{1,2}^{\mathbf{P}_0} = \pm i\omega_0$, $\lambda_3^{\mathbf{P}_0} = -d < 0$.

By the non-singular linear transformation $\mathbf{x} = \mathbf{S}\mathbf{y}$ system (12) is reduced to the form (8)

$$\frac{d\mathbf{y}}{dt} = \mathbf{A}\mathbf{y} + \mathbf{b}\varepsilon\varphi(\mathbf{u}^*\mathbf{y}), \tag{13}$$

[1] Such transformation exists for non-degenerate transfer functions.

where

$$\mathbf{A} = \begin{pmatrix} 0 & -\omega_0 & 0 \\ \omega_0 & 0 & 0 \\ 0 & 0 & -d \end{pmatrix}, \ \mathbf{b} = \begin{pmatrix} b_1 \\ b_2 \\ 1 \end{pmatrix}, \ \mathbf{c} = \begin{pmatrix} 1 \\ 0 \\ -h \end{pmatrix}.$$

The transfer function $W_{\mathbf{A}}(p)$ of system (13) can be represented as

$$W_{\mathbf{A}}(p) = \frac{-b_1 p + b_2\omega_0}{p^2 + \omega_0^2} + \frac{h}{p+d}.$$

Further, using the equality of transfer functions of systems (12) and (13) one can obtain

$$W_{\mathbf{A}}(p) = \mathbf{r}^*(\mathbf{P}_0 - p\mathbf{I})^{-1}\mathbf{q}.$$

This implies the following relations

$$\begin{aligned} k &= \frac{-\alpha(m_1 + m_1\gamma + \gamma) + \omega_0^2 - \gamma - \beta}{\alpha(1+\gamma)}, \\ d &= \frac{\alpha + \omega_0^2 - \beta + 1 + \gamma + \gamma^2}{1+\gamma}, \\ h &= \frac{\alpha(\gamma + \beta - (1+\gamma)d + d^2)}{\omega_0^2 + d^2}, \\ b_1 &= \frac{\alpha(\gamma + \beta - \omega_0^2 - (1+\gamma)d)}{\omega_0^2 + d^2}, \\ b_2 &= \frac{\alpha\big((1+\gamma-d)\omega_0^2 + (\gamma+\beta)d\big)}{\omega_0(\omega_0^2 + d^2)}. \end{aligned} \tag{14}$$

Since by the non-singular linear transformation $\mathbf{x} = \mathbf{S}\mathbf{y}$ system (12) can be reduced to the form (13) for the matrix $\mathbf{S}$ the following relations

$$\mathbf{A} = \mathbf{S}^{-1}\mathbf{P_0}\mathbf{S}, \quad \mathbf{b} = \mathbf{S}^{-1}\mathbf{q}, \quad \mathbf{c}^* = \mathbf{r}^*\mathbf{S}. \tag{15}$$

are valid. After solving these matrix equations, one can obtain the transformation matrix

$$\mathbf{S} = \begin{pmatrix} s_{11} & s_{12} & s_{13} \\ s_{21} & s_{22} & s_{23} \\ s_{31} & s_{32} & s_{33} \end{pmatrix},$$

where

$$\begin{aligned} s_{11} &= 1, \qquad s_{12} = 0, \qquad s_{13} = -h, \\ s_{21} &= m_1 + 1 + k, \qquad s_{22} = -\frac{\omega_0}{\alpha}, \\ s_{23} &= -\frac{h(\alpha(m_1+1+k) - d)}{\alpha}, \\ s_{31} &= \frac{\alpha(m_1+k) - \omega_0^2}{\alpha}, \\ s_{32} &= -\frac{\alpha(\beta+\gamma)(m_1+k) + \alpha\beta - \gamma\omega_0^2}{\alpha\omega_0}, \\ s_{33} &= h\frac{\alpha(m_1+k)(d-1) + d(1+\alpha-d)}{\alpha}. \end{aligned}$$

Using Theorem 1 one obtains the initial data

$$\mathbf{x}(0) = \mathbf{S}\mathbf{y}(0) = \mathbf{S}\begin{pmatrix} a_0 \\ 0 \\ 0 \end{pmatrix} = \begin{pmatrix} a_0\, s_{11} \\ a_0\, s_{21} \\ a_0\, s_{31} \end{pmatrix}. \tag{16}$$

Back to Chua system denotations, for the determination of the initial data of starting solution for multistage procedure, it can be obtained

$$\begin{aligned} &x(0) = a_0, \quad y(0) = a_0(m_1 + 1 + k), \\ &z(0) = a_0\,\frac{\alpha(m_1+k) - \omega_0^2}{\alpha}. \end{aligned} \tag{17}$$

Consider system (1) with the parameters

$$\alpha = 8.4562, \quad \beta = 12.0732, \quad \gamma = 0.0052, \\ m_0 = -0.1768, \quad m_1 = -1.1468. \tag{18}$$

Note that for the considered values of parameters there are three equilibria in the system: the zero equilibrium $F_0 = (0, 0, 0)$ is a stable focus-node and two symmetric equilibria

$$S_\pm = \pm\left(\frac{m_1 - m_0}{m_1 + \frac{\beta}{\beta+\gamma}}, \frac{\gamma(m_1 - m_0)}{(\gamma+\beta)m_1 + \beta}, -\frac{\beta(m_1 - m_0)}{(\gamma+\beta)m_1 + \beta}\right)$$

are saddle-foci with one-dimensional unstable manifolds.

Let us try to apply the DFM and define an initial data for periodic oscillation. Using (4) and (5) for parameters (18) one obtains following starting frequency and a coefficient of harmonic:

$$\omega_0 = 2.0392, \quad k = 0.2098. \tag{19}$$

Assuming $a \geq 1$, describing function (9) and its derivative for Chua system (1) can be rewritten as follows:

$$\Phi(a) = 2(m_0 - m_1)\left[\frac{\pi a}{2} + \sqrt{1 - \frac{1}{a^2}} - a \arccos\frac{1}{a}\right] - \pi a k,$$

$$\frac{d\Phi(a)}{da} = 2(m_0 - m_1)\left[\frac{\pi}{2} - \frac{1}{a}\sqrt{1 - \frac{1}{a^2}} - \arccos\frac{1}{a}\right] - \pi k.$$

For parameters (18) and (19) one obtains initial amplitude $a_0 = 5.8576$ that satisfies the conditions of Theorem 1. Thus, by (17) initial data for the oscillation are as follows

$$x(0) = 5.8576, \quad y(0) = 0.3694, \quad z(0) = -8.3686. \tag{20}$$

In our numerical experiments we skip the multistep procedure based on the small parameter method and apply initial data (20) for hidden attractors localization in the initial system (i.e., system (1) in the form (6), $\varepsilon = 1$). It turns out that in this case this is enough for localization of two symmetric hidden chaotic attractors $\mathcal{A}^{\text{hid}}_\pm$ in the Chua system (see Fig. 3). For attractor $\mathcal{A}^{\text{hid}}_-$ one should take symmetric initial data $x(0) = -5.8576$ $y(0) = -0.3694$, $z(0) = 8.3686$.

Consider system (1) with another values of the parameters

$$\alpha = 8.4, \quad \beta = 12, \quad \gamma = -0.005, \\ m_0 = -1.2, \quad m_1 = -0.05. \tag{21}$$

Note that for the considered values of parameters the zero equilibrium F_0 is a saddle-focus with one-dimensional unstable manifold and two symmetric equilibria $S_\pm$ are stable focus-nodes. Again let us apply the DFM and define an initial data for periodic oscillation. Note that equation (4) for parameters (21) has two positive solutions and by (5) we obtain following starting frequencies and coefficients of harmonic:

$$\omega_0 = 2.0260, \quad k = -0.8890 \tag{22}$$

and

$$\omega_0 = 3.2396, \quad k = -0.1244. \tag{23}$$

For parameters (21) and (22) one obtains initial amplitude $a_0 = 1.5187$ that satisfies the conditions of Theorem 1. Thus, by (17) initial data for the oscillation are as follows

$$x(0) = 1.5187, \quad y(0) = 0.0926, \quad z(0) = -2.1682. \tag{24}$$

Using these initial data for original system (1) it is possible to localize two symmetric hidden chaotic attractors $\mathcal{A}^{\text{hid}}_\pm$ (see Fig 4).

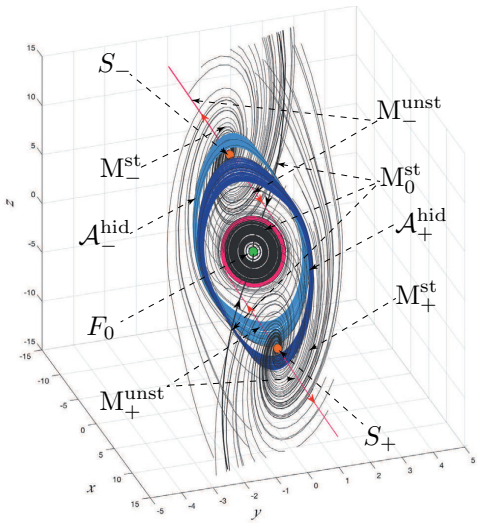

Fig. 3. Two symmetric hidden chaotic attractors ($\mathcal{A}^{\text{hid}}_\pm$ - blue domains) in the classical Chua system (1): trajectories (red) from unstable manifolds $\mathrm{M}^{\mathrm{unst}}_\pm$ of two saddle points $S_\pm$ are either attracted to locally stable zero equilibrium F_0, or tend to infinity; trajectories (black) from stable manifolds $\mathrm{M}^{\mathrm{st}}_{0,\pm}$ tend to F_0 or $S_\pm$; $\alpha = 8.4562$, $\beta = 12.0732$, $\gamma = 0.0052$, $m_0 = -0.1768$, $m_1 = -1.1468$.

For parameters (21) and (23) one obtains initial amplitude $a_0 = 11.7546$ (also satisfies the conditions of Theorem 1) which by (17) yields the following initial data

$$x(0) = 11.7546, \; y(0) = 9.7044, \; z(0) = -16.7367. \tag{25}$$

These initial data for original Chua system (1) allows to localize a hidden periodic attractor: stable limit cycle $\mathcal{A}^{\text{hid}}_{\text{limCyc}}$ (see Fig. 5). Thus, in this configuration despite the trivial attractors, i.e. equilibria $S_\pm$, for system (1) with parameters (21) we obtain the co-existence of hidden periodic attractor (stable limit cycle) and two symmetric hidden chaotic attractors.

CONCLUSIONS

In this paper we discuss the use of describing function method for searching periodic oscillations in its application to the famous Chua circuit. Despite the fact that DFM is an approximate analytical method (which does not guarantee the true results), the application of DFM to the Chua system allows us to localize hidden chaotic and periodic attractors. In particular, for certain values of parameters we obtain a new configuration of co-existing hidden attractors (two symmetric chaotic and stable limit cycle) in the Chua system.

4. ACKNOWLEDGMENTS

This work was supported by the Russian Science Foundation (14-21-00041p).

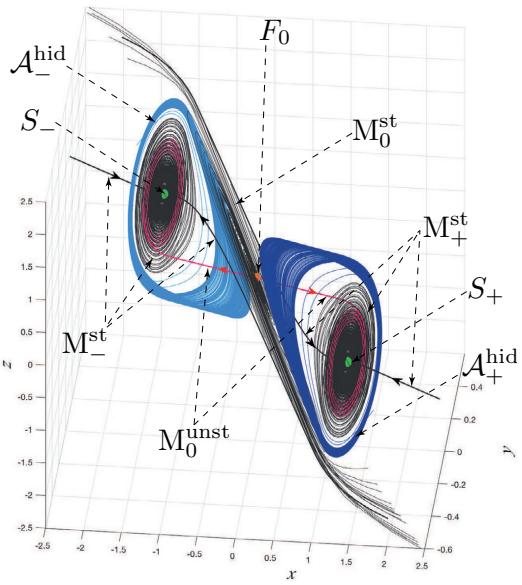

Fig. 4. Two symmetric hidden chaotic attractors ($\mathcal{A}^{\rm hid}_{\pm}$ - blue domains) in the classical Chua system (1): trajectories (red) from unstable manifold $\mathrm{M}^{\rm unst}_0$ of the saddle points F_0 are attracted to locally stable equilibria $S_{\pm}$; trajectories (black) from stable manifolds $\mathrm{M}^{\rm st}_{0,\pm}$ are attracted to F_0 or $S_{\pm}$; $\alpha = 8.4$, $\beta = 12$, $\gamma = -0.005$, $m_0 = -1.2$, $m_1 = -0.05$.

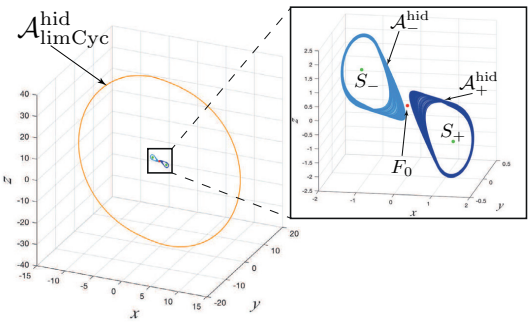

Fig. 5. Co-existence of hidden periodic attractor: the stable limit cycle $\mathcal{A}^{\rm hid}_{\rm limCyc}$, and two symmetric hidden chaotic attractors $\mathcal{A}^{\rm hid}_{\pm}$ in Chua system (1) with parameters $\alpha = 8.4$, $\beta = 12$,$\gamma = -0.005$, $m_0 = -1.2$, $m_1 = -0.05$.

REFERENCES

Alli-Oke, R., Carrasco, J., Heath, W., and Lanzon, A. (2012). A robust Kalman conjecture for first-order plants. *IFAC Proceedings Volumes (IFAC-PapersOnline)*, 7, 27–32. doi:10.3182/20120620-3-DK-2025.00161.

Andronov, A.A., Vitt, E.A., and Khaikin, S.E. (1966). *Theory of Oscillators*. Pergamon Press, Oxford.

Banerjee, T. (2012). Single amplifier biquad based inductor-free Chua's circuit. *Nonlinear Dynamics*, 68, 565–573.

Bao, B., Hu, F., Chen, M., Xu, Q., and Yu, Y. (2015). Self-excited and hidden attractors found simultaneously in a modified Chua's circuit. *International Journal of Bifurcation and Chaos*, 25(05). doi: 10.1142/S0218127415500753. art. num. 1550075.

Barabanov, N.E. (1988). On the Kalman problem. *Sib. Math. J.*, 29(3), 333–341.

Bernat, J. and Llibre, J. (1996). Counterexample to Kalman and Markus-Yamabe conjectures in dimension larger than 3. *Dynamics of Continuous, Discrete and Impulsive Systems*, 2(3), 337–379.

Bilotta, E. and Pantano, P. (2008). *A gallery of Chua attractors*, volume Series A. 61. World Scientific.

Bragin, V., Vagaitsev, V., Kuznetsov, N., and Leonov, G. (2011). Algorithms for finding hidden oscillations in nonlinear systems. The Aizerman and Kalman conjectures and Chua's circuits. *Journal of Computer and Systems Sciences International*, 50(4), 511–543. doi: 10.1134/S106423071104006X.

Brezetskyi, S., Dudkowski, D., and Kapitaniak, T. (2015). Rare and hidden attractors in van der Pol-Duffing oscillators. *European Physical Journal: Special Topics*, 224(8), 1459–1467.

Chen, M., Li, M., Yu, Q., Bao, B., Xu, Q., and Wang, J. (2015a). Dynamics of self-excited attractors and hidden attractors in generalized memristor-based Chua's circuit. *Nonlinear Dynamics*, 81, 215–226.

Chen, M., Yu, J., and Bao, B.C. (2015b). Hidden dynamics and multi-stability in an improved third-order Chua's circuit. *The Journal of Engineering*. doi: 10.1049/joe.2015.0149.

Chua, L. (1992). A zoo of strange attractors from the canonical Chua's circuits. *Proceedings of the IEEE 35th Midwest Symposium on Circuits and Systems (Cat. No.92CH3099-9)*, 2, 916–926.

Chua, L. (1995). A glimpse of nonlinear phenomena from Chua's oscillator. *Philosophical Transactions: Physical Sciences and Engineering*, 353(1701), 3–12.

Chua, L. and Lin, G. (1990). Canonical realization of Chua's circuit family. *IEEE Transactions on Circuits and Systems*, 37(4), 885–902.

Danca, M.F., Kuznetsov, N., and Chen, G. (2017). Unusual dynamics and hidden attractors of the Rabinovich–Fabrikant system. *Nonlinear Dynamics*, 88, 791–805. doi:10.1007/s11071-016-3276-1.

Danca, M.F. (2016). Hidden transient chaotic attractors of Rabinovich–Fabrikant system. *Nonlinear Dynamics*, 86(2), 1263–1270.

Dudkowski, D., Jafari, S., Kapitaniak, T., Kuznetsov, N., Leonov, G., and Prasad, A. (2016). Hidden attractors in dynamical systems. *Physics Reports*, 637, 1–50. doi: 10.1016/j.physrep.2016.05.002.

Feng, Y., Pu, J., and Wei, Z. (2015). Switched generalized function projective synchronization of two hyperchaotic systems with hidden attractors. *European Physical Journal: Special Topics*, 224(8), 1593–1604.

Feng, Y. and Wei, Z. (2015). Delayed feedback control and bifurcation analysis of the generalized Sprott B system with hidden attractors. *European Physical Journal: Special Topics*, 224(8), 1619–1636.

Fitts, R.E. (1966). Two counterexamples to Aizerman's conjecture. *Trans. IEEE*, AC-11(3), 553–556.

Heath, W.P., Carrasco, J., and de la Sen, M. (2015). Second-order counterexamples to the discrete-time Kalman conjecture. *Automatica*, 60, 140 – 144.

Jafari, S., Sprott, J., and Nazarimehr, F. (2015). Recent new examples of hidden attractors. *European Physical Journal: Special Topics*, 224(8), 1469–1476.

Jenkins, A. (2013). Self-oscillation. *Physics Reports*, 525(2), 167–222.

Khalil, H.K. (2002). *Nonlinear Systems*. Prentice Hall, N.J.

Kiseleva, M., Kuznetsov, N., and Leonov, G. (2016). Hidden attractors in electromechanical systems with and without equilibria. *IFAC-PapersOnLine*, 49(14), 51–55. doi:10.1016/j.ifacol.2016.07.975.

Krylov, N. and Bogolyubov, N. (1947). *Introduction to non-linear mechanics*. Princeton Univ. Press, Princeton.

Kuznetsov, N., Kuznetsova, O., Leonov, G., and Vagaitsev, V. (2013). Analytical-numerical localization of hidden attractor in electrical Chua's circuit. *Lecture Notes in Electrical Engineering*, 174(4), 149–158. doi: 10.1007/978-3-642-31353-0_11.

Kuznetsov, N. (2016). Hidden attractors in fundamental problems and engineering models. A short survey. *Lecture Notes in Electrical Engineering*, 371, 13–25. doi: 10.1007/978-3-319-27247-4_2. (Plenary lecture at International Conference on Advanced Engineering Theory and Applications 2015).

Kuznetsov, N., Leonov, G., and Vagaitsev, V. (2010). Analytical-numerical method for attractor localization of generalized Chua's system. *IFAC Proceedings Volumes*, 43(11), 29–33. doi:10.3182/20100826-3-TR-4016.00009.

Kuznetsov, N., Leonov, G., Yuldashev, M., and Yuldashev, R. (2017). Hidden attractors in dynamical models of phase-locked loop circuits: limitations of simulation in MATLAB and SPICE. *Commun Nonlinear Sci Numer Simulat*, 51, 39–49. doi:10.1016/j.cnsns.2017.03.010.

Leonov, G., Bragin, V., and Kuznetsov, N. (2010). Algorithm for constructing counterexamples to the Kalman problem. *Doklady Mathematics*, 82(1), 540–542. doi: 10.1134/S1064562410040101.

Leonov, G. and Kuznetsov, N. (2011). Algorithms for searching for hidden oscillations in the Aizerman and Kalman problems. *Doklady Mathematics*, 84(1), 475–481. doi:10.1134/S1064562411040120.

Leonov, G. and Kuznetsov, N. (2013). Hidden attractors in dynamical systems. From hidden oscillations in Hilbert-Kolmogorov, Aizerman, and Kalman problems to hidden chaotic attractors in Chua circuits. *International Journal of Bifurcation and Chaos*, 23(1). doi: 10.1142/S0218127413300024. art. no. 1330002.

Leonov, G., Kuznetsov, N., and Mokaev, T. (2015). Homoclinic orbits, and self-excited and hidden attractors in a Lorenz-like system describing convective fluid motion. *Eur. Phys. J. Special Topics*, 224(8), 1421–1458. doi: 10.1140/epjst/e2015-02470-3.

Leonov, G., Kuznetsov, N., and Vagaitsev, V. (2011). Localization of hidden Chua's attractors. *Physics Letters A*, 375(23), 2230–2233. doi: 10.1016/j.physleta.2011.04.037.

Leonov, G., Kuznetsov, N., and Vagaitsev, V. (2012). Hidden attractor in smooth Chua systems. *Physica D: Nonlinear Phenomena*, 241(18), 1482–1486. doi: 10.1016/j.physd.2012.05.016.

Li, C., Hu, W., Sprott, J., and Wang, X. (2015). Multistability in symmetric chaotic systems. *European Physical Journal: Special Topics*, 224(8), 1493–1506.

Lozi, R. and Ushiki, S. (1993). The theory of confinors in Chua's circuit: accurate anatysis of bifurcations and attractors. *International Journal of Bifurcation and chaos*, 3(2), 333–361.

Matsumoto, T. (1990). A chaotic attractor from Chua's circuit. *IEEE Transaction on Circuits and Systems*, 31, 1055–1058.

Menacer, T., Lozi, R., and Chua, L. (2016). Hidden bifurcations in the multispiral Chua attractor. *International Journal of Bifurcation and Chaos*, 26(14). art. num. 1630039.

Pham, V., Vaidyanathan, S., Volos, C., and Jafari, S. (2015). Hidden attractors in a chaotic system with an exponential nonlinear term. *European Physical Journal: Special Topics*, 224(8), 1507–1517.

Pliss, V.A. (1958). *Some Problems in the Theory of the Stability of Motion (in Russian)*. Izd LGU, Leningrad.

Saha, P., Saha, D., Ray, A., and Chowdhury, A. (2015). Memristive non-linear system and hidden attractor. *European Physical Journal: Special Topics*, 224(8), 1563–1574.

Semenov, V., Korneev, I., Arinushkin, P., Strelkova, G., Vadivasova, T., and Anishchenko, V. (2015). Numerical and experimental studies of attractors in memristor-based Chua's oscillator with a line of equilibria. Noise-induced effects. *European Physical Journal: Special Topics*, 224(8), 1553–1561.

Shahzad, M., Pham, V.T., Ahmad, M., Jafari, S., and Hadaeghi, F. (2015). Synchronization and circuit design of a chaotic system with coexisting hidden attractors. *European Physical Journal: Special Topics*, 224(8), 1637–1652.

Sprott, J. (2015). Strange attractors with various equilibrium types. *European Physical Journal: Special Topics*, 224(8), 1409–1419.

Tsypkin, Y.Z. (1984). *Relay Control Systems*. Cambridge Univ Press., Cambridge.

Vaidyanathan, S., Pham, V.T., and Volos, C. (2015). A 5-D hyperchaotic Rikitake dynamo system with hidden attractors. *European Physical Journal: Special Topics*, 224(8), 1575–1592.

Zelinka, I. (2016). Evolutionary identification of hidden chaotic attractors. *Engineering Applications of Artificial Intelligence*, 50, 159–167.

Zhusubaliyev, Z., Mosekilde, E., Churilov, A., and Medvedev, A. (2015). Multistability and hidden attractors in an impulsive Goodwin oscillator with time delay. *European Physical Journal: Special Topics*, 224(8), 1519–1539.

PIII

SYNCHRONIZATION OF HIDDEN CHAOTIC ATTRACTORS ON THE EXAMPLE OF RADIOPHYSICAL OSCILLATORS

by

N. V. Kuznetsov, G. A. Leonov, and N. V. Stankevich 2017

Proceeding of PIERS IEEEXplore

PIV

A FAMILY OF MODELS WITH BLUE SKY CATASTROPHES OF DIFFERENT CLASSES

by

P. V. Kuptsov, S. P. Kuznetsov, N.V. Stankevich 2017

Regular and Chaotic dynamics, Vol.5, pp. 551-565

ISSN 1560-3547, Regular and Chaotic Dynamics, 2017, Vol. 22, No. 5, pp. 551–565. © Pleiades Publishing, Ltd., 2017.

A Family of Models with Blue Sky Catastrophes of Different Classes

Pavel V. Kuptsov[1*], Sergey P. Kuznetsov[2], and Nataliya V. Stankevich[1,3***]**

[1] *Yuri Gagrin State Technical University of Saratov*
ul. Politehnicheskaya 77, Saratov, 410054 Russia

[2] *Kotel'nikov's Institute of Radio-Engineering and Electronics of RAS, Saratov Branch*
ul. Zelenaya 38, Saratov, 410019 Russia

[3] *University of Jyväskylä*
Mattilanniemi 2, FIN-40014, Finland

Received August 17, 2017; accepted September 08, 2017

Abstract—A generalized model with bifurcations associated with blue sky catastrophes is introduced. Depending on an integer index m, different kinds of attractors arise, including those associated with quasi-periodic oscillations and with hyperbolic chaos. Verification of the hyperbolicity is provided based on statistical analysis of intersection angles of stable and unstable manifolds.

MSC2010 numbers: 34C28, 34C23, 37D20, 37E99, 37G15, 37G35

DOI: 10.1134/S1560354717050069

Keywords: dynamical system, blue sky catastrophe, quasi-periodic oscillations, hyperbolic chaos, Smale – Williams solenoid

INTRODUCTION

Originally, the bifurcation called the blue sky catastrophe was described in [1]. In the simplest case it can be explained as follows. The phase trajectory departs from a vicinity of a semistable limit cycle (saddle-node periodic orbit) existing at the threshold of the bifurcation, goes around a large-size loop, and turns back to the limit cycle from the other side. As a control parameter is varied in one direction, the semistable cycle transforms into a pair of cycles, a stable and an unstable one. As the control parameter is varied in the opposite direction, two cycles meet each other, forming the semistable cycle, and then disappear, while the large-size limit cycle emerges in the domain of the above-mentioned loop containing helical coils in the phase space region of the former limit cycle pair (Fig. 1a). Conditions and mechanisms of birth of limit cycles through the blue sky catastrophe are described in detail in [2–8].

According to the analysis developed in [2], it is natural to consider actually a family of such bifurcations distinguished by an integer index m. Indeed, in general, if a phase trajectory with some angular coordinate φ departs from the saddle-node cycle, then after a travel along the large-size loop and subsequent return it will be characterized by this angular coordinate expressed by a relation containing an additive term of form $m\varphi$ (Fig. 1b). For three-dimensional phase space (the minimal dimension where the blue-sky catastrophe may take place) the integer m may be either 0 or 1. However, at higher dimensions, any integer can occur. In particular, $m = 2$ will correspond to the birth of a hyperbolic strange attractor represented by a classical Smale–Williams solenoid in a Poincaré section, and $m > 2$ to solenoids of larger rates of increase in the number of loops at successive stages of their geometric construction [3] (Fig. 2).

*E-mail: p.kuptsov@rambler.ru
**E-mail: spkuz@yandex.ru
***E-mail: stankevichnv@mail.ru

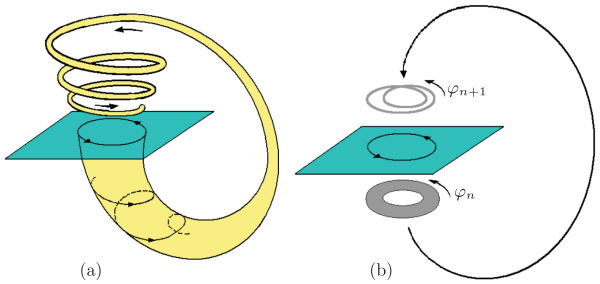

Fig. 1. Phase space structure in the case of the blue sky catastrophe in the simplest case of three dimensions (a) and schematic representation of the situation where the Smale–Williams attractor can appear in a phase space of dimension 4 and higher (b).

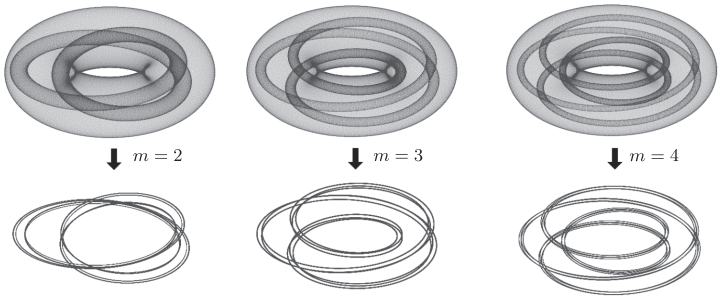

Fig. 2. Formal geometric construction of the Smale-Williams solenoids associated with the indices $m = 2$, 3, and 4: initial toroidal domain in the state space, results of its transformation in the first iteration of the mapping, and the solenoid obtained after a large number of repetitive applications of the procedure.

In a series of works, different applications were discussed in relation to the blue sky catastrophes. Remarkably, a lot was done in connection with biological models and neurons. For instance, some results demonstrating a transition between tonic-spiking and bursting in a model of leech neuron are presented in reference [9]. Also, in [10–12] it was mentioned that this kind of bifurcation can be considered as the main mechanism for the onset of the burst-spike dynamics, and it was observed in other neuron-like models. Such approaches were applied for relaxation systems with fast and slow variables, and for modeling the cardiac rhythms [13, 14]. In a recent paper [15] the authors suggest that the interaction of technology and economic policy regulations in the energy sector may be described by slow-fast systems, where the blue sky catastrophes are possible. In [16] the bifurcation associated with the blue sky catastrophe was considered as one of scenarios for the birth of chimera states in ensembles of phase oscillators, which are used for description networks of neurons and for other biological models of interaction.

In [17] the bifurcation of the blue sky catastrophe has been found in a binary mixture contained in a laterally heated cavity at small Prandtl numbers. In [18–20] the blue sky catastrophes are discussed in relation to astrophysics, in the context of the restricted four-body problem. In [21] results are presented concerning maps describing the Josephson junction, where such kind of bifurcation was observed. In [22] a blue sky catastrophe of limit cycles of van der Pol system with noise (fuzzy disturbance) was studied.

Also, theoretical investigations of the blue sky catastrophes continue to develop [23–26]. Most of these studies relate to the simplest case of the limit cycle birth in the bifurcation (index $m = 0$ according to the classification of reference [2]).

However, no concrete examples relating to the emergence of hyperbolic chaos have been considered, although recently a number of models and experimental electronic circuits manifesting this phenomenon have been proposed [27–29, 32, 33].

In the context of the present study, the most important is the four-dimensional system, in which an attractor of Smale – Williams type appears as a result of the blue sky catastrophe with the Turaev – Shilnikov index $m = 2$, which was suggested and studied numerically in reference [33]. By modifying this system, it is possible to construct models with other integer indices m representing various types of the blue-sky catastrophes; particularly, in reference [34] we considered the case $m = 1$ associated with the birth of quasi-periodicity.

In the present work we suggest a generalized model representing a family of four-dimensional dynamical systems, in which the blue sky catastrophes of different classes outlined by Turaev and Shilnikov [2, 3] take place. In Section 2 we introduce a model manifesting the blue sky catastrophes containing an index m as an integer parameter, depending on what kinds of attractors can arise due to the bifurcations. In Section 3 we review possible dynamical regimes of the model and discuss the structure of the space of control parameters. In Section 4 we consider a generalized model in the case of emergence of quasi-periodic dynamics $m = 1$. In Section 5 results of numerical simulation of the generalized model with $m = 2, 3, 4$ are presented, and the occurrence of hyperbolic chaos is demonstrated. In Section 6 we present results of verification of hyperbolicity based on analysis of statistical distributions of the angles of intersection of stable and unstable manifolds of orbits on the attractors.

1. FAMILY OF SYSTEMS WITH THE BLUE SKY CATASTROPHES

In order to construct a generalized model, let us start with a two-dimensional predator–prey system with instant state specified by two nonnegative variables r_1, r_2:

$$\begin{aligned} \dot r_1 &= 2\left(1 - r_2 + \frac{1}{2}r_1 - \frac{1}{50}r_1^2\right) r_1, \\ \dot r_2 &= 2\left(r_1 - \mu + \frac{1}{2}r_2 - \frac{1}{50}r_2^2\right) r_2. \end{aligned} \tag{1.1}$$

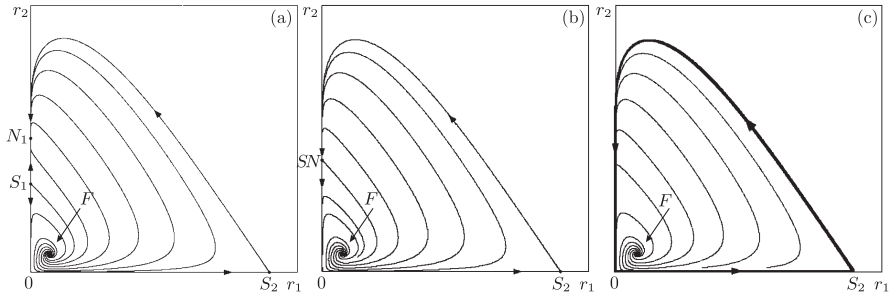

Fig. 3. Phase portraits of the system (1.1); diagrams from (a) to (c) correspond to increase in parameter μ.

These equations differ from those in reference [29] with additional nonlinear terms in the second ("predator") equation, and contain a control parameter μ. If the value of μ is slightly less than $\mu_0 = 3\frac{1}{8}$, the picture of orbits on the phase plane (r_1, r_2) looks like that shown in Fig. 3a. There are four fixed points here, an unstable focus F, saddles S_1 and S_2, and a node N_1. With increasing μ, the fixed points S_1 and N_1 move to meet each other at $\mu = \mu_0$, and then disappear (see panels (b) and (c), respectively). Instead of the former pair of fixed points, a domain of relatively slow motion appears there, while the attractor is a limit cycle, which passes close to the origin and to the saddle S_2.

Following [29], let us consider the quantities r_1 and r_2 as squared absolute values of complex amplitudes for two oscillators of some frequency ω_0, namely, $r_{1,2} = |a_{1,2}|^2$. One can write down a set of differential equations for the complex variables a_1 and a_2 and add terms of a certain form, which introduce an additional coupling between the oscillators in the following way:

$$\begin{aligned} \dot{a}_1 &= -i\omega_0 a_1 + \left(1 - |a_2|^2 + \frac{1}{2}|a_1|^2 - \frac{1}{50}|a_1|^4\right) a_1 + \frac{1}{2}\varepsilon \operatorname{Im} a_2^m, \\ \dot{a}_2 &= -i\omega_0 a_2 + \left(|a_1|^2 - \mu + \frac{1}{2}|a_2|^2 - \frac{1}{50}|a_2|^4\right) a_2 + \varepsilon \operatorname{Re} a_1. \end{aligned} \tag{1.2}$$

Here ε is a coupling coefficient and m is an integer index. At $\varepsilon = 0$, the equations for $r_{1,2} = |a_{1,2}|^2 = x_{1,2}^2 + y_{1,2}^2$ derived from (1.2) coincide precisely with Eqs. (1.1). At ε small enough, and at values of μ notably less than μ_0, the sustained dynamics presented graphically on the plane (r_1, r_2) is located close to the node N_1. For nonzero ε, this is a limit cycle of such kind that the second oscillator has some notable amplitude, while for the first one the amplitude is very small. Besides, there is an unstable limit cycle close to S_1. With gradual increase of the parameter, both cycles come closer, meet together and coincide at some $\mu = \mu_c(\varepsilon) \approx \mu_0$, forming a semistable limit cycle. At $\mu > \mu_c(\varepsilon)$ it disappears. Now the motion of a representative point on the plane (r_1, r_2) follows approximately a closed large-scale path, as in Fig. 3c, visiting again and again a neighborhood of the origin. Qualitatively, for each such passage, the following stages may be specified: excitation of the first oscillator (i), excitation of the second oscillator (ii), damping of the first oscillator (iii), and slower damping of the second oscillator (iv). Activation of the second oscillator occurs in the presence of driving from the partner, due to the coupling term proportional to ε in the second equation, so it inherits the phase from the first oscillator. During the damping stage of the second oscillator, its residual oscillations initiate the activation of the first one. The corresponding term proportional to ε in the first equation contains complex amplitude in the power of m, so this transfer of excitation is accompanied with multiplication of the argument of the complex variable that is the phase of the oscillations. Then the process repeats again and again. So the transformation of the phase at each next cycle of the excitation exchange corresponds to the circle map,

$$\varphi_{n+1} = m\varphi_n + \text{const}, \tag{1.3}$$

which is expanding for $m \geqslant 2$. At $m = 2$ it is commonly referred to as the Bernoulli map. Then let us analyze dynamical regimes in the model (1.2) for different m.

2. DYNAMICAL BEHAVIOR OF THE GENERALIZED MODEL

One of the well-known techniques for studies of dynamical systems is the method of charts of dynamical regimes [30, 31], which reveals the disposition of dynamical regimes depending on control parameters visualizing the parameter plane topography. Let us consider the system (1.2) using this method. As the control parameters we choose the basic frequency of the self-oscillations ω_0 and the parameter μ responsible for the transition through the blue sky bifurcation. We note that the index m is not regarded as a control parameter in the classical sense, since the differential equations are modified if we change m. Undertaking the computations, for each value of m we deal with a concrete four-dimensional set of differential equations (In the Appendix full representations of the equations are collected with different values of m).

Figure 4 shows the charts of dynamical regimes for $m = 1$ (a), $m = 2$ (b), $m = 3$ (c), and $m = 4$ (d). In the course of plotting the charts, for periodic regimes we evaluate the number of discrete points in the Poincaré section by a surface $\operatorname{Re}(a_1) = 0$ after excluding transients. (The legend for correspondence of the periods and colors is given in the bottom part of Fig. 4). In the case of the number of discrete points larger than 120, we regard the regime as nonperiodic (which may be either chaotic or quasi-periodic), and the respective point of the parameter plane is colored by a certain gray color tone.

For all values of m from 1 to 4, on the parameter planes of Fig. 4 one can observe two kinds of characteristic bifurcation lines, at which complex dynamics emerge. The first line $\mu_c^{BS} \approx 3\frac{1}{8}$ is that corresponding to the bifurcation of the blue sky catastrophe. The second line $\mu_c^{NS} \approx 16.5$ is that

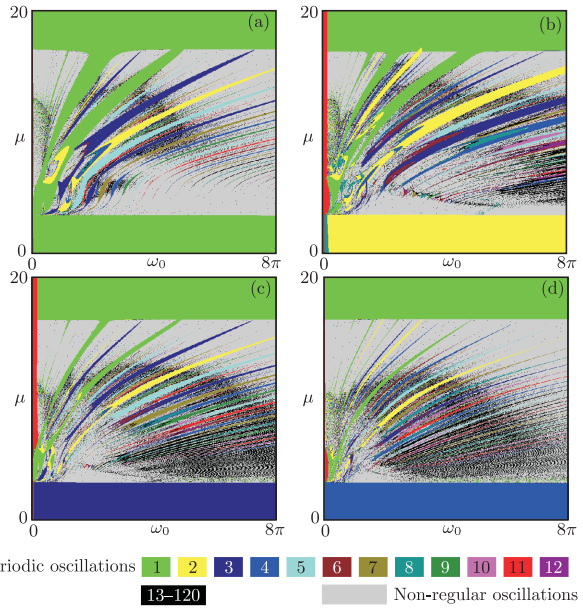

Fig. 4. Charts of dynamical regimes for the generalized model (1.2) at (a) $m = 1$, $\varepsilon = 1$; (b) $m = 2$, $\varepsilon = 0.5$; (c) $m = 3$, $\varepsilon = 0.1$; (d) $m = 4$, $\varepsilon = 0.02$.

of the Neimark – Sacker bifurcation. Arrangements of the parameter plane for all discussed values of m look similar: for $\mu_c^{NS} < \mu < \mu_c^{BS}$ periodic self-oscillations take place; inside the band between μ_c^{BS} and $\mu < \mu_c^{NS}$ there is a complex structure including resonance tongues and nonperiodic self-oscillations.

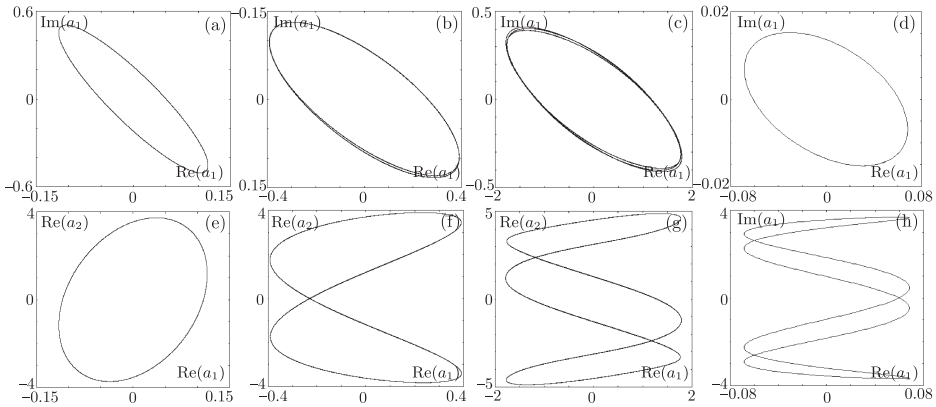

Fig. 5. Two-dimensional projections of phase portraits and Lissajous figures for the model (1.2) before the bifurcation of the blue sky at $\mu = 3.1$, $\omega_0 = 2\pi$, (a) $m = 1$, $\varepsilon = 1$; (b) $m = 2$, $\varepsilon = 0.5$; (c) $m = 3$, $\varepsilon = 0.1$; (d) $m = 4$, $\varepsilon = 0.02$.

Periods of the regimes occurring before the blue sky catastrophe ($\mu < \mu_c^{BS}$) differ depending on the index m. In Fig. 5 we show the corresponding two-dimensional projections of phase portraits on the plane of real and complex parts of the amplitude of the first oscillator $\big(\Re(a_1), \Im(a_1)\big)$ and two-dimensional projections of Lissajous figures on the planes of real parts of amplitudes of the first and the second oscillators $\big(\Re(a_1), \Re(a_2)\big)$. On the projections of phase portraits the observed numbers of rotation for the orbits correspond to the index m. On the projections of the Lissajous figures with increase of the index m one can see the appearance of self-intersections of the trajectory; the number of self-intersections is equal to $m - 1$.

Inside the area between the bifurcation lines μ_c^{BS} and μ_c^{NS} sets of synchronization tongues occur on the parameter plane, and among them one can distinguish main tongues of period 1. The upper bases of the tongues are placed along the Neimark – Sacker bifurcation line; the last tongue of period-1 is located on the parameter plane at frequency $\omega_0 = 4.8\pi$, other tongues at $\omega_{02} = \omega_0/2$, $\omega_{03} = \omega_0/3$, $\omega_{04} = \omega_0/4$, $\omega_{05} = \omega_0/5$, $\omega_{06} = \omega_0/6$; the frequencies of the successive tongues decrease geometrically. Between the period-1 tongues, narrower tongues of higher order are observed. The bottom base of the main diagonal line of period-1 ($\omega_0 = 4.8\pi$) leans on the line of bifurcation associated with the blue sky catastrophe; to the right of this only resonances of higher orders are observed, but to the left of this the same repeating structures of tongues are observed, which lean on the main diagonal tongue of period-1 instead of the line of blue sky catastrophe.

Apart from that, we discuss quasi-periodic and chaotic oscillations (domains of gray color on the parameter planes). As mentioned above, the horizontal line $\mu_c^{NS} \approx 16.5$ corresponds to the Neimark – Sacker bifurcation; as a result of this bifurcation a two-dimensional torus emerges for any m as we go downward in the parameter plane. Tongues of synchronization with different winding numbers lean on the line of the Neimark – Sacker bifurcation. With decreasing μ the synchronization tongues overlap, and chaotic dynamics develops. Inside several tongues one can observe transition to chaos via period-doubling bifurcation cascades.

The structure of the parameter plane near the line of bifurcation of the blue sky catastrophe differs essentially for different m. The synchronization tongues at the bottom bifurcation line tighten at one point. Note that the formation of complex dynamics in the course of the blue sky bifurcation has specific features for different values of index m. For example, for $m = 1$ one can see that the synchronization tongues of high order approach very close the bifurcation line and tend to one point along this line (Fig. 4a). It was checked in [34] that for this case, as a result of the blue sky catastrophe, a two-frequency torus is born; see also Section 4. For $m = 2, 3, 4$ one can see homogeneous domains of chaotic dynamics (gray color) on the parameter planes above the bifurcation line of blue sky catastrophe in several intervals of ω_0, which correspond to robust hyperbolic chaos (Figs. 4b–4d). In Section 5 we consider in detail the features of formation of hyperbolic chaos. In Section 6 we present results of computer verification of the hyperbolicity.

3. QUASI-PERIODIC DYNAMICS

Quasi-periodic oscillations are typical of systems of coupled oscillators. As one can see from Fig. 4, quasi-periodic dynamics take place in the generalized model (1.2), arising as a result of the Neimark – Sacker bifurcation for $\mu_c^{NS} \approx 16.5$. The topography of the parameter plane has a specific characteristic structure manifesting sets of tongues of synchronization on multiple frequencies embedded in the area of quasi-periodicity.

In Fig. 6 two-dimensional projections (gray color) and Poincaré sections (black color) of typical phase portraits for the generalized model (1.2) are presented for different values of index m. Projections of the attractors are projections of tori. In the Poincaré section an invariant curve is visualized[1)].

Quasi-periodic oscillations in the model (1.2) with index $m = 1$ occur as a result of the blue sky catastrophe. Figure 7 shows a two-dimensional projection of phase portrait (a), and its Poincaré section formed by the intersection with the surface $\mathrm{Re}(a_1) = 0$ (b). In the Poincaré section we observe a smooth invariant curve. The diagram in panel (c) demonstrates the evolution of phases at successive crossings of the surface $|a_1| = |a_2|$ corresponding to the Poincaré section in the correct

[1)]For this case we realized the Poincaré section by the surface $\mathrm{Re}(a_1) = 0$.

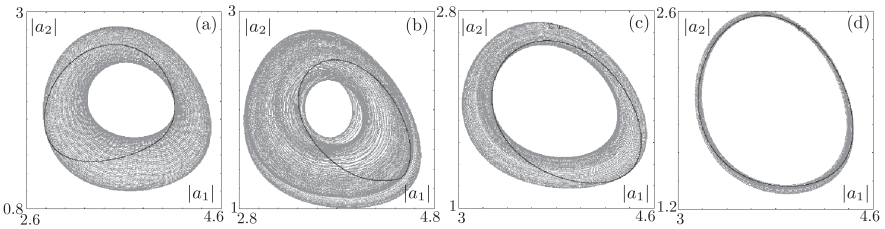

Fig. 6. Two-dimensional projections (gray) and Poincaré sections formed by the intersection with the plane $\mathrm{Re}(a_1) = 0$ of two-frequency quasi-periodic oscillations born as a result of the Neimark – Sacker bifurcation, (a) $m = 1$, $\varepsilon = 1$, $\omega_0 = 3\pi$, $\mu = 16$; (b) $m = 2$, $\varepsilon = 0.5$, $\omega_0 = 2\pi$, $\mu = 16$; (c) $m = 3$, $\varepsilon = 0.1$, $\omega_0 = 2\pi$, $\mu = 16$; (d) $m = 4$, $\varepsilon = 0.02$, $\omega_0 = 2\pi$, $\mu = 16$.

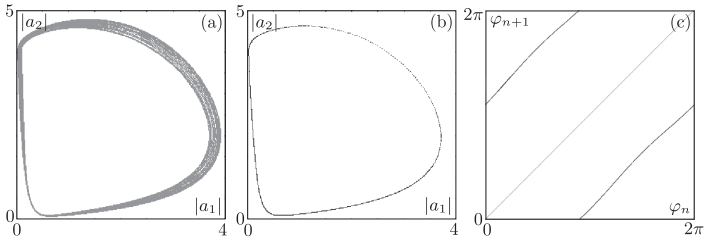

Fig. 7. Two-dimensional phase portrait (a) and its Poincaré section (b) for a quasi-periodic regime; (c) map of phases for the first oscillator in the Poincaré section formed by the intersection with the plane $|a_1| = |a_2|$, for $m = 1$, $\varepsilon = 1$, $\omega_0 = 3\pi$, $\mu = 3.15$.

direction of increase of $|a_2|$. The phase φ_n relates to the first oscillator at $t = t_n$, which is the nth crossing. In computations, it is determined as $\varphi_n = \arg\big(a_1(t_n)\big)$. The plot for the map of phases contains two almost parallel lines, without intersection with the bisector, and it looks like the map (1.3) for $m = 1$.

4. HYPERBOLIC CHAOS AND OTHER PHENOMENA

According to the theory of Shilnikov and Turaev, for $m \geqslant 2$ hyperbolic chaos is expected in the system. Now we consider some features of formation of the hyperbolic chaotic attractors.

As mentioned above, in Figs. 4b–4d nearly above the boundary line of the blue sky catastrophe bifurcation line one can observe chaotic dynamics that correspond at $m \geqslant 2$ to regimes of hyperbolic chaos. Consider some illustrations of this kind of dynamics.

Figure 8 shows two-dimensional projections of phase portraits in the regime of hyperbolic chaos for m from 2 to 4 (top row) together with the respective iterative diagrams for phases at successive passages of the Poincaré section formed by the intersection with the surface $|a_1| = |a_2|$. Observe that for $m = 2$ topologically the discrete-step evolution of the phases corresponds to the Bernoulli map: one full revolution for the preimage φ_n gives rise to two revolutions for the image φ_{n+1}. For $m = 3$ and $m = 4$ the transformation of the phases corresponds to the triple and quadruple expanding circle map (1.3): one full revolution for the preimage φ_n gives rise to three and four revolutions for the image φ_{n+1}, respectively. It supports the qualitative arguments that the case $m \geqslant 2$ occurs here, associated with the presence of the Smale – Williams solenoid in the Poincaré map according to the Shilnikov – Turaev theory.

Figure 9 shows, for the same values of parameters, the waveforms produced by two oscillators constituting the system. Here we observe the process of exchange of excitation between the subsystems according to its description in Section 2. The waveforms of the second subsystem are smooth enough, and those of the first one have small-scale oscillations near zero, while the second

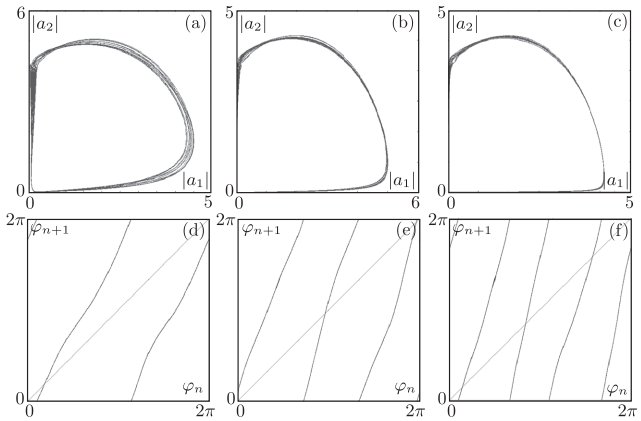

Fig. 8. Two-dimensional projections of phase portraits and the map of phases of the generalized model (1.2) in the regime of hyperbolic chaos for different values of index m: (a) $m = 2$, $\varepsilon = 0.5$, $\omega_0 = 2\pi$, $\mu = 3.15$; (b) $m = 3$, $\varepsilon = 0.1$, $\omega_0 = 2\pi$, $\mu = 3.15$; (c) $m = 4$, $\varepsilon = 0.02$, $\omega_0 = 2\pi$, $\mu = 3.15$.

subsystem has a large amplitude. They correspond to oscillations on the helical coils, which occur in the vicinity of the small-scale limit cycles before the blue sky catastrophe. These fluctuations are well seen in two-dimensional projections of phase portraits in Fig. 8.

Let us consider in detail each case of different values of index m. Firstly, we turn to a one-parameter analysis. In Fig. 10a bifurcation diagrams for $m = 2$ and $\omega_0 = 3\pi$ are shown. In Figs. 10b and 10c magnified fragments are presented for vicinities of critical values of control parameters μ_c^{BS} and μ_c^{NS}. As in the case $m = 1$, near the Neimark – Sacker bifurcation a soft birth of a torus takes place. In the vicinity of the blue sky bifurcation, a hard birth of a two-frequency torus occurs.

Figure 10d–10i shows two-dimensional projections of phase portraits in the Poincaré section formed by the intersection with the plane $\mathrm{Re}(a_1) = 0$. As one can see, at $\mu = 3.15$ in the Poincaré section the phase portrait is close to a smooth invariant curve, but it has a small loop extending from the invariant curve. With increasing μ this loop grows, but in the diagrams for phases corresponds topologically to the Bernoulli map (Figs. 10e and 10j, $\mu = 4.3$). When we observe the transition to nonhyperbolic chaos in the bifurcation diagram, in the Poincaré section this loop becomes larger, and the map of phases becomes more complex and ceases to correspond to the Bernoulli map (Figs. 10f and 10k, $\mu = 6.3$). As one goes up to the Neimark – Sacker bifurcation line, this loop in the Poincaré section disappears gradually. For the quasi-periodic regime ($\mu = 12$) the iterative diagram of phases tends to a straight line of unit slope.

Now let us turn to two-parametric analysis and consider in more detail the structure of the parameter plane in the domain where hyperbolic chaos takes place. Figure 11 shows magnified fragments of the chart of dynamical regimes of the model (1.2) for values of index m from 2 to 4. A wide homogeneous domain of gray color corresponds to hyperbolic chaos. Thus, with increasing parameter μ, at μ_c^{BS} hyperbolic chaos emerges. With further increase of μ tongues of synchronization appear on the charts, which gradually become wider and start to overlap. This process accompanies the destruction (collapse) of hyperbolic chaos.

In [35], one of possible scenarios of birth and collapse of strange hyperbolic attractors associated with Smale – Williams solenoids was suggested. The outlined mechanism of transition, as the control parameter is varied, consists in merging orbits belonging to the attractor with orbits belonging to the unstable invariant set, which are in one-to-one correspondence, in some parameter interval of finite width through saddle-node bifurcations. The same type of behavior is observed in the generalized model (1.2) for values of index m from 2 to 4.

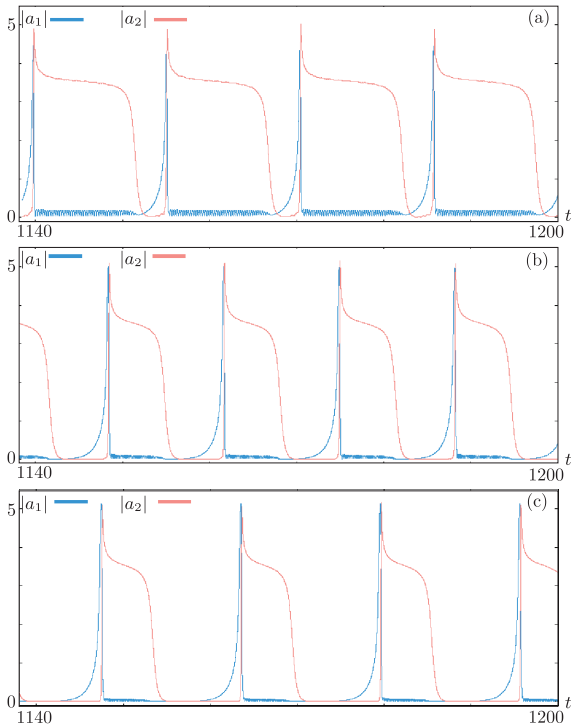

Fig. 9. Waveforms produced by the generalized model (1.2) in regimes of hyperbolic chaos for different values of index m: (a) $m = 2$, $\varepsilon = 0.5$, $\omega_0 = 2\pi$, $\mu = 3.15$; (b) $m = 3$, $\varepsilon = 0.1$, $\omega_0 = 2\pi$, $\mu = 3.15$; (c) $m = 4$, $\varepsilon = 0.02$, $\omega_0 = 2\pi$, $\mu = 3.15$.

5. LYAPUNOV EXPONENTS AND VERIFICATION OF HYPERBOLICITY

Consider Lyapunov exponents for the flow system (1.2) at different m, employing the standard algorithm [36, 37]. The computed values of the exponents λ_i, $i = 1, \ldots, 4$ are collected in Table 1. Note that for all three cases $m = 2, 3$ and 4 there is only one positive Lyapunov exponent. The second one is zero within a numerical error. Using the Lyapunov exponents, we can estimate the attractor dimension via the Kaplan – Yorke formula [38], see column D_{KY} in Table 1. Observe that the dimensions are remarkably close to each other for all three cases.

Table 1. Lyapunov exponents and Kaplan – Yorke dimension for the system (1.2) and the corresponding Poincaré map.

m	λ_1	λ_2	λ_3	λ_4	D_{KY}	Λ_1	T	$\lambda_1 T$
2	0.0439	−0.0001	−8.7588	−8.8606	2.0050	0.6793	15	0.6590
3	0.0810	−0.0001	−5.9709	−6.3186	2.0136	1.0729	14	1.1346
4	0.0817	−0.0003	−4.6255	−5.0960	2.0176	1.3635	17	1.3890

To perform the hyperbolicity test, a Poincaré map is required that represents the states of the flow system at successive excitation stages. We define this map in the same way as it was done previously, when the iteration diagrams for phases were plotted, with the section surface $|a_1| = |a_2|$.

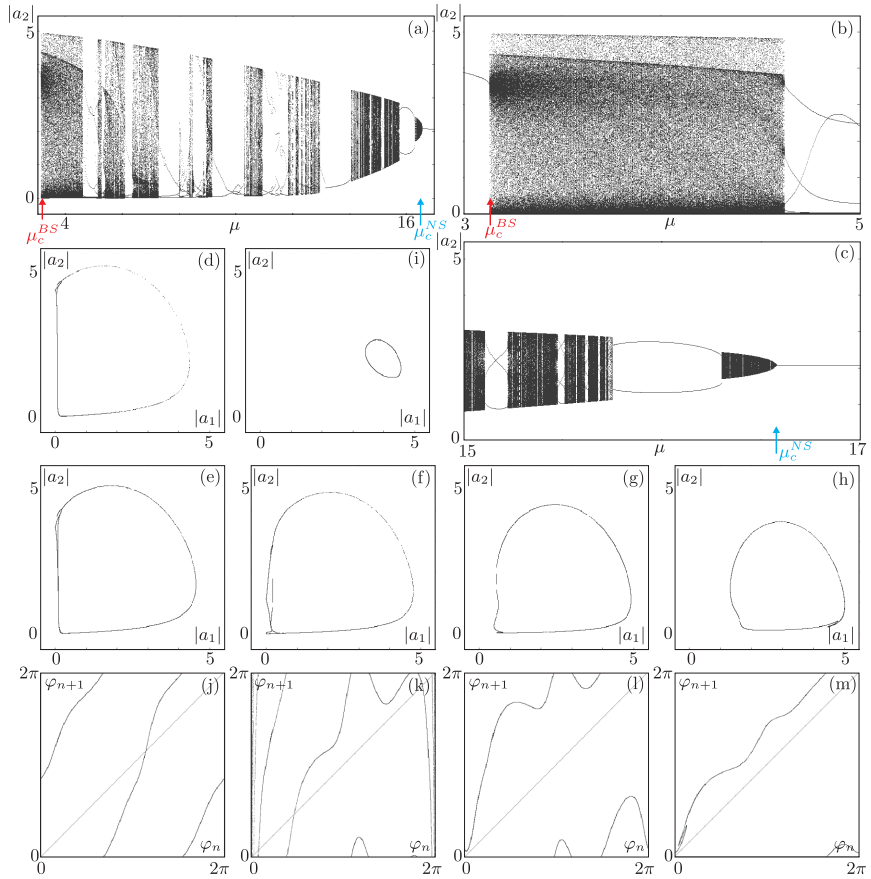

Fig. 10. Bifurcation diagrams and their magnified fragments in the vicinity of bifurcation lines of the generalized model (1.2) for $m = 2$, $\omega_0 = 3\pi$ (a)–(c); two-dimensional projections of phase portraits in the Poincaré section formed by the intersection with the plane $\mathrm{Re}(a_1) = 0$ for different values of parameter μ: (d) $\mu = 3.15$, (e) $\mu = 4.3$, (f) $\mu = 6.1$, (g) $\mu = 8.8$, (h) $\mu = 12.0$, (i) $\mu = 16.0$; and the corresponding map of phases (j) $\mu = 4.3$, (k) $\mu = 6.1$, (l) $\mu = 8.8$, (m) $\mu = 12.0$.

The comparison of the Lyapunov exponents for the map with exponents for the original flow system requires an average time T between the excitation stages, or, which is the same, between the Poincaré section crossings. We have computed it by analyzing the trajectories of the flow system; see the corresponding column in Table 1. Observe that the product $\lambda_1 T$ equals approximately the corresponding Λ_1.

The first Lyapunov exponent for the Poincaré map, see column Λ_1 of Table 1, equals approximately $\ln m$.

Let us now turn to the numerical test of hyperbolicity. The fast method of angles will be applied, see reference [39] for details. In reference [40] the theoretical background for this method is formulated.

All trajectories on a chaotic hyperbolic attractor are known to be of saddle type. This means that their manifolds, i.e., expanding, contracting and neutral, if any, always intersect transversally,

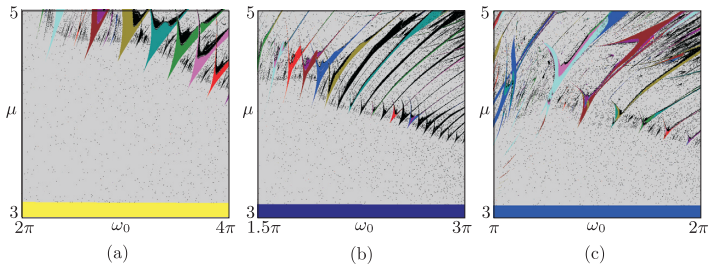

Fig. 11. Magnified fragments of the charts of dynamical regimes for the model (1.2) with $m = 2$ (a), 3 (b), and 4 (c), which contain the areas of hyperbolic chaos and their vicinities.

and no tangencies between them can occur. The method of angles consists in testing for this property: moving along a trajectory, we compute the angles between the subspaces tangent to the trajectory manifolds. The hyperbolicity is confirmed if the angles never vanish, while for nonhyperbolic attractors zero angles are encountered with a nonzero probability.

The fast method of angles [39] consists in passing forward and back in time along the same trajectory. The forward-time pass is identical with that performed for the Lyapunov exponents computation. The equations under consideration are integrated simultaneously with a required number, say K, of copies of the corresponding variation equations. Periodically, the orthonormalization of a matrix whose columns are solutions of the variational equations is performed. But unlike the routine for Lyapunov exponents, the matrices after the orthonormalizations are saved for further use.

For the backward-time pass, an adjoint variational equation has to be derived. For the system under consideration we merely have to transpose the Jacobian matrix and invert its sign. The adjoint variational equations are integrated in backward time. The number of equations is the same as on the forward pass, i. e., K. In quite the same way solutions of the adjoint equations provide columns of the matrix, which have to be periodically orthonormalized. This has to be done exactly at the same trajectory points as on the forward pass. The resulting orthogonal matrices together with the corresponding matrices saved on the forward pass are used for computation of the angles. A matrix of pairwise inner products of their columns is built; then for each of its top left submatrices the smallest singular value σ_i is computed, where $i = 1, \ldots, K$, and the angle is computed as $\theta_i = \frac{\pi}{2} - \arccos(\sigma_i)$ [39].

As discussed above, the flow systems with $m = 2, 3, 4$ exhibit chaotic regimes with one positive Lyapunov exponent, and due to the invariance under time shifts the second exponent is zero, see Table 1. This means that the respective trajectories have one-dimensional expanding and one-dimensional neutral manifolds. As we deal with the Poincaré map, we exclude the neutral manifold from consideration. Thus, testing the hyperbolicity, we need to compute the angle between expanding and contracting manifolds only. However, to actually exclude the neutral manifold in the course of computations, we should project the solutions of the variational and adjoint equations onto the Poincaré section surface, which complicates the routines. Instead we check if the original flow system on the section surface fulfills the conditions imposed on Anosov flows [41, 42]. This automatically implies hyperbolicity for the corresponding Poincaré map.

Thus, we need to compute two angles for the flow system: θ_1 between the expanding subspace and a direct sum of the neutral and contracting subspaces, and θ_2 between a direct sum of the expanding and neutral subspace and the contracting subspace. This means that $K = 2$, i. e., we need to solve two copies of the variational as well as the adjoint equations. The hyperbolicity will be confirmed if both of these angles never vanish.

Figures 12a–12c show the distributions of angles θ_1 and θ_2 computed for the system (1.2) $m = 2, 3$ and 4, respectively. In all three cases the distributions are well separated from the origin, which confirms the hyperbolicity of the corresponding attractors.

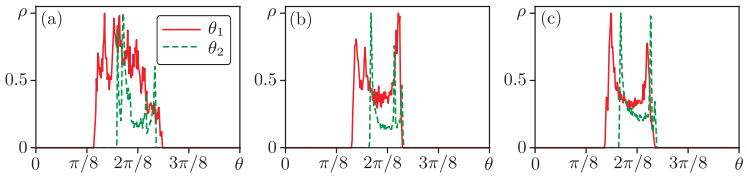

Fig. 12. Distributions of angles between subspaces tangent to trajectory manifolds of the system (1.2). Panels (a), (b) and (c) correspond to $m = 2$, 3 and 4, respectively. The parameters correspond to those given in the caption of Fig. 9. Angles are computed on the Poincaré section surface. The clear separation of the distributions confirms the hyperbolicity of the corresponding Poincaré map in all three cases.

6. CONCLUSIONS

We have introduced a family of systems governed by ordinary fourth-order differential equations in which, depending on an integer index m, different variants of the blue sky catastrophe occur. The latter is a bifurcation event consisting in the appearance of a large-scale attractor after merging and disappearance of a pair of small-scale stable and unstable limit cycles, when a control parameter is varied. In accordance with the Shilnikov – Turaev theory, the type of the resulting attractor is determined by the index m; its role is that it determines the m-fold expansion for an angular variable acquired by the trajectory at the entrance to the region of spiral movements in the phase space, where the former missing pair of limit cycles existed, in comparison with its initial value at the exit from that region. The cases $m = 1, 2, 3, 4$ are discussed in some detail. For $m = 1$, the result of bifurcation is the emergence of an attractive torus, and for $m \geqslant 2$ the result is the appearance of hyperbolic chaos associated with the attractor corresponding to a Smale – Williams solenoid in the Poincaré map. The topological type of the solenoid is determined by the index m, which characterizes the rate of increase in the number of loops of the solenoid winding for successive iterations of the Poincaré map. Results of a numerical study of the dynamics are discussed and illustrated in detail, including the parameter plane charts of dynamic regimes, bifurcation diagrams, portraits of the attractors of the flow system and of the Poincaré map. On the charts of dynamical regimes, various nontrivial dynamical behaviors take place in a band between the line corresponding to the blue sky catastrophe and the line associated with the Neimark – Sacker bifurcation. Hyperbolic chaos occurs over the entire areas near the blue sky catastrophe line. The destruction of hyperbolic chaos upon departure from these areas in other directions is associated with the emergence of periodic dynamics represented by synchronization tongues in the parameter plane. It is believed possible to implement systems representing the introduced family of dynamical systems as electronic devices. This may be of interest when it comes to constructing electronic generators characterized by insensitivity to variation of parameters, manufacturing errors, interferences etc., since a fundamental attribute of hyperbolic chaos is its property of roughness (structural stability).

APPENDIX

Full systems of ODE which were used in numerical experiments for different values of index m.
$m = 1$

$$\begin{aligned}
\dot{x}_1 &= \omega_0 y_1 + \Big[1 - (x_2^2 + y_2^2) + \frac{1}{2}(x_1^2 + y_1^2) - \frac{1}{50}(x_1^4 + 2x_1^2 y_1^2 + y_1^4)\Big] x_1 + \frac{1}{2}\varepsilon y_2,\\
\dot{y}_1 &= -\omega_0 x_1 + \Big[1 - (x_2^2 + y_2^2) + \frac{1}{2}(x_1^2 + y_1^2) - \frac{1}{50}(x_1^4 + 2x_1^2 y_1^2 + y_1^4)\Big] y_1,\\
\dot{x}_2 &= \omega_0 y_2 + \Big[(x_1^2 + y_1^2) - \mu + \frac{1}{2}(x_2^2 + y_2^2) - \frac{1}{50}(x_2^4 + 2x_2^2 y_2^2 + y_2^4)\Big] x_2 + \varepsilon x_1,\\
\dot{y}_2 &= -\omega_0 x_2 + \Big[(x_1^2 + y_1^2) - \mu + \frac{1}{2}(x_2^2 + y_2^2) - \frac{1}{50}(x_2^4 + 2x_2^2 y_2^2 + y_2^4)\Big] y_2.
\end{aligned} \tag{A.1}$$

$m = 2$

$$\begin{aligned}
\dot{x}_1 &= \omega_0 y_1 + \Big[1 - (x_2^2 + y_2^2) + \frac{1}{2}(x_1^2 + y_1^2) - \frac{1}{50}(x_1^4 + 2x_1^2 y_1^2 + y_1^4)\Big] x_1 + \varepsilon x_2 y_2,\\
\dot{y}_1 &= -\omega_0 x_1 + \Big[1 - (x_2^2 + y_2^2) + \frac{1}{2}(x_1^2 + y_1^2) - \frac{1}{50}(x_1^4 + 2x_1^2 y_1^2 + y_1^4)\Big] y_1,\\
\dot{x}_2 &= \omega_0 y_2 + \Big[(x_1^2 + y_1^2) - \mu + \frac{1}{2}(x_2^2 + y_2^2) - \frac{1}{50}(x_2^4 + 2x_2^2 y_2^2 + y_2^4)\Big] x_2 + \varepsilon x_1,\\
\dot{y}_2 &= -\omega_0 x_2 + \Big[(x_1^2 + y_1^2) - \mu + \frac{1}{2}(x_2^2 + y_2^2) - \frac{1}{50}(x_2^4 + 2x_2^2 y_2^2 + y_2^4)\Big] y_2.
\end{aligned} \tag{A.2}$$

$m = 3$

$$\begin{aligned}
\dot{x}_1 &= \omega_0 y_1 + \Big[1 - (x_2^2 + y_2^2) + \frac{1}{2}(x_1^2 + y_1^2) - \frac{1}{50}(x_1^4 + 2x_1^2 y_1^2 + y_1^4)\Big] x_1 + \frac{1}{2}\varepsilon(3x_2^2 y_2 - y_2^3),\\
\dot{y}_1 &= -\omega_0 x_1 + \Big[1 - (x_2^2 + y_2^2) + \frac{1}{2}(x_1^2 + y_1^2) - \frac{1}{50}(x_1^4 + 2x_1^2 y_1^2 + y_1^4)\Big] y_1,\\
\dot{x}_2 &= \omega_0 y_2 + \Big[(x_1^2 + y_1^2) - \mu + \frac{1}{2}(x_2^2 + y_2^2) - \frac{1}{50}(x_2^4 + 2x_2^2 y_2^2 + y_2^4)\Big] x_2 + \varepsilon x_1,\\
\dot{y}_2 &= -\omega_0 x_2 + \Big[(x_1^2 + y_1^2) - \mu + \frac{1}{2}(x_2^2 + y_2^2) - \frac{1}{50}(x_2^4 + 2x_2^2 y_2^2 + y_2^4)\Big] y_2.
\end{aligned} \tag{A.3}$$

$m = 4$

$$\begin{aligned}
\dot{x}_1 &= \omega_0 y_1 + \Big[1 - (x_2^2 + y_2^2) + \frac{1}{2}(x_1^2 + y_1^2) - \frac{1}{50}(x_1^4 + 2x_1^2 y_1^2 + y_1^4)\Big] x_1 + 2\varepsilon x_2 y_2 (x_2^2 - y_2^2),\\
\dot{y}_1 &= -\omega_0 x_1 + \Big[1 - (x_2^2 + y_2^2) + \frac{1}{2}(x_1^2 + y_1^2) - \frac{1}{50}(x_1^4 + 2x_1^2 y_1^2 + y_1^4)\Big] y_1,\\
\dot{x}_2 &= \omega_0 y_2 + \Big[(x_1^2 + y_1^2) - \mu + \frac{1}{2}(x_2^2 + y_2^2) - \frac{1}{50}(x_2^4 + 2x_2^2 y_2^2 + y_2^4)\Big] x_2 + \varepsilon x_1,\\
\dot{y}_2 &= -\omega_0 x_2 + \Big[(x_1^2 + y_1^2) - \mu + \frac{1}{2}(x_2^2 + y_2^2) - \frac{1}{50}(x_2^4 + 2x_2^2 y_2^2 + y_2^4)\Big] y_2.
\end{aligned} \tag{A.4}$$

ACKNOWLEDGMENTS

The work of SPK and NVS including the model formulation and its qualitative and numerical analysis (Sections 2–5) was supported by RSF grant No 17-12-01008. The work of PVK on Lyapunov analysis and hyperbolicity verification (Section 6) was supported by RFBR grant No 16-02-00135.

REFERENCES

1. Palis, J. and Pugh, C. C., Fifty Problems in Dynamical Systems, in *Dynamical Systems: Proc. Sympos. Appl. Topology and Dynamical Systems (Univ. Warwick, Coventry, 1973/1974): Presented to E. C. Zeeman on His Fiftieth Birthday,* Lecture Notes in Math., vol. 468, Berlin: Springer, 1975, pp. 345–353.
2. Turaev, D. V. and Shil'nikov, L. P., Blue Sky Catastrophes, *Dokl. Math.,* 1995, vol. 51, pp. 404–407; see also: *Dokl. Akad. Nauk,* 1995, vol. 342, no. 5, pp. 596–599.
3. Shil'nikov, L. P. and Turaev, D. V., Simple Bifurcations Leading to Hyperbolic Attractors: Computational Tools of Complex Systems: 1, *Comput. Math. Appl.,* 1997, vol. 34, nos. 2–4, pp. 173–193.
4. Shilnikov, L. P. and Turaev, D. V., A New Simple Bifurcation of a Periodic Orbit of ¡¡Blue Sky Catastrophe¿¿ Type, in *Methods of Qualitative Theory of Differential Equations and Related Topics,* Amer. Math. Soc. Transl. Ser. 2, vol. 200, Providence, R.I.: AMS, 2000, pp. 165–188.
5. Gavrilov, N. and Shilnikov, A., Example of a Blue Sky Catastrophe, in *Methods of Qualitative Theory of Differential Equations and Related Topics,* Amer. Math. Soc. Transl. Ser. 2, vol. 200, Providence, R.I.: AMS, 2000, pp. 99–105.
6. Shilnikov, A. L., Shilnikov, L. P., and Turaev, D. V., Blue-Sky Catastrophe in Singularly Perturbed Systems, *Mosc. Math. J.,* 2005, vol. 5, no. 1, pp. 269–282.
7. Shilnikov, A. and Turaev, D., Blue-Sky Catastrophe, *Scholarpedia,* 2007, vol. 2, no. 8, p. 1889.
8. Shilnikov, L. P., Shilnikov, A. L., and Turaev, D. V., Showcase of Blue Sky Catastrophes, *Internat. J. Bifur. Chaos Appl. Sci. Engrg.,* 2014, vol. 24, no. 8, 1440003, 10 pp.

9. Shilnikov, A. and Cymbalyuk, G., Transition between Tonic Spiking and Bursting in a Neuron Model via the Blue-Sky Catastrophe, *Phys. Rev. Lett.,* 2005, vol. 94, no. 4, 048101, 4 pp.
10. Shilnikov, A., Complete Dynamical Analysis of a Neuron Model, *Nonlinear Dynam.,* 2012, vol. 68, no. 3, pp. 305–328.
11. Barnett, W., O'Brien, G., and Cymbalyuk, G., A Family of Mechanisms Controlling Bursting Activity and Pulse-Triggered Responses of a Neuron Model, in *Proc. of the 29th Southern Biomedical Engineering Conference (SBEC),* 2013, pp. 53–54.
12. Barnett, W. H. and Cymbalyuk, G. S., A Codimension-2 Bifurcation Controlling Endogenous Bursting Activity and Pulse-Triggered Responses of a Neuron Model, *PLoS ONE,* 2014, vol. 9, no. 1, e85451.
13. Glyzin, S. D., Kolesov, A. Yu., and Rozov, N. Kh., The Blue Sky Catastrophe in Relaxation Systems with One Fast and Two Slow Variables, *Differ. Equ.,* 2008, vol. 44, no. 2, pp. 161–175; see also: *Differ. Uravn.,* 2008, vol. 44, no. 2, pp. 158–171, 285.
14. Glyzin, S. D., Kolesov, A. Yu., and Rozov, N. Kh., Blue Sky Catastrophe As Applied to Modeling of Cardiac Rhythms, *Comput. Math. Math. Phys.,* 2015, vol. 55, no. 7, pp. 1120–1137; see also: *Zh. Vychisl. Mat. Mat. Fiz.,* 2015, vol. 55, no. 7, pp. 1136–1155.
15. Bondarev, A. A. and Weigt, H., Sensitivity of Energy System Investments to Policy Regulation Changes: Application of the Blue Sky Catastrophe, https://ssrn.com/abstract=2968230 (May 11, 2017), 23 pp.
16. Maistrenko, Yu. L., Vasylenko, A., Sudakov, O., Levchenko, R., and Maistrenko, V. L., Cascades of Multiheaded Chimera States for Coupled Phase Oscillators, *Internat. J. Bifur. Chaos Appl. Sci. Engrg.,* 2014, vol. 24, no. 8, 1440014, 17 pp.
17. Meca, E., Mercader, I., Batiste, O., and Ramírez-Piscina, L., Blue Sky Catastrophe in Double-Diffusive Convection, *Phys. Rev. Lett.,* 2004, vol. 92, no. 23, 234501, 4 pp.
18. Burgos-García, J. and Delgado, J., On the "Blue Sky Catastrophe" Termination in the Restricted Four-Body Problem, *Celestial Mech. Dynam. Astronom.,* 2013, vol. 117, no. 2, pp. 113–136.
19. Burgos-García, J. and Delgado, J., Periodic Orbits in the Restricted Four-Body Problem with Two Equal Masses, *Astrophys. Space Sci.,* 2013, vol. 345, no. 2, pp. 247–263.
20. Alvarez-Ramírez, M. and Barrabés, E., Transport Orbits in an Equilateral Restricted Four-Body Problem, *Celestial Mech. Dynam. Astronom.,* 2015, vol. 121, no. 2, pp. 191–210.
21. Botha, A. E., Shukrinov, Yu. M., and Kolahchi, M. R., A Farey Staircase from the Two-Extremum Return Map of a Josephson Junction, *Nonlinear Dynam.,* 2016, vol. 84, no. 3, pp. 1363–1372.
22. Hong, L. and Sun, J.-Q., A Fuzzy Blue Sky Catastrophe, *Nonlinear Dynam.,* 2009, vol. 55, no. 3, pp. 261–267.
23. Van Gorder, R. A., Triple Mode Alignment in a Canonical Model of the Blue-Sky Catastrophe, *Nonlinear Dynam.,* 2013, vol. 73, nos. 1–2, pp. 397–403.
24. Leonov, G. A., Cascade of Bifurcations in Lorenz-Like Systems: Birth of a Strange Attractor, Blue Sky Catastrophe Bifurcation, and Nine Homoclinic Bifurcations, *Dokl. Math.,* 2015, vol. 92, no. 2, pp. 563–567; see also: *Dokl. Akad. Nauk,* 2015, vol. 464, no. 4, pp. 391–395.
25. Leonov, G. A., Necessary and Sufficient Conditions of the Existence of Homoclinic Trajectories and Cascade of Bifurcations in Lorenz-Like Systems: Birth of Strange Attractor and 9 Homoclinic Bifurcations, *Nonlinear Dynam.,* 2016, vol. 84, no. 2, pp. 1055–1062.
26. Battelli, F. and Feckan, M., Blue Sky-Like Catastrophe for Reversible Nonlinear Implicit ODEs, *Discrete Contin. Dyn. Syst. Ser. S,* 2016, vol. 9, no. 4, pp. 895–922.
27. Kuznetsov, S. P., Example of a Physical System with a Hyperbolic Attractor of the Smale – Williams Type, *Phys. Rev. Lett.,* 2005, vol. 95, no. 14, 144101, 4 pp.
28. Kuznetsov, S. P. and Seleznev, E. P., Strange Attractor of Smale – Williams Type in the Chaotic Dynamics of a Physical System, *J. Exp. Theor. Phys.,* 2006, vol. 102, no. 2, pp. 355–364; see also: *Zh. Èksper. Teoret. Fiz.,* 2006, vol. 129, no. 2, pp. 400–412.
29. Kuznetsov, S. P. and Pikovsky, A., Autonomous Coupled Oscillators with Hyperbolic Strange Attractors, *Phys. D,* 2007, vol. 232, no. 2, pp. 87–102.
30. Kuznetsov, S. P., *Dynamical Chaos,* 2nd ed., Moscow: Fizmatlit, 2006 (Russian).
31. Kuznetsov, A. P., Kuznetsov, S. P., Sataev, I. R., and Chua, L. O., Two-Parameter Study of Transition to Chaos in Chua's Circuit: Renormalization Group, Universality and Scaling, *Internat. J. Bifur. Chaos Appl. Sci. Engrg.,* 1993, vol. 3, no. 4, pp. 943–962.
32. Isaeva, O. B., Kuznetsov, S. P., and Mosekilde, E., Hyperbolic Chaotic Attractor in Amplitude Dynamics of Coupled Self-Oscillators with Periodic Parameter Modulation, *Phys. Rev. E,* 2011, vol. 84, no. 1, 016228, 10 pp.
33. Kuznetsov, S. P., Example of Blue Sky Catastrophe Accompanied by a Birth of Smale – Williams Attractor, *Regul. Chaotic Dyn.,* 2010, vol. 15, nos. 2–3, pp. 348–353.
34. Kuznetsov, A. P., Kuznetsov, S. P., and Stankevich, N. V., Four-Dimensional System with Torus Attractor Birth via Saddle-Node Bifurcation of Limit Cycles in Context of Family of Blue Sky Catastrophes, *Izv. Vyssh. Uchebn. Zaved. Prikl. Nelin. Dinam.,* 2015, vol. 23, no. 4, pp. 32–39.
35. Isaeva, O. B., Kuznetsov, S. P., and Sataev, I. R., A "saddle–node" Bifurcation Scenario for Birth or Destruction of a Smale – Williams Solenoid, *Chaos,* 2012, vol. 22, no. 4, 043111, 7 pp.

36. Benettin, G., Galgani, L., Giorgilli, A., and Strelcyn, J.-M., Lyapunov Characteristic Exponents for Smooth Dynamical Systems and for Hamiltonian Systems: A Method for Computing All of Them: P. 1: Theory, *Meccanica,* 1980, vol. 15, pp. 9–20.
37. Shimada, I. and Nagashima, T., A Numerical Approach to Ergodic Problem of Dissipative Dynamical Systems, *Progr. Theoret. Phys.,* 1979, vol. 61, no. 6, pp. 1605–1616.
38. Kaplan, J. L. and Yorke, J. A., A Chaotic Behavior of Multi-Dimensional Differential Equations, in *Functional Differential Equations and Approximations of Fixed Points,* H.-O. Peitgen, H.-O. Walther (Eds.), Lecture Notes in Math., vol. 730, Berlin: Springer, 1979, pp. 204–227.
39. Kuptsov, P. V., Fast Numerical Test of Hyperbolic Chaos, *Phys. Rev. E,* 2012, vol. 85, no. 1, 015203, 4 pp.
40. Kuptsov, P. V. and Parlitz, U., Theory and Computation of Covariant Lyapunov Vectors, *J. Nonlinear Sci.,* 2012, vol. 22, no. 5, pp. 727–762.
41. Katok, A. and Hasselblatt, B., *Introduction to the Modern Theory of Dynamical Systems,* Encyclopedia Math. Appl., vol. 54, Cambridge: Cambridge Univ. Press, 1995.
42. *Dynamical Systems 9: Dynamical Systems with Hyperbolic Behaviour,* D. V. Anosov (Ed.), Encyclopaedia Math. Sci., vol. 66, Berlin: Springer, 1995.

PV

HYPERBOLIC CHAOS AND QUASIPERIODIC DYNAMICS IN EXPERIMENTAL NONAUTONOMOUS SYSTEMS OF COUPLED OSCILLATORS

by

O. B. Isaeva, D. V. Savin, E. P. Seleznev, and N. V. Stankevich 2017

Proceeding of PIERS IEEEXplore

PVI

GENERATION OF CHAOTIC AND QUASI-PERIODIC OSCILLATIONS IN MULTI-CONTOUR SELF-GENERATOR

by

N. V. Stankevich, O. V. Astakhov, E. P. Seleznev 2017

Proceeding of PIERS IEEEXplore

PVII

COEXISTENCE BETWEEN BURSTING AND SILENT STATES IN A BIOPHYSICAL MODEL OF HODGKIN-HUXLEY-TYPE

by

N. V. Stankevich, E. Mosekilde 2017

CHAOS, Vol.27, Issue 11, accepted

Coexistence between bursting and silent states in a biophysical model of Hodgkin-Huxley-type

Nataliya Stankevich[1,2,3,a)] and Erik Mosekilde[4]

[1] *Department of Radio-Electronics and Telecommunications, Yuri Gagarin State Technical University of Saratov, 77, Politechnicheskaya, Saratov 410054, Russian Federation*

[2] *Faculty of Information Technology, University of Jyväskylä, P.O. Box 35, FI-40014 Jyväskylä, Finland*

[3] *Faculty of Mathematics and Mechanics, St. Petersburg State University, 28, Peterhof, Universitetskiy proezd, St. Petersburg 198504, Russian Federation*

[4] *Department of Physics, Technical University of Denmark, 2800 Lyngby, Denmark*

(Received 5 June 2017; accepted 9 November 2017; published online xx xx xxxx)

Classification of the dynamical mechanisms that support bistability between bursting oscillations and silence has not yet been clarified in detail. The purpose of this paper is to demonstrate that the coexistence of a stable equilibrium point with a state of continuous bursting can occur in a slightly modified well-known biophysical model, which describe the dynamics of pancreatic beta-cells. To realize this form of coexistence, we have introduced an additional voltage-dependent potassium current that is activated in the region around the original equilibrium point. It is interesting to note that this modification also leads the model to display a blue-sky catastrophe in the transitions region between chaotic and bursting states. *Published by AIP Publishing.*

https://doi.org/10.1063/1.4986401

Multistability is a characteristic feature of many types of cells, neural networks, and other forms of oscillatory biophysical systems. This feature is particularly significant in connection with the study of interacting ensembles of many, nearly identical subsystems. It is well-known that, for instance, a variety of unusual phenomena that emerge in ensembles of coupled oscillators can lead to significant reconstructions of an oscillator population, and the presence of coexisting states can significantly influence on the dynamics of all ensemble. In this paper, we introduce a modified version of the well-known model describing dynamics of pancreatic beta-cells obtained by introducing a new type of potassium-like ion channel with a characteristic set of channel parameters selected in accordance with a standard Hodgkin-Huxley formalism. The suggested modification is designed to be local and small enough to allow for the existence of an attracting state inside the regime of stable bursting dynamics. This provides for the presence of multistability in the modified beta-cell model and, at the same time, serves as an example of a biophysical system that allows for the coexistence of a stable equilibrium point with large amplitude bursting.

I. INTRODUCTION

Multistability, or coexistence of dynamical regimes, is a characteristic feature of many types of cells, neural networks,[1–4] and other forms of oscillatory biophysical systems.[5–11] This feature is particularly significant in connection with the study of interacting ensembles of many, nearly identical subsystems. It is well-known that, for instance, a variety of unusual phenomena that emerge in ensembles of coupled oscillators can lead to significant reconstructions of an oscillator population or to its total collapse. It is broadly accepted that, for instance, synchronization plays an important role in the pathogenesis of neurological diseases such as Parkinson's disease and essential tremor[10–12] and, more specifically, Parkinson's disease is associated with asynchronous pacemaker activity involving a population of many thousands of neurons in the basal ganglia.[13,14] Another fundamental phenomenon that can emerge in ensembles of coupled system is oscillator quenching.[15] The biomedical significance of this phenomenon again hinges on the fact that the suppression or disruption of oscillations is involved in the treatment of a variety of neuronal disorders such as Alzheimer's and Parkinson's disease.

In this context, the coexisting states of the single element of the system play a significant role. Special attention should be paid to hidden or rare attractors. In line with the recent survey papers by Leonov and Kuznetsov *et al.*,[16–18] an attracting state may be classified as either "hidden" or "self-excited," with hidden attractors representing all those attractors that do not connect to a stable equilibrium state. The presence of hidden or rare attractors in a system leads to multistability, and in some cases finding of hidden or rare attractor may be a challenging task, but it can influence the dynamics as of the single subsystem, as in ensembles.

At present, the mechanisms that allow bistability, such as the coexistence of tonic spiking and silence or the coexistence of tonic spiking and bursting, appear to be relatively well described. On the other hand, the dynamical mechanisms that support bistability between bursting and silence have not yet been examined to the same extent.[4] Classification of mechanisms that support the coexistence of oscillatory and

[a)]Author to whom correspondence should be addressed: stankevichnv@mail.ru

silent regimes is so far incomplete, and this remains a challenge both in relation to the progress of dynamical systems theory and in relation to important issues in neuroscience. An example of a system that displays coexistence of silence and bursting oscillations was presented in the recent paper by Malashchenko *et al.*.[4] Yet, further attention to this problem is clearly desirable.

This study takes a point of departure in the classic Sherman model that has been widely used to describe the spiking and bursting dynamics of insulin-secreting pancreatic beta-cells,[19,20] and also this model is widely used for description of the dynamics of neuron. Experimentally, one can observe, for instance, how the secretion of insulin increases with the fraction of time that the cells spend in the spiking state. On the other hand, the duration of the silent phase between two bursts is regulated by the rate at which calcium is removed from the interior of the cell. The spiking oscillations typically display a period of 1–10 s, whereas the duration of the bursting period typically varies from 0.2 to 5.0 min. It is interesting to note that, however, individual beta-cells do not burst.[21–23] The opening probability for the potassium channels is too small for the individual cell to present a regular spiking signal and, only in the form of clusters of 30–100 synchronized cells, a regular spiking oscillations will occur. Both electrical coupling and so-called glucose sensing are involved in the cellular synchronization.

We have previously performed a variety of one- and two-dimensional bifurcation analyses[21] for the considered beta-cell model[20,21] and demonstrated how the dynamics of this system after an initial Hopf bifurcation may display an unusual structure of overlapping resonance tongues. We have also outlined the main bifurcation structure for a model of two coupled, identical pancreatic cells[24] and we have described an interesting form of phase synchronization that can occur when the uncoupled oscillators can synchronize in a variety of different configurations.[25] Most recently, we have contributed to a study of the co-existence of hidden attractors in a variety of different systems,[26] and we used fluorescence microscopy to demonstrate how externally forced glucose oscillations can induce distinct 1:1 and 1:2 entrainment of oscillations in islet Ca^{2+} concentrations and mitochondrial membrane potential.[27]

In this paper, we introduce a modified version of the Sherman model obtained by introducing a new type of potassium-like ion channel with a characteristic set of channel parameters selected in accordance with a standard Hodgkin-Huxley formalism. The suggested modification is designed to be local and small enough to allow for the existence of an attracting state inside the regime of stable bursting dynamics. This provides for the presence of multistability in the modified beta-cell model and, at the same time, serves as an example of a biophysical system that allows for the coexistence of a stable equilibrium point with large amplitude bursting. Besides the possibility of observing hidden attractors in a type of beta-cell like model, our interest in the considered system originates from the possibility of observing processes such as the intracellular dynamics of Ca^{2+}-sensitive K^{+}-channel dynamics[28] or the effect of alternative controls on the cell dynamics.[29] We first present the structure of the original model and describe some of the characteristic bifurcation structure of that model. Hereafter follows a description of the modified cell model and the associated characteristic phenomena. Finally, in the last section, we discuss the modified beta cell model in the light of its underlying biological mechanisms.

II. PRESENTATION OF THE BURSTING MODEL

It is well known that the electrical activity of pancreatic beta-cells and other biological cells relies on a number of different types of voltage- and ligand-gated ion channels that are permeable to inorganic ions such as sodium, potassium, chloride, and calcium. Increasing evidence suggests that ion channels not only regulate membrane potential, ion homeostasis, and electrical signaling of these cells but also play an important role in cell proliferation, migration, apoptosis, and differentiation. Recently, the role of ion channels in different oncogenic processes was demonstrated.[30–32]

Over the years, studies of complex pancreatic systems have been performed on individual beta-cells from mice, on small and larger groups of interacting beta-cells, and on clusters of interacting islets. Together these studies have contributed significantly to a better understanding of the role of the inhomogeneity that exists at different levels of the interaction including, for instance, the more or less random mix of different cell types across the pancreatic tissue, the anisotropy associated with the preferential arrangement of the beta-cells along the pancreatic blood vessels, and the variation of the tissue properties along the edges of the islets. However, as mentioned above, only reasonably large and uniform clusters of pancreatic beta-cells display the characteristic bursting dynamics with its alternation between of rapid spiking and periods of silence.

As the starting point for our analysis, let us use the following simplified pancreatic beta-cell model based on the Hodgkin-Huxley formalism as suggested by Sherman *et al.*:[20]

$$\begin{aligned} \tau\dot{V} &= -I_{Ca}(V) - I_K(V,n) - I_S(V,S), \\ \tau\dot{n} &= \sigma(n_\infty(V) - n), \\ \tau_S\dot{S} &= S_\infty(V) - S. \end{aligned} \tag{1}$$

Here, V represents the membrane potential, n may be interpreted as the opening probability of the potassium channels, and S accounts for the presence of a slow variable in the system. As previously noted, the precise biophysical interpretation of this variable remains unclear. The variables $I_{Ca}(V)$ and $I_K(V,n)$ are the calcium and potassium currents, $g_{Ca} = 3.6$ and $g_K = 10.0$ are the associated conductances, and $V_{Ca} = 25$ mV and $V_K = -75$ mV are the respective Nernst (or reversal) potentials. Together with $I_S(V, S)$, the slow calcium current I_{Ca} and the potassium current I_K define the three transmembrane currents of our basic system

$$I_{Ca}(V) = g_{Ca} m_\infty(V)(V - V_{Ca}), \tag{2}$$

$$I_K(V,n) = g_K n(V - V_K), \tag{3}$$

$$I_S(V,n) = g_S S(V - V_K), \tag{4}$$

TABLE I. Parameters for model (1).[18]

$\tau = 0.02$ s	$\tau_S = 35$ s	$\sigma = 0.93$
$g_{Ca} = 3.6$	$g_K = 10.0$	$g_S = 4.0$
$V_{Ca} = 25.0$ mV	$V_K = -75$ mV	
$\theta_m = 12.0$ mV	$\theta_n = 5.6$ mV	$\theta_S = 10.0$ mV
$V_m = -20.0$ mV	$V_n = -16.0$ mV	$V_S = -35$ mV

with the gating variables for m, n, and S representing the opening probabilities of the fast and slow potassium channels

$$\omega_\infty(V) = \left[1 + \exp\frac{V_\omega - V}{\theta_\omega}\right]^{-1}, \quad \omega = m, n, S. \qquad (5)$$

Table I lists the parameter values corresponding to the observed bursting dynamics for the model (1). In principle, the characteristic time constant for the membrane potential is determined by the membrane capacity and the corresponding electrical conductance. In accordance with the original formulation of the model,[20] there is no electrical capacitance in Eq. (1), and the conductances are all dimensionless. To eliminate the dependence on cell size, the conductances have thus been scaled relative to some appropriate conductance. With time constants of $\tau = 0.02$ s and $\tau_S = 35$ s, the ratio $k_S = \tau/\tau_S$ is quite small, and the model is numerically stiff.

Figures 1(a) and 1(b) show typical examples of the time series obtained for the fast variable V and slow variable S. Calcium functions as an essential part of a double-sided feedback loop that controls the bursting process and involves modulations of both electrical activity and hormonal secretion.[19] Calcium removal leads to depolarization and controls the silent phase through deactivation of calcium activated potassium channels. This depolarization activates both the voltage-gated calcium channels and the Hodgkin-Huxley like potassium channels until a renewed influx of calcium takes place and the spiking dynamics is initiated again.

Following Izhikevich,[3] the bursting attractor in the model (1) is born through simultaneous Hopf and saddle-node bifurcations. As long as $V_S < -44.7$ mV, the equilibrium point is stable [examples of fast and slow manifolds are presented in Fig. 1(d)]. For $V_S = -44.7$ mV, a Hopf bifurcation has occurred, the equilibrium point has turned unstable, and the bursting attractor exists [Fig. 1(e)]. The parameter V_S only controls the slow manifold, and with increasing values of this parameter, the slow manifold moves upwards relatively to the fast manifold. The bursting attractor is born in the vicinity of the equilibrium point, but after the bifurcation that occurs for increasing values of V_S, the equilibrium point moves far away from the bursting attractor. Finally, at $V_S = -33.7$ mV, the bursting attractor turns into the spiking attractor as shown in Fig. 1(f).

An interesting feature of the biological bursting system is the large variation one often observes for the bursting period. We have already referred to this variability in relation to the discussion of slow and fast bursters. Besides variations associated with differences in clusters size, the most obvious reason for variations to occur is inhomogeneity in the cell clusters. This has inspired a number of authors[19,20] to propose a so-called phantom burster model that allows fast and slow bursting to occur simultaneous, i.e., by replacing the original equation for the slow potassium current by a set of two (or more) parallel potassium currents. The idea has been to use a multiple degree-of-freedom approach to generate a broader range of interacting bursting oscillators while maintaining the overall structure of the system. If the conductance is large, the bursting that results from this feedback will be fast. On the other hand, if the conductance is small, this feedback has little influence, and the bursting that results from it will be slow. In this way, it has been possible

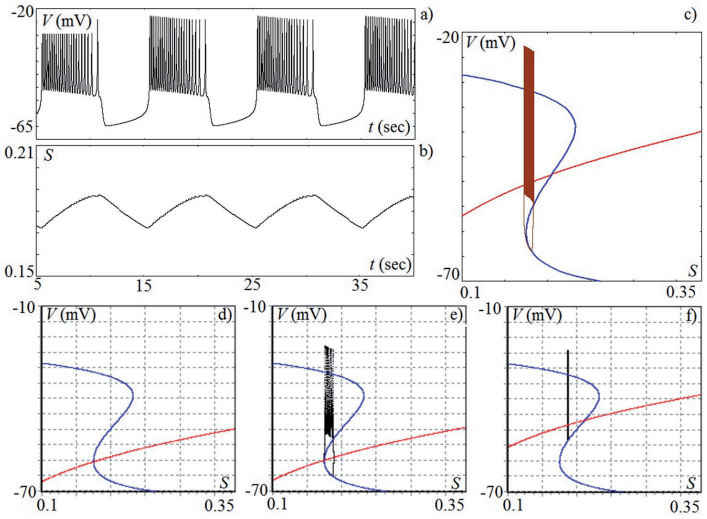

FIG. 1. Time series of the fast (a) and slow (b) variables; (c) fast (blue) and slow (red) manifolds together with a two-dimensional projection of phase portrait for the original Sherman model.[18] During the spiking phase, Ca^{2+}-ions flow into the cells and, during the silent phases, Ca^{2+}-ions are pumped out. The fast (spiking) dynamics is related to the flow of K^+-ions. (d) $V_S = -45$ mV; (e) $V_S = -44.7$ mV; and (f) $V_S = -33.7$ mV.

to account for a range of biomedical phenomena, including the ubiquitous tri-phase response to a step increase in glucose, the response to perturbations of intra-cellular Ca^{2+} stores, and different intracellular functions of potassium.[20,29]

III. MODIFICATION OF THE MODEL

Figure 1(c) shows the two-dimensional projection of the phase portrait (brown color) together with the fast and slow manifolds for $V_S = -35$ mV. For these parameters, the (periodic) trajectories do not intersect the neighborhood of the equilibrium point, but the bursting state terminates in a homoclinic bifurcation as the trajectory hits the slow manifold at some other point. Hence, it appears possible to reorganize the conditions around the equilibrium point in such a way that this point is stabilized while the bursting trajectory continues to exist. Between the stable equilibrium point and the bursting state, we expect to find some rejecting structure and, under these conditions, the bursting state represents a hidden attractor.

To achieve stabilization of the equilibrium point, we propose a form of the voltage-dependent potassium current that varies strongly with the membrane potential right near this equilibrium point and, hence, its stability can exist without affecting the global flow in the model. The suggested form of the potassium current is specified by the equation:

$$I_{K2}(V) = g_{K2} p_\infty(V)(V - V_K), \tag{6}$$

where the function

$$p_\infty(V) = \left[\exp\frac{V - V_p}{\theta_p} + \exp\frac{V_p - V}{\theta_p}\right]^{-1} \tag{7}$$

represents the opening probability for the suggested new type of potassium channel. The same probability functions for the normal channels are represented by sigmoidal function (5) [see Figs. 2(a) and 2(b)]. When the membrane voltage reaches a threshold voltage, the potassium channel will open with probability $n_\infty(V) = 1.0$. For the new channels, the opening function never equals to 1.0. When the membrane voltage reaches a threshold voltage, the opening probability will be equal only to 0.5 [this probability function is presented in Fig. 2(c)]. From the physiological point of view, such situation can be interpreted as some dysfunction of ion channel, for instance, like blocking of potassium channel or inactivation.[33] Also we have to remind that for the individual potassium channels of pancreatic beta-cell the opening probability is very small.[21,22]

Thus, the modified model has the form

$$\begin{aligned} \tau\dot{V} &= -I_{Ca}(V) - I_K(V,n) - I_{K2}(V) - I_S(V,S), \\ \tau\dot{n} &= \sigma(n_\infty(V) - n), \\ \tau_S\dot{S} &= S_\infty(V) - S, \end{aligned} \tag{8}$$

with $I_{K2}(V)$ and $p_\infty(V)$ as given by (6) and (7).

All the parameters of the original model (1) still apply. However, the modified model has three additional parameters g_{K2}, V_p, and θ_p, which can be used to characterize the new ion channel. Figure 2(e) shows the null-clines of the modified model (8). These curves illustrate how one can

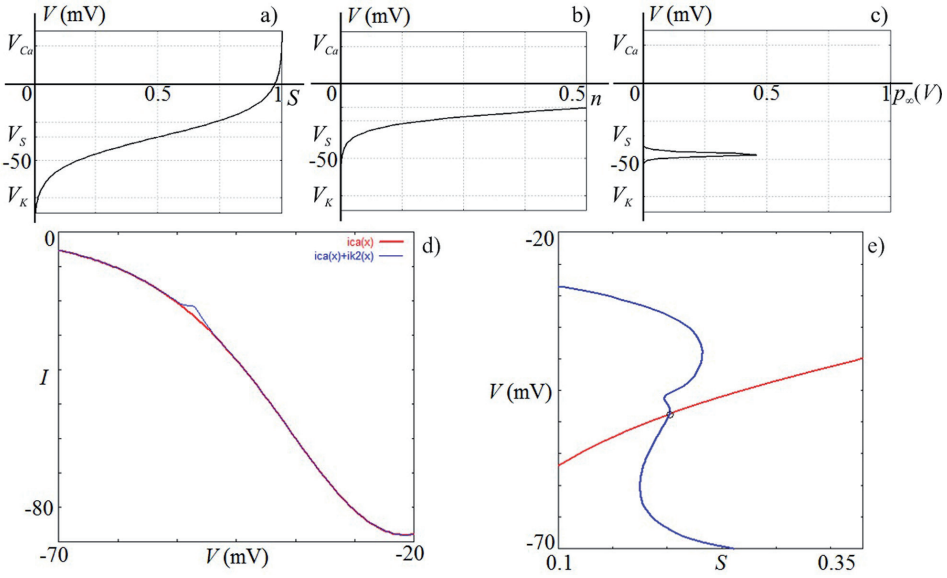

FIG. 2. Dependence of the membrane potential on the different ions: (a) calcium channel; (b) potassium channel; (c) probability function of new ion channel; (d) current of Ca^{2+} (2) (red) and sum of current Ca^{2+} (2) and current of new channel (6) (blue); (e) fast (blue) and slow (red) manifolds of the modified model (8). Supplementing parameters for the new ion channel: g_{K2}=0.14, θ_p=1 mV, and V_p=−46 mV.

introduce new types of ion channels to the model, each leading to the appearance of new pairs of extreme points (minima and maxima) on the fast manifold without affecting the slow manifold. By changing the parameter V_p, one can determine the extreme points or the range of voltage where the system is most sensitive. The parameter θ_p=1 controls the voltage range in which the new ion channel is active in dependence of the membrane potential V. In this situation, the equilibrium point can be stable, but bursting dynamics can develop on the same branch of manifold as in the original model (1). Figure 2(d) illustrates the variation of Ca^{2+}-current (red) and of the sum of the Ca^{2+}-currents and the current associated with new ion channel. One can see that, however, changing of the current can only be local, very small, and without major changes of the system. Figure 2(e) shows the fast (blue) and slow (red) manifolds of the modified Sherman model (8).

IV. DYNAMICAL REGIMES

Let us now consider the mode distribution across a plane spanned by the parameters V_p and g_{K2} that characterize the new ion channel in the model. Figure 3 shows charts of dynamical modes for the modified system (8) with different initial conditions and different magnifications. These charts were constructed in the following way: Using a standard Poincaré section technique, the parameter plane was scanned in small steps. The dynamical state was determined by using a sufficiently long transient for each point in the Poincaré section defined by $n = 0.02$. The distribution of points in the Poincaré section and the corresponding number/colors in Fig. 3 are shown below. If the number of points exceeded 120, the corresponding region was considered to represent a chaotic mode. Charts (a) and (b) were constructed with different initial conditions. Chart (c) is a magnified part of chart (b). In Figs. 3(a) and 3(b), the line of Hopf bifurcation of the equilibrium point is indicated by blue color. This curve was obtained by the use of the software package XPP AUTO.

As the control parameters, we have used the parameter g_{K2} that characterizes the conductance of the new ion channel and parameter V_p that determines the point on the fast-slow manifold where the transition occurs. By varying V_p, we can move the fast manifold relatively to the slow manifold, and in this way we can shift the equilibrium point. In the original model, the unstable equilibrium point falls in the point $EP_0(V_0, n_0, S_0) = (-48.578, 0.0029663, 0.2046)$. In the following, we will vary parameter V_p in the vicinity of V_0. In Fig. 3, the vertical green line is the line that corresponds to line $V_p = V_0$.

For small values of the conductance $g_{K2} = (0–0.05)$, one observes a broad range with different shades of purple. This color represents bursting dynamics in our model. Different shades of purple reflect different number of spikes per burst. For vanishing supply of g_{K2}, one can see bursting regime with a few spikes per burst. This implies that the influence of the new ion channel on the dynamic of the model (8) is still of limited significance, and the overall dynamics is practically similar to that of the original model (1). When parameter g_{K2} increases, one can observe an increasing number of spikes per burst. The equilibrium point may become unstable under such variations.

Finally, to the left in the chart of modes, where g_{K2}>0.05, one observes a cascade of period-doubling bifurcations. Green represents a limit cycle of period-1. Period doubling bifurcations take place with decreasing parameter g_{K2} and increasing parameter V_p. This dynamical regime represents only spiking dynamics. Figure 4(a) shows the corresponding bifurcation diagram. With increasing values of the parameter V_p, the spiking limit cycle is transformed into a period-2 cycle via a period-doubling bifurcation. In the chart of modes, we can hereafter follow the mode lines for the period-doubling bifurcations. Figures 4(b)–4(e) show the examples of spiking attractors, and via projections on the plane (S, V), we can follow how the equilibrium point moves and how the spiking attractor is placed in relation to the form of the fast-slow manifolds. With the increasing values of parameter V_p, the fast manifold moves upwards relatively to slow manifold, and equilibrium point is shifted into a position between the two extrema.

Lines of period-doublings converge onto individual points located in a corner of the area of a stable equilibrium point. Such regions of parameter space are characteristic for the formation of bursting dynamics associated with a blue sky catastrophe.[34] A similar phenomenon was observed in a model of a heart interneuron from the medical leech.[34] We should also notice that the formation of bursting attractor according to this type of scenario is possible only for values of parameter V_p less than V_0 ($V_p < V_0$).

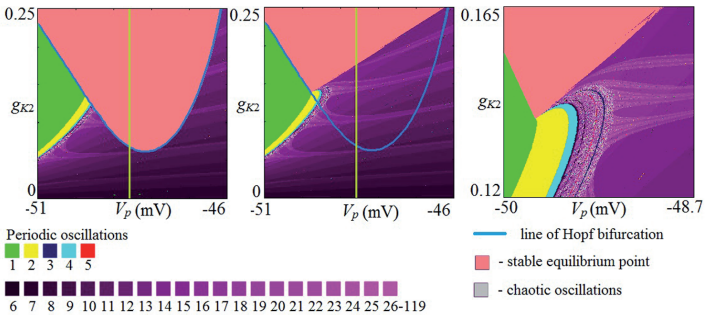

FIG. 3. Charts of dynamical modes for the modified model (8). All parameters from Table I remain unchanged and θ_p=1 mV. Initial conditions for charts: (a) $V_0 = -50$ mV, $n_0 = 0.002$, and $S_0 = 0.1984$ and (b) $V_0 = -40$ mV, $n_0 = 0.02$, and $S_0 = 0.1$. (c) Magnified part of Fig. 3(b). In part of the region above the Hopf bifurcation (blue curve), the system displays coexistence of the stable equilibrium point and a variety of periodic and chaotic solutions.

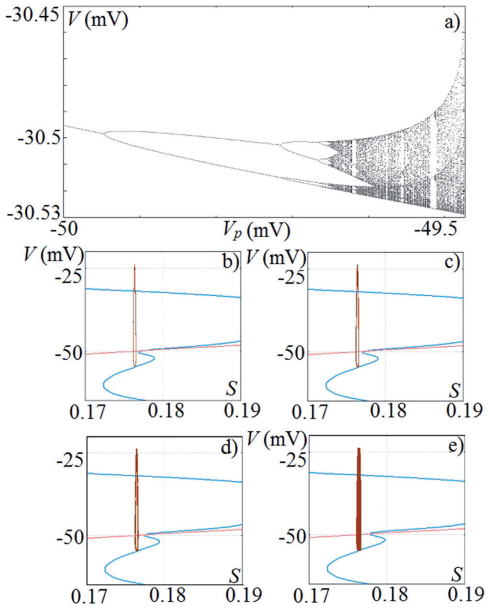

FIG. 4. (a) Bifurcation diagram for the modified model (8) for $g_{K2} = 0.12$ and $\theta_p = 1$. Two-dimensional projections of phase portraits on the V-S plane demonstrating the transition to chaos through period doubling bifurcations. Only spiking oscillations occur: $g_{K2} = 0.12$ and $\theta_p = 1$. (b) $V_p = -50$ mV; (c) $V_p = -49.9$ mV; (d) $V_p = -49.7$ mV; and (e) $V_p = -49.5$ mV.

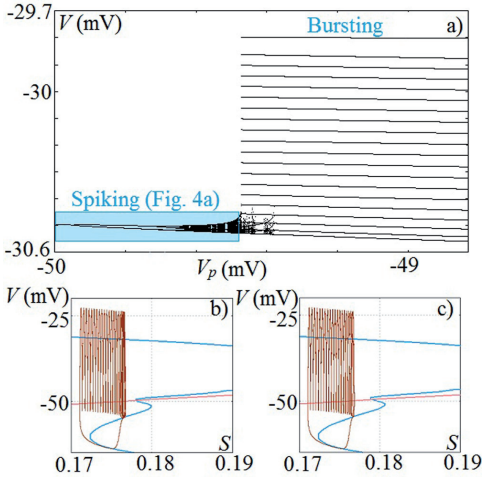

FIG. 5. (a) Bifurcation diagram for the modified model (8) for g_{K2}=0.12 and $\theta_p = 1$. Two-dimensional projections of phase portraits on the V-S plane demonstrating the transition from chaos to stable bursting dynamics. (b) $V_p = -49.4$ mV and (c) $V_p = -49$ mV.

On the right hand side of the chart of modes ($V_p > V_0$), one can observe a broad region with different shades of purple representing bursting dynamics. The bifurcation diagram for the bursting and spiking areas is depicted in Fig. 5(a), and Figs. 5(b) and 5(c) show examples of phase portraits for this form of regime. On the fast-slow manifold, we can see that, when the equilibrium point moves to the maximum, the upper branch of fast manifold becomes unstable, the attractor is shifted to the lower branch, and a long period of oscillations occur. As mentioned above, this transition from spiking to bursting dynamics is associated with a blue-sky catastrophe that occurs at $V_p \approx -49.47$ mV. This transition take place in accordance with the description presented by Shilnikov and Cymbalyuk.[34] For such kind transformation of the dynamics, the multistability with silent state is possible for larger values of parameter g_{K2}, but there is no coexistence between spiking and bursting.

The bifurcation diagram in Fig. 4(a) is a magnified part of the diagram in Fig. 5(a). Due to the transition associated with blue-sky catastrophe, the areas of spiking and bursting have different scales in respect to variable V. In the simplest version, a blue sky catastrophe occurs in three-dimensional phase space. At the bifurcation, a saddle-node limit cycle takes place, whose two-dimensional unstable manifold returns to the periodic orbit making infinitely many rotations in the node region. With a shift of a value of the control parameter in one direction, the saddle-node cycle disappears and a long large-scale stable periodic orbit containing helical coils near the former saddle-node cycle is born. In Fig. 5(b), one can see helical coils on the place of spiking attractors.

With further increase of parameter g_{K2}, one can see line of Hopf bifurcation. This line corresponds to stabilization of equilibrium point. In Sec. V, we describe in detail the formation of coexistence of regime bursting and regime of silent.

V. COEXISTING (HIDDEN) ATTRACTORS

Let us now focus on the coexistent regimes of bursting and of silence (stable equilibrium) as they appear in our modified model. In the charts of dynamical modes (Fig. 3), the red area, representing a region of stable equilibrium, and the purple area, representing a region bursting dynamics, overlap. Hence, depending on the initial conditions, either the stable equilibrium point or the bursting oscillator may be the final state.

In Fig. 6(a), we have plotted the trajectories for a pair of coexisting attracting states in three-dimensional phase space. The purple trajectory represents the stable bursting attractor and the pink curve represents a phase space trajectory that goes to the silent regime. Hence, we conclude that the bursting oscillator (for a range of initial conditions) can operate with a stable equilibrium state in its middle.

Figure 6(b) shows a two-dimensional section of the basin of attraction for the attractors depicted in Fig. 6(a). The section covers the (S_0, V_0) plane while the third variable n_0 was fixed near the equilibrium point at n_0=0.00275. The dynamical regimes was obtained by Poincare section at the plane n_0=0.02. Red color represents initial conditions that lead to the stable equilibrium point and purple represents initial conditions that lead to the bursting state. The black curves in Fig. 6(b) represent the lines of the fast and slow

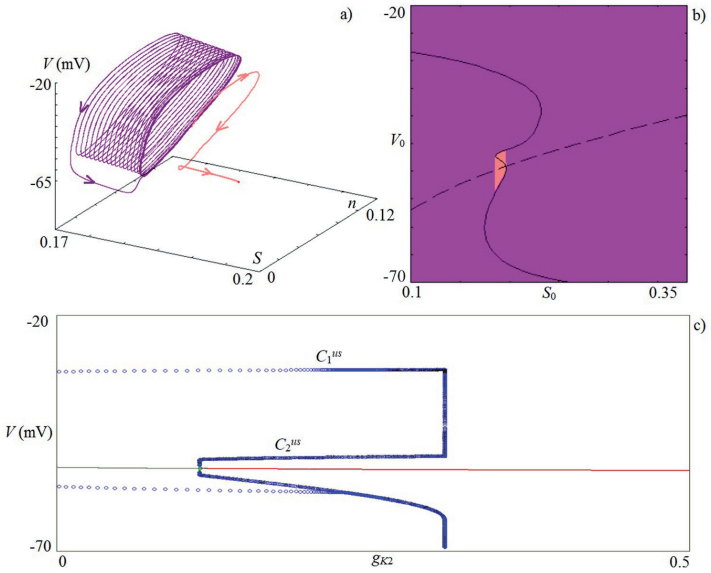

FIG. 6. (a) Three dimensional phase portrait of the modified model (8), $g_{K2} = 0.2$, $V_p = -47$ mV, and $\theta_p = 1$. The figure shows the co-existence of the bursting dynamics and the stable equilibrium point; purple and red trajectories have different initial conditions: red [$V_0 = -40$ mV, $n_0 = 0.02$, and $S_0 = 0.187$] and purple [$V_0 = -40$ mV, $n_0 = 0.02$, $S_0 = 0.181$]; (b) basin of attraction for co-existing bursting attractor (purple) and stable equilibrium point (red), $g_{K2} = 0.2$, $V_p = -47$ mV, $\theta_p = 1$, and $n_0 = 0.00275$; (c) bifurcation diagram in dependence on the parameter g_{K2}, $V_p = -47$ mV.

manifolds. In this way, we can demonstrate that the basin of attraction for the bursting oscillator surrounds a three-dimensional region in which the dynamics is controlled by the stable equilibrium point. This island of stable equilibrium dynamics is located between two extrema of null-clines, which occur as a result of the introduction of the new ion channel.

We suppose that the boundary of the basin of attraction for the stable equilibrium point involves an unstable limit cycle together, presumably, with other structures. In order to detect this unstable cycle, we have used numerical bifurcation analysis. In Fig. 6(c), the bifurcation diagram is obtained with XPP AUTO using g_{K2} as a bifurcation parameter. Red and black lines mark stable and unstable equilibrium point. Blue and green circles mark stable and unstable auto-oscillations. As we can see from Fig. 6(c), at small values of g_{K2}, there is an unstable equilibrium point together with an unstable cycle (C_2^{us}).

This unstable cycle associates with the bursting attractor of the original model. At small values of the conductivity g_{K2}, the influence of new ion channel is insignificant and does not change the dynamic of the model. At g_{K2}=0.1137, this point is stabilized as a result of Hopf bifurcation. This bifurcation is supercritical, and the result of bifurcation is the birth of an unstable and stable limit cycle birth in the vicinity of equilibrium point, but hereafter limit cycle became unstable (C_1^{us}). Thus, the island of regime of silent is limited by unstable cycle (C_1^{us}), which occur as a result of Hopf bifurcation by adding the new ion channel, but another unstable orbit (C_2^{us}) which correspond to original bursting attractor persists. At certain value of the parameter g_{K2} ($g_{K2} \approx 0.3$), a collision of the two unstable orbits take place to leave only a regime of silent.

VI. CONCLUSIONS

The qualitative theory of dynamical systems provides a rigorous description of the scenarios that produce multi-stability of regimes in nonlinear dynamical systems. Early studies by Rinzel[35] and by Guttman *et al.*[36] have formulated and answered a number of questions that describe the basic scenario of bistability between tonic spiking and silence. The answer provided is based on the presence of a repelling periodic orbit separating the basin of attraction of the tonic spiking periodic orbit from the state of equilibrium that represents the silent regime. The same scenario also describes the modulation of the neuron dynamics in response to the variations of a bifurcation parameter. According to this scenario, the unstable limit cycle emerges through a subcritical Andronov-Hopf bifurcation and disappears through a saddle-node bifurcation for periodic orbits. These bifurcations define the boundaries of bistability.

In this paper, we have used a modified well-known biophysical model, which describe dynamics of pancreatic beta-cells to demonstrate the coexistence of a bursting regime and a silent regime. For the considered modification of the model, this type of bistability occurs at the introduction of an additional voltage-dependent potassium current that is activated in the region around the original unstable equilibrium point. The mechanism of bistability is associated with the birth of an unstable cycle as the result of a subcritical Hopf-bifurcation inside the bursting attractor. From the point of view of hidden attractors, the bursting regime is a hidden attractor that cannot be reached from initial conditions in the vicinity of the equilibrium point. At the same time, we have shown that the transition from spiking dynamics to bursting dynamics occurs as a result of a blue sky catastrophe.

ACKNOWLEDGMENTS

N.V.S. acknowledges the partial support from the Russian Science Foundation under Grant No. 14-21-00041.

[1]P. Heyward, M. Ennis, A. Keller, and M. T. Shipley, "Membrane bistability in olfactory bulb mitral cells," J. Neurosci. **21**(14), 5311–5320 (2001).
[2]Y. Loewenstein, S. Mahon, P. Chadderton, K. Kitamura, H. Sompolinsky, Y. Yarom, and M. Häusser, "Bistability of cerebellar Purkinje cells modulated by sensory stimulation," Nat. Neurosci. **8**(2), 202–211 (2005).
[3]E. M. Izhikevich, "Neural excitability, spiking and bursting," Int. J. Bifurcation Chaos **10**(06), 1171–1266 (2000).
[4]T. Malashchenko, A. Shilnikov, and G. Cymbalyuk, "Six types of multistability in a neuronal model based on slow calcium current," PloS One **6**(7), e21782 (2011).
[5]A. N. Pisarchik and U. Feudel, "Control of multistability," Phys. Rep. **540**, 167–218 (2014).
[6]J. R. Pomerening, E. D. Sontag, and J. E. Ferrell, "Building a cell cycle oscillator: Hysteresis and bistability in the activation of Cdc2," Nat. Cell Biol. **5**(4), 346–351 (2003).
[7]K. Tsaneva-Atanasova, C. L. Zimliki, R. Bertram, and A. Sherman, "Diffusion of calcium and metabolites in pancreatic islets: Killing oscillations with a pitchfork," Biophys. J. **90**(10), 3434–3446 (2006).
[8]D. K. Wells, W. L. Kath, and A. E. Motter, "Control of stochastic and induced switching in biophysical networks," Phys. Rev. X **5**, 031036 (2015).
[9]B. N. Kholodenko, "Cell-signalling dynamics in time and space," Nat. Rev. Mol. Cell Biol. **7**(3), 165–176 (2006).
[10]P. A. Tass, *Phase Resetting in Medicine and Biology: Stochastic Modelling and Data Analysis* (Springer Science & Business Media, 2007).
[11]J. G. Milton, "Epilepsy as a dynamic disease: A tutorial of the past with an eye to the future," Epilepsy Behav. **18**(1), 33–44 (2010).
[12]G. Buzsáki and A. Draguhn, "Neuronal oscillations in cortical networks," Science **304**(5679), 1926–1929 (2004).
[13]H. Bergman, A. Feingold, A. Nini, A. Raz, H. Slovin, M. Abeles, and E. Vaadia, "Physiological aspects of information processing in the basal ganglia of normal and parkinsonian primates," Trends Neurosci. **21**(1), 32–38 (1998).
[14]J. Sarnthein, A. Morel, A. Von Stein, and D. Jeanmonod, "Thalamic theta field potentials and EEG: High thalamocortical coherence in patients with neurogenic pain, epilepsy and movement disorders," Thalamus Relat. Syst. **2**(03), 231–238 (2003).
[15]A. Koseska, E. Volkov, and J. Kurths, "Oscillation quenching mechanisms: Amplitude vs. oscillation death," Phys. Rep. **531**(4), 173–199 (2013).
[16]G. A. Leonov and N. V. Kuznetsov, "Hidden attractors in dynamical systems. From hidden oscillations in Hilbert-Kolmogorov, Aizerman, and Kalman problems to hidden chaotic attractor in Chua circuits," Int. J. Bifurcation Chaos **23**(1), 1330002 (2013).
[17]G. A. Leonov, N. V. Kuznetsov, and T. N. Mokaev, "Homoclinic orbits, and self-excited and hidden attractors in a Lorenz-like system describing convective fluid motion," Eur. Phys. J. Spec. Top. **224**, 1421 (2015).
[18]D. Dudkowski, S. Jafari, T. Kapitaniak, N. V. Kuznetsov, G. A. Leonov, and A. Prasad, "Hidden attractors in dynamical systems," Phys. Rep. **637**, 1–50 (2016).
[19]T. R. Chay and J. Keizer, "Minimal model for membrane oscillations in the pancreatic beta-cell," Biophys. J. **42**(2), 181–189 (1983).
[20]A. Sherman, J. Rinzel, and J. Keizer, "Emergence of organized bursting in clusters of pancreatic beta-cells by channel sharing," Biophys. J. **54**(3), 411–425 (1988).
[21]P. Smolen, J. Rinzel, and A. Sherman, "Why pancreatic islets burst but single beta cells do not. The heterogeneity hypothesis," Biophys. J. **64**(6), 1668–1680 (1993).
[22]E. Gylfe, E. Grapengiesser, and B. Hellman, "Propagation of cytoplasmic Ca^{2+} oscillations in clusters of pancreatic β-cells exposed to glucose," Cell Calcium **12**(2-3), 229–240 (1991).
[23]E. Mosekilde, B. Lading, S. Yanchuk, and Y. Maistrenko, "Bifurcation structure of a model of bursting pancreatic cells," BioSystems **63**(1), 3–13 (2001).
[24]B. Lading, E. Mosekilde, S. Yanchuk, and Y. Maistrenko, "Chaotic synchronization between coupled pancreatic β-cells," Prog. Theor. Phys. Suppl. **139**, 164–177 (2000).
[25]D. E. Postnov, O. V. Sosnovtseva, S. Y. Malova, and E. Mosekilde, "Complex phase dynamics in coupled bursters," Phys. Rev. E **67**(1), 016215 (2003).
[26]A. P. Kuznetsov, S. P. Kuznetsov, E. Mosekilde, and N. V. Stankevich, "Co-existing hidden attractors in a radio-physical oscillator system," J. Phys. A: Math. Theor. **48**(12), 125101 (2015).
[27]M. G. Pedersen, E. Mosekilde, K. S. Polonsky, and D. S. Luciani, "Complex patterns of metabolic and Ca^{2+} entrainment in pancreatic islets by oscillatory glucose," Biophys. J. **105**(1), 29–39 (2013).
[28]T. R. Chay, "On the effect of the intracellular calcium-sensitive K+ channel in the bursting pancreatic beta-cell," Biophys. J. **50**(5), 765–777 (1986).
[29]E. Heart and P. J. Smith, "Rhythm of the β-cell oscillator is not governed by a single regulator: Multiple systems contribute to oscillatory behavior," Am. J. Physiol.-Endocrinol. Metab. **292**(5), E1295–E1300 (2007).
[30]G. R. Monteith, D. McAndrew, H. M. Faddy, and S. J. Roberts-Thomson, "Calcium and cancer: Targeting Ca^{2+} transport," Nat. Rev. Cancer **7**(7), 519–530 (2007).
[31]X. Huang and L. Y. Jan, "Targeting potassium channels in cancer," J. Cell Biol. **206**(2), 151–162 (2014).
[32]A. Litan and S. A. Langhans, "Cancer as a channelopathy: Ion channels and pumps in tumor development and progression," Front. Cell. Neurosci. **9**, 86 (2015).
[33]B. A. Simms and G. W. Zamponi, "Neuronal voltage-gated calcium channels: Structure, function, and dysfunction," Neuron **82**(1), 24–45 (2014).
[34]A. Shilnikov and G. Cymbalyuk, "Transition between tonic spiking and bursting in a neuron model via the blue-sky catastrophe," Phys. Rev. Lett. **94**(4), 048101 (2005).
[35]J. Rinzel, "On repetitive activity in nerve," Fed. Proc. **37**(14), 2793–2802 (1978).
[36]R. Guttman, S. Lewis, and J. Rinzel, "Control of repetitive firing in squid axon membrane as a model for a neuroneoscillator," J. Physiol. **305**, 377–395 (1980).